USHER SYNDROME TYPE 3A: RETINAL PHENOTYPE AND GENE THERAPY APPROACHES

By

RACHEL MICHELLE STUPAY

A DISSERTATION PRESENTED TO THE GRADUATE SCHOOL
OF THE UNIVERSITY OF FLORIDA IN PARTIAL FULFILLMENT
OF THE REQUIREMENTS FOR THE DEGREE OF
DOCTOR OF PHILOSOPHY

UNIVERSITY OF FLORIDA

2017

To my mother Cynthia Kachnik for her continued support through my many endeavors over the years, and to my boyfriend Marcus Hooper for surviving the Ph.D process with me. Words cannot express my gratitude to you both.

ACKNOWLEDGMENTS

I thank my mentor Dr. William Hauswirth and all the members that have been a part of the Dr. Hauswirth lab over my time in the lab particularly my co-mentor Dr. Astra Dinculescu for working with me on a daily basis and for training me with everything I have learned. I thank my committee members Dr. John Ash, Dr. Alfred Lewin, and Dr. Wesley Clay Smith for their continued support and assistance throughout my Ph.D and their effort in helping to train me as a scientist. I thank the Genetics Chair, Dr. Margret Wallace, for her continued guidance, mentoring, and training during this process and for allowing me opportunities that were not readily available for most graduate students. I thank my boyfriend Marcus Hooper for his continued support over the years, helping out with Loki, my beloved dog, and for helping to edit this dissertation. I finally thank my family, particularly my mother, Cynthia Kachnik, for her continued support over the years from almost 2 decades in ballet, to a very productive undergraduate career, and finally during an extensive Ph.D program.

TABLE OF CONTENTS

LIST OF TABLES

LIST OF FIGURES

LIST OF ABBREVIATIONS

AAV	Adeno-Associated Virus
ABR	Auditory Brainstem Response
Aipl1	Aryl Hydrocarbon Receptor Interacting Protein-Like 1
ANOVA	Analysis of Variance
BBS	Bardet Biedl Syndrome
BBSome	Bardet Biedl Syndrome Interactome
bp	Base Pairs
BPC(s)	Bipolar Cell
CC	Connecting Cilium of Photoreceptors
Cdh23	Cadherin Protein number 23
cDNA	Complimentary DNA
Clrn1/Clrn1	Clarin-1 Gene/Protein mouse
CLRN1/CLRN1	Clarin-1 Gene/Protein human
CLS	Ciliary Localization Signal
DAPI	4',6-diamidino-2-phenylindole
DNA	Deoxyribonucleic Acid
ER	Endoplasmic Reticulum
ERG	Electroretinogram
GC1	Guanylate Cyclase 1
GCL	Ganglion Cell Layer
GFAP	Glial Filamental Acidic Protein
GFP	Green Fluorescent Protein
GPCR	G-Protein Coupled Receptor
GRK1	G-Protein-Coupled Receptor Kinase 1 Promoter

HA	Hemagglutinin Sequence Tag
IFT	Intraflagellar Transport
ILM	Inner Limiting Membrane
INL	Inner Nuclear Layer
IPL	Inner Plexiform Layer
IRBPE	Interphotoreceptor Retinoid Binding Protein Enhancer
IS	Inner Segment of Photoreceptors (PR)
N48K KI	Clarin-1-N48K Knock-in mouse
Clrn1 $^{-/-}$ KO	Clarin-1 Knock-out mouse
ml	Milliliters
MKS	Meckel-Grouber Syndrome, including protein complex
NB	Novus Biologicals
NB-CLRN1	Novus Biologicals-CLARIN1 antibody
NPHP	Nephronopthesis, including protein complex
OCT	Optical Coherence Tomography
OLM	Outer Limiting Membrane
ONL	Outer Nuclear Layer
OPs	Oscillatory Potentials
OPL	Outer Plexiform Layer
OS	Outer Segment of Photoreceptors (PR)
PBS	Phosphate Buffered Saline
PC	Primary Cilia
PFA	Paraformaldehyde
Pch15	Protocadherin number 15
PCR	Polymerase Chain Reaction

PDZ	Post Synaptic Density Protein (PSD95), Drosophila Disc Large Tumor Suppressor (Dlg1), and Zonula Occludens-1 Protein (zo-1) Protein Sequence
PR(s)	Photoreceptor(s)
RGC(s)	Retinal Ganglion Cells
RNA	Ribonucleic Acid
RPE	Retinal Pigmented Epithelium
RPE65	Retinal Pigmented Epithelium-Specific Protein,65kDa Molecular Weight
RT-PCR	Reverse Transcriptase-Polymerase Chain Reaction
sc	Self-Complimentary
scAAV2Q-Y-F	scAAV2-Quadruple Capsid Protein Mutant (Y272F+Y444F+Y500F+Y730F)
scAAV2Quad-T491V	scAAV2-Quadruple Capsid Protein Mutant (Y272F+Y444F+Y500F+Y730F) plus T491V Mutation
SDS-PAGE	Sodium Dodecyl Sulfate Polyacrylamide Gel Electrophoresis
SEM	Standard Error of the Mean
smCBA	Small Chicken Beta-Actin Promoter
SNAREs	soluble *N*-ethylmaleimide sensitive factor receptors
Spata7	Spermatogenesis-Associated Protein 7
TZ	Transition Zone
ul	Microliters
USH	Usher Syndrome
USH3A	Usher Syndrome Type 3A
UTR	Untranslated Region
vg	Vector Genomes

Abstract of Dissertation Presented to the Graduate School
of the University of Florida in Partial Fulfillment of the
Requirements for the Degree of Doctor of Philosophy

USHER SYNDROME TYPE 3A: RETINAL PHENOTYPE AND GENE THERAPY APPROACHES

By

Rachel Michelle Stupay

December 2017

Chair: William W. Hauswirth
Co – chair: Astra Dinculescu
Major: Medical Science – Genetics

Primary cilia (PC) are extracellular microtubule-based sensory organelles which can be found on almost every cell type in the mammalian system. Defects in PC result in a broad range of phenotypes including polycystic kidneys, retinal degeneration, hearing loss, obesity, polydactyly, and severe cerebral malformations. As a class these diseases are termed ciliopathies. While some mutations are more pleiotropic, other mutations only affect certain cell types such as the human sensory organ systems, including rod and cone photoreceptors in the retina and cochlea hair cells in the inner ear which have highly modified PC. For my project I have chosen to work on a select class of ciliopathies termed Usher syndrome (USH). USH is an autosomal recessive disorder that affects both hearing and vision in patients and accounts for more than 50% of combined deafness and blindness cases. Usher Syndrome Type 3A (USH3A) is caused by mutations in the Clarin-1 (*CLRN1*/CLRN1) gene and there is no cure for this devastating disorder. Therefore, my major goal was to develop a gene replacement based therapeutic approach for USH3A. In order to accomplish this, I first needed to identify the endogenous localization of Clrn1 in the retina by utilizing commercially

available antibodies against CLRN1 allowing us to target the correct retinal cell type for treatment and to avoid off-target toxicity. In addition, I sought to identify a retinal phenotype in *Clrn1* deficient mouse models in order to design and evaluate an effective gene therapy approach, and be able to efficiently assay for phenotype rescue. My results show that both *Clrn1* $^{-/-}$ knockout (KO) and N48K knock-in (KI) mice display a novel retinal phenotype with a delay in arrestin-1 movement upon exposure to light in photoreceptor cells. My final goal was to determine the effects of AAV-mediated delivery of Clrn1 on retinal function and morphology in USH3A mouse models. I show that all neuronal cell types in the retina sustain AAV-mediated CLRN1 expression after intravitreal and subretinal vector delivery as detected by anti-GFP and anti-HA tag antibodies. In addition, the previously utilized CLRN1 antibody can recognize AAV-expressed CLRN1 through co-localization experiments.

CHAPTER 1
INTRODUCTION

Primary Cilia

Cilia Structure and Function

Primary cilia (PC) was first identified in 1675 by Anton Van Leeuwenhoek and were believed to be vestigial organelles not essential for cell survival and/or function (41). Today, it is known that PC are found on almost every cell type in the body and are conserved from the green algae *Chlamydomonas reinhardtii,* to the nematodes *Caenorhabditis elegans*, all the way up to humans (85). PC have a diverse range of physiological roles including embryonic development, control of cell growth, and signal transduction (45, 56, 228). Tissue-specific modified PC also act as chemical, physical, or ligand-based sensors, which will be discussed in Sensory Cilia. Overall, PC play a vital role in the development and function of a wide range cell types and organ systems.

PC are microtubule-based organelles that extend from the apical surface of the plasma membrane and are present on almost all eukaryotic cell types (18, 41, 64, 85, 113, 195). During the cell cycle, in mitosis the centrioles act to separate a single cell into two daughter cells. Once the nuclear envelope re-forms the mother centriole duplicates a neighboring daughter centriole. Once established, the mother and daughter centrioles proceed to dock along the plasma membrane in G0/G1 phase and become the basal bodies that generate the ciliary axoneme (41, 85, 113). The mother centriole contacts a ciliary vesicle, analogous to the plasma membrane, which tethers the mother centriole to a bilayer membrane by centriole distal appendages called transition fibers. In the ciliary vesicle, a ciliary bud begins to form and will elongate from the base to the tip, forming the cilia membrane. The mother centriole will elongate the alpha-tubulin and

beta-tubulin to generate the ciliary axoneme, while the gamma-tubulin will remain exclusively at the mother centriole. Once the cilium is fully formed, the ciliary vesicle will dock and merge with the plasma membrane and the ciliary axoneme will be projected outside the cell. (85, 113, 195, 228). Once a cilium is formed, the cell is no longer able to divide until the cell resorbs the ciliary axoneme and disassociates the basal bodies from the plasma membrane to then act as centrioles for cell division once again.

PC exist as motile and non-motile PC. All have a ring of 9 parallel microtubule doublets that extend from the basal bodies at the cell surface. The basal bodies consist of alpha- beta- and gamma-tubulin while the PC axoneme consists of alpha- and beta-tubulin (18, 41, 64, 85, 113). The outer ring microtubule doublets are also susceptible to post-translational modifications including acetylation, glycylation, and glutamylation (113). These additions allow for greater stability and provide additional interaction foci for other proteins. Motile cilia contain an additional microtubule doublet in the middle of the axoneme that is tethered to the outer ring by radial spokes and dynein arms that allow for regulated movement and active bending of the axoneme (56, 143, 195). Motile cilia are preferentially found on the surface of epithelial cells in the trachea and the ependymal cells lining the ventricles in the brain. Unique 9 + 2 microtubules exist on olfactory sensory neurons that coincidentally are non-motile cilia. There is an additional role for non-motile cilia on the embryonic node pericardium on the developing heart which helps to regulate fluid flow in the abdomen during embryonic development and is responsible for the specification of the left-right body axis (18, 85, 113).

The base of the ciliary membrane is continuous with the plasma membrane and a distinct region, just above the basal bodies, will become differentiated into a transition

zone (TZ) with structurally distinct protein complexes that act as a gate to regulate protein entry and exit within the cilium. The TZ consists of Y-links connecting the ciliary membrane to the microtubule axoneme. They are tethered to the membrane through transmembrane proteins that associate with beaded extracellular proteins that form an outer ring termed a ciliary necklace (45, 195, 216, 231). At the TZ, there are two primary protein complexes that functionally interact with each other, the Meckel-Grouber Syndrome (MKS) complex and the Nephronopthesis (NPHP) complex. Interactions between these two complexes are critical for the early stages of ciliogenesis including membrane docking and fusion of the ciliary vesicle (56, 195, 216, 231). The MKS complex consists of MKS-1/ MKSR-1/ MKSR-2/ MKS-3/ / MKS-5/ MKS-6 and the NPHP complex consists of NPHP-1/NPHP-4. Furthermore, there is a hierarchal interaction between the proteins within each individual complex, as well as between the two complexes. MKS-5 is essential for TZ localization of all MKS and NPHP complex components. Loss of MKS-5 in combination with MKSR-1, MKSR-2, MKS-6, and NPHP-4 all result in abnormal cilia morphology; and MKS-5 is required for proper TZ localization of MKS-1, MKSR-1, MKSR-2, MKS-3, and MKS-6 (the entire MKS complex). Additionally, MKS-5 is also responsible for complete localization of NPHP-1 and NPHP-4 at the transition zone (231). Together, this indicates that MKS-5 is a critical component of the TZ and may act as a key regulator of the ciliary gating mechanism.

In addition to the TZ as a ciliary gate, protein trafficking into and out of the cilia is also regulated by intracellular trafficking. Due to the fact that protein synthesis takes place within the endoplasmic reticulum (ER) and cytoplasm of the cell, ciliary proteins need to be trafficked to the PC through intraflagellar transport (IFT) as well as the

BBSome (BBS: Bardet-Biedl Syndrome) complex. IFT is an intracellular trafficking system that moves uni-directionally along microtubules using Dynein and Kinesin microtubule motors. Kinesin2 regulates anterograde transport and Dynein regulates retrograde transport. These motors are associated with two primary protein complexes comprised of IFTA and IFTB (85, 113, 202, 203, 234). The BBSome is a hetero-octameric complex of 8 core proteins with up to 8 associated proteins that traffics cargo bi-directionally through the cytoplasm and cilia. The BBSome is not essential for PC formation as IFT is; however, mutations in BBS proteins result in altered membrane protein composition (122, 159). One mechanism that helps to regulate the selective trafficking of certain receptors to cilia is that they contain a ciliary localization sequence (CLS) within the protein that allows it to be recognized by the IFT and/or BBSome machinery (85, 216). Membrane trafficking from the ER and/or Golgi apparatus is also regulated by the Rab family of small GTPases as well as SNAREs (soluble *N*-ethylmaleimide sensitive factor receptors) (113, 216, 228). SNAREs are a component of the exocyst complex, this will allow trafficking across the ciliary membrane indicating that there is a potential active transport mechanism in place utilizing importins and exportins. It has been proposed that this process functions similarly to that of the nuclear pore complex, and nucleoporins that regulates protein trafficking across the nuclear envelope. Indeed, recently, it has also been shown that nucleoporins localize to the basal bodies at the PC in cell culture as well as in tracheal epithelial cells (85, 130, 161). Not all nucleoporins localize to the basal bodies, only those aligning with the outer nuclear membrane ring, transmembrane ring, and linker nucleoporins, indicating that there are cilia-specific gating proteins as well in addition to the TZ proteins (130).

Sensory Cilia

In addition to the standard PC found on almost every cell type, certain tissues possess modified PC unique to its particular cell type, tissue type, and function. The primary examples are olefactory cilia in nasal tissue, stereocilia and kinocilia in the cochlea, and photoreceptor (PR) connecting cilia (CC) in the retina. One common feature of all three cell types is that their PC have adjacent actin-based microvilli, either on the same cell or adjacent cells, which act to assist in cilia function (80).

Olfactory neurons are first order neurons and are the initial cell types in the olfactory system that responds to external stimuli, primarily odorants, and are responsible for our sense of smell. Olfactory neurons also have adjacent sustentacular cells that act as supporting cells and they possess a dense layer of microvilli on their apical surface (20). The olfactory system is unique in that the olfactory epithelium has a basal cell layer consisting of horizontal and globular basal cells that acts as olfactory stem cells and can regenerate the olfactory neurons if they die and need to be replaced (20). Olfactory neurons contain between 10-30 primary cilia per cell, and as mentioned previously, olfactory neuronal cilia are non-motile cilia even though they possess a central doublet of microtubules (80, 120, 121, 125, 151). Odorants will bind to their respective G-protein-coupled receptors (GPCRs) within the cilia of olfactory neurons and will then consecutively relay the activation signal to the olfactory glomeruli in the olfactory bulb which will stimulate mitral cells in the olfactory tract to relay the signal to the brain (156). In general, each olfactory neuron only expresses a single type of GPCR, and humans possess approximately 400 odorant GPCR genes. Although each GPCR is specific for a particular odorant, they all signal through the activation of

adenylyl cyclase III, which will act to increase the intracellular levels of cAMP and the consecutive opening of cyclic nucleotide gated channels (80, 121, 125, 151).

In contrast to the multi-ciliated olfactory neurons, ciliated cells in the cochlea have a single PC with adjacent actin-based microvilli structures. PC in the cochlea act to receive and process sound waves and the adjacent vestibular system coincides with sensing motion and balance (21, 111). At the surface of each cochlear hair cell there is a modified PC called a kinocilium which contains a central microtubule doublet in addition to the 9 doublets of the axoneme. Each kinocilia has adjacent rows of stereocilia (similar to microvilli) that are composed of actin, arranged in semi-circle rows, and are stacked in a staircase-like fashion moving away from the kinocilium (80, 84). The result is a V-shaped bundle that is connected together by both ankle and tip links that, upon sound stimuli, will bend and initiate an intracellular signaling cascade to relay the stimulus through the cochlear nerve and into the brain to process the signal (80, 111). The direction of kinocilium formation will predict the direction and orientation of the stereocilia bundle and is believed to be responsible for any positional information required for proper hair cell development (3, 10, 21, 54, 80, 111, 157, 242, 246).

In contrast to both olfactory and cochlear cilia, the cilia in PR cells in the retina exist as a single highly modified PC called a CC ((15, 67, 78)133, 170). Rod PR are designed for response to very dim levels of light and cone PR are designed for response to bright levels of light. They each have a similar cellular structure in that their ribbon synapses are located in the outer plexiform layer (OPL) in the retina, their nuclei are localized in the outer nuclear layer (ONL), their inner segments (IS) contain the majority of intracellular content, and they have a small CC that connects the IS to the

outer segment (OS). Just below the CC, around the basal bodies, is a periciliary ridge complex that helps to facilitate disk membrane biogenesis as well as general membrane protein trafficking into the cilium (112, 145, 161, 214). There are additional actin-based microvilli-like structures that are extensions of IS membrane, and these filamentous structures are termed calyceal processes which are only present in amphibians, birds, and primates (133, 168). Along the OS of PR cells are membrane invaginations termed incisures that are associated with these calyceal processes (72, 73). This periciliary membrane as well as the calyceal processes are highly concentrated with scaffolding and adhesion molecules that are very large transmembrane proteins. These proteins act to connect the OS incisures to the calyceal processes and allow for structural integrity of the OS as well as potentially help to facilitate protein trafficking into the OS of PR cells (72, 73, 200). These proteins when mutated or missing result in Usher Syndrome (USH) which will be discussed below in Usher Syndrome (147, 233).

The rod OS is composed of very densely stacked disc membranes that are separate from the plasma membrane whereas the cone OS is composed of folds of plasma membrane (80, 106). PR cilia are in a 9 + 0 arrangement and the TZ occupies the entire length of the CC, which is unique to PR cells (112, 145). The OS contains the axoneme of the cilia and it also contains the light absorbing components of the PR. OS discs are shed distally on a daily basis and are phagocytized by the retinal pigmented epithelium (RPE) while new discs are replenished at the base of the OS at the CC. All components of the OS are synthesized in the IS and they are trafficked to the OS through molecular motors within the cell (147, 187, 190, 202, 203, 234). Through some more recent data, it was identified that primates have well developed additional actin-

based structures on their PR cells that extend from the IS and are localized all around the OS termed calyceal processes. They are present on both rod and cone PR cells and are absent from lower level mammals, including mice. These processes are composed of actin filaments and contain all of the USH proteins, indicating that these processes are involved in an elongated periciliary ridge complex and assist with protein trafficking to the OS (198). The OS of rod PRs have membrane invaginations termed incisures which are associated with microtubule tracks that allow for protein trafficking along the OS. Calyceal processes are tethered to the OS incisure microtubule tracks by the USH transmembrane proteins. They are believed to help facilitate OS protein trafficking as well as possibly provide additional structural integrity to the rod OS (75, 76). This is believed to be why USH syndrome mouse models do not display retinal degeneration, whereas patients that carry similar mutations develop retinal degeneration (198), and will be discussed further in Autosomal Recessive Retinal Dystrophies. PR function and the rhodopsin signaling cascade will be discussed in Phototransduction Cascade.

Diseases Associated with Primary Cilia (Ciliopathies)

Ciliopathies are a class of disorders that result from defects and/or abnormalities in PC structure and/or function. Ciliopathies are primarily autosomal recessive disorders that present with a very broad range of phenotypes even with mutations in the same gene. Autosomal recessive polycystic kidney disease is defined by bilateral renal cysts and is caused by mutations in the PKHD1 gene. Nephronopthesis (NPHP) is caused by renal cysts and 11 causative genes have been identified, NPHP1-11 (18, 64, 78, 109). Leber's Congenital Amaurosis is an early onset blindness due to retinal degeneration that presents as retinitis pigmentosa caused by PR cell death. There are 14 known causative genes. Not all of these are cilia related genes, as there are several that are

crucial for the visual signaling cascade, but the disease is characterized based on patient presentation (1, 187, 188). Senior-Løken Syndrome is combined polycystic kidney disease with retinal degeneration and is believed to be a result in mutations in select NPHP genes (1, 109, 187, 188). Usher Syndrome (USH) is combined hearing and vision loss due to mutations in any of 11 genes. The three forms of USH are classified by the severity and age of onset of symptoms and USH will be discussed further in Usher Syndrome (1, 187, 188, 230). Joubert's syndrome, in addition to renal cysts, also presents with retinal coloboma as well as mental retardation and ataxia as a result of hypoplasia of the cerebellum. Mutations in several NPHP and MKS genes can result in Joubert's Syndrome. The primary diagnostic characteristic is a "molar tooth sign" that is observed in a brain MRI, as a result of cerebral hypoplasia (41, 109). Bardet Biedl Syndrome (BBS) is caused by mutations in the BBSome proteins as well as some MKS and NPHP genes. BBS is characterized by juvenile-onset obesity caused by altered leptin signaling in the brain. BBS also presents with retinitis pigmentosa, polycystic kidneys, and mental retardation (1, 41, 109, 188, 230). Meckel-Grouber Syndrome (MKS) is the most severe form of ciliopathy and is embryonic lethal. In addition to the earlier mentioned symptoms, it is primarily characterized by lung hypoplasia, post-axial polydactyly, and occipital meningoencephalocele (41, 109).

Recently, different recessive mutations have been seen in many cilia genes and can present with a wide range of organ involvement based on the causative mutation, or combination of mutations (109, 127). There is also the possibility that certain mutations will present differently based on the genetic background of the patient and the effect of modifier alleles on the causative mutation(s) (127). This is becoming more widely

accepted in the field of ciliopathy research over the last decade as researchers begin to identify the cellular mechanisms underlying the respective disease phenotypes (127).

The Biology of Vision

Retinal Structure

The eye is a highly specialized organ that allows for the perception of light and vision. The visual system is a highly complex signaling system with multiple integrated components that are required for visual processing. Light passes through the cornea and lens and is received in the retina in the back of the eye to sense a visual stimulus. This stimulus is further processed by the inner retina and then by the brain into cohesive images. The retina possesses five primary classes of neurons that perform the initial image processing including rod and cone PRs, bipolar cells (BPCs), amacrine cells, horizontal cells, and retinal ganglion cells (RGCs). In addition to retinal neurons, there are two supporting cells in the retina, the RPE and Müller glial cells (106, 214). Rod and cone PRs are first order neurons in the ONL that initially respond to light. Rod PRs mediate dim light vision while cone PRs mediate bright light and color vision. The rod scotopic response range is 10^{-6} – 10^{2} cd/m^2, while the cone photopic response range is10^{-2} – 10^{6} cd/m^2. Mesopic vision refers to a mixed rod-cone response and is at the high response end of rods and the low end of cones between 10^{-2} – 10 cd/m^2. Humans have one type of rod cell that responds maximally to a wavelength of 498 nm and 3 cone pigment cells, blue cones (short wavelength cones: s-cones) responding maximally to a wavelength of 437nm, green cones (medium wavelength cones: m-cones) responding maximally to a wavelength of 533 nm, and red cones (long wavelength cones: l-cones) responding maximally to a wavelength of 564 nm (106).

At the base of PR cells are their synapses that connect to BPCs. Rod synapses are termed the rod spherule and cone synapses are termed the cone pedicle. Both rod and cone synapses contain a ribbon synapse that is adjacent to post-synaptic structures (106). In addition to synaptic communication between PRs and BPCs, there are also lateral contacts between rods and cones as well as cones to cones in the retina. These exist between the synaptic membranes as well as small gap junctions along the outer limiting membrane (OLM) that also connect both rod and cone PRs to the Müller cell end feet (106). BPCs are second order neurons in the INL that synapse to PRs and act to amplify the visual signal. There is one type of BPC for rods, the rod on BPC, which connects to multiple rod cells. Cones have two types of BPCs, on and off BPCs. These BPCs relay the amplified signal to the third order RGCs which communicate the visual signal through the optic nerve to the brain. Within the brain, communication and interpretation between the left and right eyes occurs across the optic chiasm. Finally, the lateral geniculate nucleus in the thalamus is responsible for visual perception in the brain and this signal is forwarded to the visual cortex for final visual processing (214).

In addition to bipolar cells, the INL has horizontal cells and amacrine cells that provide lateral interactions between rod and cone cells as well as between PRs across the retina. Horizontal cells are responsible for close and global communication across the retina between rods and cones. Amacrine cells have synaptic connections with the axons of bipolar cells and RGCs (106). On the apical side of the OS of PR cells lies the RPE cell layer. The RPE absorbs much of the excess light that is not received by the PR cells, and provides nutrients and oxygen to PRs. The RPE is also responsible for phagocytosing the OS of PRs on a daily basis. Approximately 10% of the distal OS is

digested by the RPE every morning and this is an integrin-mediated process (106). Müller cells are another cell type found in the retina that span the entire retina from their basal lamina at the inner limiting membrane (ILM) adjacent to the RGCs, with the nucleus in the INL, and the Müller cell end-feet creating the OLM at the apical side of the ONL. Müller cells act as supporting glial cells for all cell types in the retina and are responsible for neuroprotective pathways as well as facilitating cone-opsin recycling through a Müller cell-specific pathway. Additionally, Müller cells are believed to act as photon guides to direct incoming light directly onto the PR OS (106).

Human retinas have a highly dense cone region near the center of the retina along the visual axis called a fovea centralis, which is approximately 2.5 mm in diameter and appears as a shallow depression in retinal optical coherence tomography images. Surrounding the fovea is a narrow ring called the macula lutea. These areas are adjacent to the optic nerve, which is localized nasally to the fovea. The fovea consists of only cone PRs with a lower density of cones spread across the remainder of the retina. Adjacent to the fovea, approximately 4.5 mm just outside of the foveal pit, is the densest region of rod PRs that gradually decreases towards the retinal periphery. There are between 60-125 million rod PRs and approximately 3.2-6.5 million cones in the human retina. Cones account for only 10% of the retina but they are responsible for our daytime vision and normal daylight visual acuity (106). The foveal cone system allows for greater resolution than the rest of the retina in that each cone PR synapses to only one bipolar cell, termed a midget cone BPC, and one ganglion cell, termed a midget ganglion cell. In the periphery of the retina, each rod BPC connects with multiple PRs and each cone BPC and ganglion cell interact with multiple PRs (106, 214). The foveal

region is specific to primates, however some species have modified regions of the retina that act in a similar fashion, for example the area centralis in dogs (16).

Phototransduction Cascade

In rod PR cells, rhodopsin is the primary component of the OS. It is a 40 kDa seven-transmembrane GPCR with an associated chromophore molecule 11-cis retinal. The C-terminal sequence of rhodopsin is critical because it not only contains a sequence of five amino acids (aa) (QVXPX) at the C-terminus that targets rhodopsin to the OS, but the C-terminus and intracellular loop regions are also responsible for binding of rhodopsin to its associated G-protein complex (161, 215). In the dark, the cyclic nucleotide gated channel is open with an intracellular charge of approximately 40mV and there is a continuous glutamate neurotransmitter release at the PR ribbon synapse (106). Upon exposure to light, the 11-cis retinal undergoes photoisomerization to the all-trans confirmation. Activated rhodopsin is now able to bind and activate the G protein transducin by catalyzing a GDP exchange for a GTP on the Gα transducing subunit of the G-protein membrane associated complex which is then released from the complex (206). Once activated, transducin stimulates the activation of cGMP phosphodiesterase that then hydrolyzes cGMP to GMP. This results in the closing of the cyclic nucleotide gated channels in the membrane and causes a hyperpolarization in membrane potential to approximately 70 mV, thus inhibiting the inflow of Na^+ and Ca^{2+} ions into rods (106, 214). For the recovery phase, activated rhodopsin is phosphorylated by the G-protein rhodopsin kinase (GRK1) which then allows for arrestin-1 to bind the C-terminus and cytoplasmic loops of rhodopsin. In the dark, with high levels of intracellular Ca^{2+}, a recoverin-Ca^{2+} complex binds to GRK1 to reduce GRK1 activity and inhibit rhodopsin phosphorylation. Upon exposure to light, when the cyclic nucleotide

gated channels close, the levels of intracellular Ca^{2+} drop and therefore results in the disassociation of the recoverin-Ca^{2+}-GRK1 complex, allowing GRK1 to then phosphorylate the C-terminus of rhodopsin and allow arrestin-1 binding. Guanylyl cyclase activating proteins (GCAP) will replenish cGMP to levels sufficient to open cyclic nucleotide gated channels once more. Additionally, the isomerized all trans-retinal is reduced to all trans-retinol, and is actively transported to the RPE, converted back to 11-cis-retinal and returned to the PR OS through the interstitial retinoid binding protein. 11-cis-retinal is then inserted back into rhodopsin. Upon return to the dark-adapted state, arrestin-1 dissociates from rhodopsin and returns to the IS, ONL, and OPL, thus completing the phototransduction cycle (106, 112, 214).

Retinal Function and Morphological Assays

Electroretinogram

The Electroretinogram (ERG) is a standard ophthalmological assay used to measure retinal function through the stimulation of an electrical activity across the eye upon exposure to flashes of light. Upon illumination there is a change in electrical potential on the surface of the cornea relative to the retina (106). The ERG was first implemented in the early 1900's. Dr. Gotch was the first to establish that there were two electrical changes that occurred, first the cornea was negatively charged compared to the baseline, and then it became positively charged (106). Today the ERG is defined as a subset of 3 functions. The a-wave is an initial depolarization due to the electrical potential change in the OS as a result of activated rhodopsin. The b-wave is a positive change in electrical potential as a result of the INL cells receiving signal input from PR cells. Additionally, there is a c-wave that appears later as a result RPE cell responses (106, 175, 184). Accompanying the rising phase of the b-wave are a series of oscillatory

potentials (OPs) that are believed to originate from via communication between cells in the INL in response to the ERG. OPs are visible but they cannot accurately be measured until a digital filter to amplify the signal is applied called a Fast Fourier Transform that reduces out the signal from the a-wave and b-wave in order to obtain a quantitative measure for their frequency and amplitude (106, 227). Additionally, prior to the a-wave, there is an early receptor potential signal that is a small dip prior to the full a-wave and is due to the initial chromophore activation (106). There are two types of ERG, scotopic and the photopic. The scotopic ERG is measured in response to dim light flashes and measures the response from rod PRs. The photopic ERG is measured at bright light flashes and therefore measures cone function. As mentioned previously, there is some overlap of rod and cone response under intermediate flash intensities, termed mesopic conditions. Therefore, the brightest light flash measured in the scotopic ERG will contain some cone responses as well. Similarly, the dimmest light flash measured in the photopic ERG will contain some rod function.

Spectral-Domain Optical Coherence Tomography

Spectral-Domain Optical Coherence Tomography (SD-OCT) provides a method for imaging cross-sections of the retina in a live animal and is non-invasive. It is the only imaging method that can provide a visualization of the multiple layers of the retina without sacrificing the animal. SD-OCT generates high quality images that are generated through two scans, an A-scan and a B-scan. The A-scan registers the interface between the retinal tissue and the B-scan is the reflected output of the light scattering through the retina that is then registered by the camera (110). Our current OCT system is a Bioptigen instrument. This system provides images of horizontal sections of the retina as well as a fundus image of the surface of the retina. SD-OCT

scans can be used to measure retinal layer thickness in an animal over time. Delineations of the ganglion cell layer (GCL), INL, and ONL are fairly easy to deduce, however the demarcation of the IS/OS/RPE is much more difficult. This can be overcome by averaging multiple scans taken at the same slice in the retina and merging these images (19, 81, 238). SD-OCT is currently the best tool for assessing subretinal vector injection damage because any subretinal detachment can be observed through this methodology *in vivo*. OCT can be used in combination with histological sections to assay for retinal damage and subretinal detachment over time and was utilized to assay for post-injection damage and retinal degeneration (19).

Autosomal Recessive Retinal Dystrophies

Patient Phenotypes

Approximately 2 million patients worldwide are affected by retinal dystrophies (1, 92). Retinal dystrophies are inherited one of four ways: autosomal dominant, autosomal recessive, X-linked, or mitochondrially (1, 92). Autosomal recessive retinal diseases are Mendelian recessive inherited disorders caused by mutations leading to the lack of protein function that will result in cellular dysfunction and eventually cell death, which in this case will present phenotypically as vision loss. The different forms of retinal dystrophies are due to mutations in over 100 different genes (92). The patient phenotypes observed in retinopathies can be classified based on the primary cell type(s) involved. Pure rod and cone dystrophies present as congenital stationary night blindness and achromatopsia, respectively. There can also be presentation of pathogenesis first in rods and then cones, a hallmark of retinitis pigmentosa. Retinitis pigmentosa typically presents as night blindness with restricted peripheral vision followed by cone loss and a decline in visual acuity. Cone/rod diseases occur when the

cones are more affected initially. Patients will exhibit photophobia and poor visual acuity with the possibility of color blindness. For this project I will specifically focus on autosomal recessive retinitis pigmentosa.

Autosomal recessive retinitis pigmentosa onset can vary depending on the gene mutated and the age at initial vision loss ranging from infants to mid-20's or later. The initial presentation is typically night vision defects due to a loss of rod PR function with increasing loss of peripheral vision over time. Subsequent extensive loss of rods will result in tunnel vision. Subsequent cone leads to declining visual acuity, color vision defects, and eventually in some cases almost complete vision loss (1, 158, 199, 213, 225, 236). Utilizing imaging of the retinal tissue through a fundus exam, there is typically visible dark pigmented deposits, due to the loss of PR cells, optic nerve pallor, and thinning of central blood vessels (199, 213). Additional phenotypic assays that can help identify the retinal pathology include the ERG which would present as a gradual decrease in the rod response and SD-OCT which would present as a thinning of the ONL over time beginning in the periphery and gradually moving towards the fovea and might include retinal fluid accumulation (158, 213). Once the overt pathology of the patient is defined, the next step to understanding potential treatment therapies is identifying the genetic mutation(s) causing the disease. Recent advances in whole genome sequencing, along with more thorough databases of characterized retinal mutations, has allowed for more accurate gene specific treatments (11, 24, 25, 43, 44, 55, 70, 92, 118, 123, 124, 132, 150, 171, 172, 185, 186, 188, 200, 201, 212, 213, 221, 239). This also provides the patients with a somewhat more accurate disease prognosis and pattern for disease progression and allows for more appropriate patient selection

for early phase gene therapy trials (20, 29, 66, 96, 104, 108, 119, 181). Unfortunately, even if the causative mutations are known, potential available treatments are often limited due to the lack of animal models that accurately recapitulate the disease phenotype, the lack of therapeutic outcomes in animal models, or the patient's inability to qualify for a given clinical trial. There is also a concern in patients that present with very early autosomal recessive retinitis pigmentosa because, although some of the more successful treatment trials have employed gene replacement therapies, if PR cells are lost, there is no way currently to generate more in the retina (49, 50, 58, 86, 116, 118).

Current Treatment Methods for Retinal Degeneration

Current treatment modalities for retinitis pigmentosa are dependent on the age of onset and the severity of the retinal degeneration. In the most severe forms of retinitis pigmentosa, patients have lost the majority of their vision and only maintain a small fraction, if any, of their PR cells in their central retina. In these patients, INL cells may also be damaged or lost, but the primary degeneration is in PR cells. These are the most difficult to treat because there are few or no PR cells left to transduce, as PR are terminally differentiated cells that do not divide, and there are no natural retinal progenitor cells that can give rise to new PR cells (136).

The Argus II, the first commercially available prosthesis for retinitis pigmentosa, is a 6x10 grid electrode array that is surgically implanted on the surface of the retina adjacent to the GCL on the ILM with a receiving antenna that is sutured to the temporal region of the face. The external component is a transmitting antenna attached to a pair of glasses with a small video camera that will record the external environment. There is an additional video unit that will process the images received through the video camera

and transform them into an electrical signal that is sent through the antenna to initiate a focal electrical stimulation of small subsets of RGCs. This results in a vision like signal being transmitted to the brain. The Argus II clinical trial was approved by the FDA in 2013 and patients have been monitored over the course of the trial for improvement in visual task performance, SD-OCT, and a Functional Low-Vision Observer Rated Assessment. After 5 years of performance and safety validation, the patients presented with an overall improvement in quality of life. They were able to perform everyday tasks such as sidewalk tracking and direction discrimination statistically better when the system is turned on vs off. The Argus II is now the sole retinal prosthesis that is approved by the US, Canada, and Europe (58, 59, 74, 91, 174).

An alternative approach is the use of optogenetics to stimulate normally light insensitive retinal cells to respond to a light stimulus, for example turning the bipolar cells and/or RGCs into new light sensors to generate a visual response to the environment (50). Currently, optogenetics therapies have made advances in pre-clinical studies, and in August of 2016 RetroSense therapeutics enrolled 3 patients in an FDA approved Phase I/II clinical trial funded by the Foundation for Fighting Blindness. The treatment was applied as an AAV-mediated gene therapy using channelrhodopsins targeting RGCs in order to stimulate retinal activity (ClinicalTrials.gov, NCT02556736).

The most novel approach that has recently been studied is the use of stem cells to regenerate retinal cells In vivo through the injection of embryonic stem cells (ESC) and induced pluripotent stem cells (iPSC). Previously, there has been some progress in generating successful gene therapy trials for diseases of the RPE including macular degeneration and Stargardt macular dystrophy through transplanted ESCs and iPSCs

to the subretinal space between PR and the RPE (20, 86). There has also been progress made on generating large quantities of mammalian cochlea cells in culture in order to generate sufficient cells to administer for cochlear iPSC gene therapy (155). There still needs to be extensive work done to assess whether these cells can integrate accurately and efficiently into degenerated retinas and cochleas. If these organoids are able to recapitulate both cell types *in vivo*, this would be a promising treatment not only for general forms of retinitis pigmentosa, but also for the more severe forms of disease that occur at varying ages from infancy to adulthood, such as USH, since the age of onset will no longer be an issue, and because this would help to circumvent problems with gene therapy treatments for large genes.

In patients that present with later onset retinitis pigmentosa or slowly progressive retinitis pigmentosa, there are more available treatment options, especially if regions of the retina are relatively intact. Gene therapy is simply defined as the administration of a therapeutic DNA to cure a defective cell. By restoring the wild-type (WT) gene or cDNA, there is the potential to achieve a therapeutic amount of WT protein that was previously absent from the cell. Alternatively, the delivered gene of interest may act to silence a detrimental gain-of-function gene. Some of the most hopeful progress in gene therapy has been achieved for retinal diseases due to the fact that the eye is a relatively immune privileged organ that is isolated from other tissue systems and therapeutic treatment can be administered fairly easily through an intraocular injection.

There are two primary gene delivery methods for therapeutic treatments, nanoparticles that are bound to the DNA of interest and viral delivery vectors that will encapsulate the DNA of interest. These two methods can further be modified with

additional mechanisms of gene therapy once the cell type(s) of interest is/are identified (108). The initial gene therapy treatments began with non-viral gene therapy in animal models, not in humans, and employed plasmid DNAs transfecting cells at the site of injection. These can be delivered as naked plasmid DNAs through electroporation, sonication, or with the DNA bound to polymers or cationic lipids to increase cellular uptake and gene expression. Non-viral gene therapy is an interesting delivery option due to its ability to carry genes of any size and it has an extremely low immunogenicity. However, with time the DNA will be naturally degraded, or if the cells divide, the gene of interest will be diluted with each cell division. If the delivered DNA integrates into chromosomal loci it may stably persist but there is a significant risk of endogenous gene disruption or gene activation that may have deleterious consequences, including tumor initiation. Some clinical applications of non-viral delivery therapy trials include intramuscular injection of naked DNA, a melanoma cancer vaccine using cationic lipids, chronic limb ischemia, and a canine melanoma vaccine (108, 222).

There are several different types of viral vectors for gene delivery, each with its own advantages and disadvantages. The primary methods for retinitis pigmentosa treatment therapy are Adenovirus, lentivirus, and Adeno-associated virus (AAV). I will first discuss is Adenovirus vectors which are fairly widely used and have a broad range of therapeutic applications. Adenovirus is an icosahedral capsid DNA virus with a nascent DNA of 36 kb. Adenovirus is a potentially useful gene therapy delivery tool because it can package up to 38kb of DNA. The Adenovirus capsid will preferentially infect hepatocytes in the liver, but different co-factors as well as different capsid mutations allow for the virus to evade initial liver infection and allow the virus to travel

through the circulatory system to reach the tissue of interest. Adenovirus has been utilized in a broad range of treatments including multiple types of cancers and cardiovascular treatments. One of the primary complications with Adenoviral therapy is that it has a strong inherent immunogenicity and this will in turn stimulate a host immune response against the therapeutic vector construct. This has been an ongoing concern with the use of Adenovirus for clinical therapies (108).

Because Adenovirus can package very large DNA constructs it may be the best possible delivery system for some genes of interest. There have been several Adenoviral gene therapies tested in the retina, but most had low transduction efficiencies or infected the wrong cell type (108). Recently, there have been some significant advances in the optimization of the Adenoviral vector for optimal retinal delivery to the cell type of interest. For example, in 2014 Dr. Hu developed a helper-dependent adenoviral vector retinal gene therapy to deliver large DNA constructs. This new delivery system has the inverted terminal repeats necessary for DNA replication without the presence of the viral coding genes. They tested a ubiquitous CAG promoter, along with a separate construct containing the interphotoreceptor retinoid binding protein enhancer (IRBPE) in order to specifically target PR cells. This system increased the transduction efficiency which resulted in a greater number of viral particles per cell. As a result, they observed sustained expression throughout the RPE with a subretinal injection using low viral doses for at least 4 months (140). This suggests that it may be possible use Adenoviral vectors to treat the retina with larger genes, such as in USH, to develop gene therapy treatments for retinitis pigmentosa.

Lentiviral vectors are another mode of viral gene therapy which is an HIV RNA based virus that can package up to 10 kb of a therapeutic construct. Lentivirus can infect dividing and non-dividing cells and stable transfection has been demonstrated for multiple organ systems. Similar to the other viral therapies, lentivirus can be pseudo-typed to optimize for cell type specific targeting of the gene of interest. Additionally, the promoter and regulatory regions flanking the gene of interest can also modify the level of cell-type specific expression. Integration-deficient vectors have also been designed for infection in non-dividing cells, however, this is not ideal for dividing cells since, like in all cases, the gene of interest will be diluted out over time as the cell divides. As with the other two viral methods, lentivirus also poses a risk of an innate or adaptive immune response to the capsid (108, 222). Most recently in 2014 Dr. Cosgrove developed an EIAV-lentiviral vector to develop a gene therapy for Myosin7A, the causative gene for USH1B. He utilized a CMV driven Myosin7A vector with a subretinal injection. Affected mice were analyzed 1 month post-injection and they reported expression of Myosin7A in both PR and RPE cells (240). Previously, they showed that Myosin7A KO mice have a delay in transducin translocation upon exposure to light. He also showed that after short-term 6 day continuous light exposure (2500 lux) and long term cyclic light/dark exposure of medium light (1500 lux) induced significant PR degeneration in Myosin7A KO vs WT mice (176, 219). Post-EIAV-lentiviral treatment with CMV-Myosin7A revealed a significant rescue of both the transducin translocation and light damage phenotypes. They also validated the safety and tolerability in non-human primates and proved that the gene therapy was safe and well-tolerated (51, 240). This is extremely promising for the progress of large gene therapy in the retina, particularly for USH diseases.

AAV is the most prevalent method of viral gene therapy to date and has had the most clinical success, particularly in the retina. In patients that present with later onset retinitis pigmentosa, gene therapy is an available treatment option, particularly if there are relatively intact remaining regions of the retina. The eye is a relatively immune privileged organ that is isolated from other tissue systems, and therapeutic treatment can be administered fairly easily through an intraocular injection. Additionally, retinal and RPE cells are terminally differentiated, meaning that any AAV-DNA that is delivered and taken up by the retinal cells will remain within those cells for the remainder of their life since it will not become diluted out over time as the cells divide (108).

AAV is a non-pathogenic parvovirus that can infect both dividing and non-dividing cells. AAV has the smallest packaging capacity of all the viral vectors with a size of only 5kb. The AAV genome is a linear strand of DNA that consists of two reading frames containing the replication, capsid, and assembly coding genes. There are 9 or more gene products that are controlled by 3 promoters with the addition of differential splicing and alternative translation start site. Flanking these sequences are the inverted terminal repeat sequences that are necessary for packaging (66, 108, 222). The replication gene codes for 4 proteins that are involved with viral replication and packaging of the virus (Rep40, Rep52, Rep68, and Rep78). The capsid proteins form the outer surface of the viral capsid (165). There are 3 capsid proteins that are composed of two smaller proteins (VP1 and VP2) and one larger protein (VP3). These capsid proteins are in a ratio of 1:1:10, with VP3 being the most abundant. There are multiple different capsid serotypes that have been identified to date as well as multiple different capsid-serotype-specific mutations that have been identified to optimize for better cell type-specific

transduction. This will be discussed later in Chapter 5: Serotypes and modifications. The AAV constructs that are utilized for gene therapy have all of the replication and capsid genes removed so that all that remains are the inverted terminal repeat sequences for packaging and then the promoter, enhancers, and gene of interest are inserted in the middle along with a poly-adenylation sequence at the end (108). There are many studies looking at the success of AAV-mediated gene therapy in the retina and the optimization of targeting specific cell types with different capsid mutants. The early gene therapy studies in the late 1990's looked at cell-type specific transduction after subretinal and intravitreal injection as well as long term expression, stability, and toxicity (108, 222). These preliminary studies initiated the development of successful gene therapy replacement treatments for several animal models of retinitis pigmentosa.

The first most extensively studied model was for mutations in the *RPE65* gene. Part of the early success for this clinical trial was that there were both naturally occurring mouse and dog models (47, 48, 102, 115). They showed that subretinal treatment of an AAV2-CBA-RPE65 lead to increased improvement in ERG post-treatment. This was also shown with several other serotypes, and was additionally assessed in both mice and dogs (46-48, 102, 115, 117). After initial treatment in humans, it was shown that treatment mediated improved vision, however it could not altogether halt the PR degeneration over several years in patients. It was also reported that the only way to halt PR cell death in dogs was to treat prior to any onset of degeneration (27, 28, 47-49, 102). Patients have been monitored for several years with some treated patients developing the ability to utilize a "pseudo-fovea" at the sight of injection in order to gain visual acuity. This indicated that the patients were able to

undergo cortical learning in order for the brain to receive a useful visual signal where it did not previously exist (20, 46, 47, 102, 117). Similar preliminary studies have been done for other autosomal recessive retinal conditions, but so far only in animal models, particularly in LCA mouse models including aryl hydrocarbon receptor interacting protein-like 1 (Aipl1), guanylate cyclase 1 (GC1), and spermatogenesis-associated protein 7 (Spata7) (28, 30-32, 137, 244). Retinal gene therapy has also been assessed in the BBS retinitis pigmentosa mouse models which show that PR cell death and rhodopsin miss-localization can be rescued post-treatment in both BBS4 and BBS1 KO mice (42, 205, 209). Similarly, BBS AAV gene therapy has also been utilized for other organ systems including olfactory epithelia and Adenovirus gene therapy has also been used for other ciliopathy genes such as Ift88 (153, 154, 232). Some cilia genes are too large to fit in a standard AAV vector for gene therapy, and therefore other methods of delivery need to be utilized such as a dual vector AAV system to deliver large genes in two parts, allowing them to recombine in the cell. This was used for USH1B rather than a lentiviral or Adenoviral vector carrier (144). Most recently in February of 2017, it was shown that AAV-mediated delivery of USH1C can prolong auditory hair cell survival, rescue sensory transduction, and rescue the auditory brain stem response post-treatment (173). Together, these results confirm the therapeutic potential for the use of AAV as gene therapy tool, not only in the retina but several other cell types as well.

Usher Syndrome

Usher Syndrome (USH) is a recessively inherited class of diseases defined as combined hearing and vision loss due to mutations in nine known genes. Recently, it has also been shown that USH mouse models possess a defect in their odorant detection abilities as well that may also provide an additional diagnostic tool for patients

(120). USH disorders affect approximately 1/23,000 people in the US and are the cause of about 50% of combined blind-deaf patients. USH was first reported by Charles Usher in 1914 in a patient cohort (233). There are three forms of USH that are classified by the severity and age of onset of symptoms as well as additional vestibular dysfunctions.

USH1 is the earliest onset and is the most severe. It presents with severe bilateral hearing loss at birth and children are either born completely deaf or will present with profound hearing loss by one year of age. USH1 patients also present with extensive vestibular dysfunction in addition to hearing loss and often have delays in motor development (236). Retinitis pigmentosa in USH1 patients presents very early in childhood and first displays as tunnel vision along with decreased visual acuity followed by rapid vision loss (10, 158, 233, 236). USH1 is known to be caused by five known genes. USH1B is caused by mutations in the Myosin7A (MYO7A) gene. MYO7A mutations are the most prevalent of all USH mutations resulting in ~50% of all USH cases based on the genetic population. MYO7A is an actin-based motor domain protein that is a non-conventional myosin. It is composed of a motor head domain, two FERM (F for 4.1 protein, E for ezrin, R for radixin, and M for moesin) domains, two MyTh4 domains, five IQ calmodulin-binding motifs, and a Src homology 3 (SH3) domain (192). USH1C is caused by mutations in the harmonin gene. USH1C is the most prevalent mutation among the Acadian population in Louisiana (236). Harmonin is a scaffolding protein that has three isoforms. All isoforms contain two PDZ (Post-synaptic density 95 (PSD95), disc large, ZO1 proteins) domains, class A and B isoforms contain an additional PDZ domain and class B isoforms also have a 2nd coil-coil domain (192). USH1D and UDH1E are caused by mutations either in the cadherin 23 (Cdh23) or

protocadherin 15 (Pch15) genes, both cadherin-related proteins. Cadherin proteins are very large calcium dependent single-pass transmembrane cell adhesion proteins that are indirectly connected to the actin cytoskeleton through their C-terminal PDZ binding motif (192). Recently, M. Zallocchi has shown that Pch15 functionally interacts with the USH3A protein CLARIN1 (CLRN1) in zebrafish cochlear hair cells via immuno-precipitation and the fact that Pch15 is mislocalized when the C-terminus of Clrn1 is deleted (169). Finally, USH1F is caused by mutations in the SANS gene which encodes a scaffolding protein (10). Sans contains three Ankyrin domains with a CT PDZ binding motif (192, 236). In addition to USH1 proteins being present in PRs and cochlear hair cells, it has recently been reported that harmonin, SANS, Cdh23, and Pch15 are all present in olfactory sensory neurons at both the mRNA and protein levels (120).

USH2 patients are characterized by the age of onset of hearing loss in their early teens, although some can present earlier on in life or in their adolescence, and hearing loss tends to be stable throughout the patients' life with no known vestibular dysfunction. Retinitis pigmentosa also arises later in USH2 patients and usually is not diagnosed until after puberty (158). Interestingly, it has been shown that USH2 patients also present with a significant reduction in choroidal thickness that is correlated with age (52). It has been shown that in retinitis pigmentosa patients there can be altered choroidal blood flow which could provide additional confounding variables with disease progression (141). This is significant because analyzing choroidal thickness may also help to provide an additional monitor for disease progression and help researchers to understand more about the disease mechanism. USH2 is known to be caused by three genes. USH2A patients carry mutations in the gene usherin which causes between 50-

90% of USH2 cases depending on the genetic population. There appears to be a founder effect in the French-Canadian population, accounting for approximately 50% of the USH2A cases with a secondary founder population of European origin accounting for approximately 15-45% of all mutated alleles (158). There are two isoforms of usherin, the short isoform is a laminin type EGF (epidermal growth factor) - like protein with 4 fibronectin domains. The long isoform is a transmembrane protein with a C-terminal protein binding motif (192, 236). USH2C is caused by mutations in the VLGR1 (very large G-protein coupled receptor) gene, which is the largest of all USH genes. VLGR1 is a seven transmembrane Ca2+ exchanger that only appears to account for a small percentage of USH2 cases at 3-6% of patients (158, 236). VLGR1 is believed to play a role of adhesion in the synaptic membranes and assist in G-protein signaling during synaptogenesis (192). USH2D is caused by mutations in the whirlin gene and is a proline-rich protein with 3 PDZ domains. Whirlin mutations appear to be extremely rare compared to other USH mutations (10, 158, 236). Similar to the USH1 proteins, the USH2 proteins usherin and Vlgr1 have also been reported to be present in olfactory sensory neurons at both the mRNA and protein levels (120).

USH3A is the latest onset of all the USH disorders and is caused by mutations in only one gene to date, Clarin1 (*CLRN1*/CLRN1). USH3A is the least prevalent of all USH forms but mutations in *CLRN1* are mostly seen among the Finnish and Ashkenazi Jewish populations which accounts for more than 40% of patients due to a strong founder effect in both cohorts. USH3A patients present with progressive retinitis pigmentosa in their 20’s to 30’s (131, 239). Affected patients will experience progressive tunnel vision and reduced visual acuity over time. Different from the other types of USH,

USH3A hearing loss will present between the 1st and 2nd decade of life, but will become profound over time (171, 172, 239). This is unique compared to USH1 and 2 because hearing loss in USH3A presents post-lingually and allows for patients to develop fairly normal speech abilities. This also suggests that USH3A may be the most detrimental in terms of patient quality of life because patients are born with normal hearing and vision, but progressively lose both senses later in life (10, 158, 185, 186, 225). Patients show a significant level of visual field loss and analysis of patient retinas by ERG show definitive PR dysfunction, with a greater deficit in rod function than in cones, and their fundus exams show significant retinitis pigmentosa phenotypes in the peripheral retina. Upon SD-OCT analysis, the ONL was significantly thinner than the standard thickness and the IS/OS band was disrupted within 4 degrees of the fovea (189). As stated previously, there is currently no treatment for retinitis pigmentosa in USH3A patients, however many patients have received cochlear implants. Those patients with cochlear implants show a significant improvement in hearing and also showed a significant improvement in word recognition post-treatment (183, 185).

CLRN1 is a tetraspanin TM protein with 3 isoforms. The main isoform contains an N48 glycosylation residue with a proposed PDZ binding motif on the intracellular C-terminus (4, 132, 192, 218, 241). The true function of CLRN1 is unknown but it is believed to localize at the CC, kinocilia, and stereocilia as other USH proteins (53, 146, 241). Although the other USH proteins were recently shown to be expressed in the olfactory epithelium, there is no evidence as of yet whether there is any CLRN1 expression as well. Clrn1/CLRN1 will be discussed in Chapter 3 background.

Usher Interactome

The USH proteins are believed to functionally interact with each other along the stereocilia and kinocilia in the inner ear and along the CC, calyceal processes, and incisures in PR cells (5, 198). Each of the proteins in this network have different functions that provide membrane-membrane connections, scaffolding proteins for structural maintenance, and motor proteins that allow for the movement of cargos. MYO7A is the only known motor protein associated with this functional network and has been shown to interact with harmonin and whirlin to connect the USH interactome to the intracellular actin cytoskeleton (135, 147, 192). MYO7A has also been shown to directly interact with Pch15 in the inner hair cells (204) with additional protein-protein specific interactions between the C-terminal PDZ binding motif in SANS to the PDZ domains in whirlin (3, 5, 35, 135, 147, 170, 191, 192, 229). Of all the USH proteins, CLRN1 is the only protein that has not yet been conclusively linked to the interactome. As stated previously, recent studies showed that the C-terminal domain of Clrn1 functionally interacts with Pch15 in zebrafish neuromast hair cells and this interaction is essential for Pch15 incorporation into cochlear hair cell bundles and its proper localization at the tip links of stereocilia. Interestingly, a Pch15 deletion did not alter Clrn1 localization suggesting that Clrn1 is required for proper Pch15 localization and function but that Clrn1 can localize independently of Pch15 (146, 169). Clrn1 was also found to be essential for the hair cell synaptic ribbon arrangement. *Clrn1* zebrafish morpholinos displayed a definitive increase of synaptic ribeye puncta and an increase in puncta mislocalization. This phenotype could be rescued with the full-length *Clrn1*, however, the C-terminal deletion of Clrn1 did not. This indicates the C-terminus is required for proper ribeye localization at the ribbon synapses as well as for synaptic formation (169).

Furthermore, Clrn1 was shown to be required for normal vesicle recycling at the ribbon synapses and the C-terminus was not required for proper vesicle recycling (169). The USH interactome proteins are also linked to other ciliopathy proteins including Cep290, RPGR, RPGRIP1, lebercilin, and BBS6. In particular, SANS has been shown to directly interact with Cep290 (211). The defects in Clrn1 vesicle recycling was also assessed using a rab11a/b cilia marker for trafficking and it was shown that Clrn1 was required for accumulation of rab11a/b at the apical pole in inner hair cells (169).

Given that this interactome is present in both cochlear hair cells and PR cells, its functions appear to be cell-type specific, although little information relates to the function of USH proteins in olfactory neurons (120). In the cochlea, this interactome is believed to play a role in sensing sound waves through cilia bending and interactions at the tip and lateral links on the inner ear stereocilia (5, 54). When the tympanic membrane senses a sound it relays a vibration that is sent through the fluid matrix in the cochlea, and the stereocilia will bend in response to fluid movement. The USH interactome proteins are believed to activate when the stereocilia move, relaying the signal into the cell and results in neurotransmitter release at the cellular synapses (23, 148). Additionally, harmonin functionally acts as a scaffold for ion channel complexes at the ribbon synapses in order to regulate Ca2+ signaling and electrical signaling at inner hair cell synapses (84, 147, 211). In PR cells, the USH interactome functions as an adhesion complex along the CC, periciliary membrane, and the calyceal processes (54, 158, 199). As mentioned previously, they are present in frogs, birds, and primates but are lacking in mice. They are believed to act as stabilizers of the OS, and USH proteins help facilitate OS disc formation and biogenesis (148, 211).

Usher Syndrome Animal Models

Many of the naturally occurring mouse models display a distinctive behavior of head-tossing and circling around themselves. This is believed to be a consequence of inner ear vestibular dysfunction and abnormal balance issues. This behavior seems to be restricted to the USH1 mutations, however there is one model for USH2 that does, indicating that some USH2 patients could perhaps have mild vestibular problems. A commonality of all USH mouse models is that they present with definitive inner ear defects, having a loss of stereocilia and kinocilia that result in hearing loss. However, they have very mild, if any, retinal phenotypes that have been extremely difficult to characterize (233). Although there does not appear to be any structural abnormalities in the retina, there is a reduced a- and b-wave ERG in some of the USH1 and 2 mouse models. A mouse model for USH1C shows mild peripheral degeneration and USH2D mice have shortened PR OS (237). MYO7A KO mice have an accumulation of rhodopsin in their OS and their RPE have an abnormal accumulation of melanosomes (51, 144). Currently, the only USH mouse model that has been reported to have measurable PR loss is an USH2A mouse which loses approximately 50% of PR by 2 years of age (233). Recently, in a new USH3A mouse model, Y. Imanishi has reported a slight decrease in b-wave ERG at 7 months of age, but as the WT animals age, their ERG will drop to KO levels at 9 months of age (217). This late onset loss of function is believed to be a result of abnormal RPE function in this mouse strain as well as an increase in inflammation (160). There are also some additional retinal phenotypes of delayed phototransduction protein localization upon exposure to light. This has been seen in mouse models for all three forms of USH (72, 176, 219, 220). The USH3A mouse models and phenotypes will be discussed further in Chapter 3 and 4.

Recently, several zebrafish morpholino models have also been generated in order to attempt to identify additional retinal phenotypes as well as study USH protein localization and function in a model organism. Zebrafish have a much shorter developmental time frame and their retinas are more cone-dominant, making them relatively more similar to a primate retina than a mouse. They are also diurnal and more dependent on visual processing (22). Zebrafish are a good model to test a potential for a gene therapy treatment because the zebrafish retina can also regenerate PR cells *in vivo* (22). There are currently zebrafish models for all three USH syndromes and successful therapeutic treatments have been of recent growing interest in these models in order to validate the effectiveness of treatments.

CHAPTER 2
OVERVIEW, RATIONALE, AND SPECIFIC AIMS

USH retinal diseases are caused by a group of autosomal recessive genetic disorders that present with combined hearing and vision loss in patients. The three classifications of USH account for 50% of combined blindness/deafness in humans and affects 1/25,000 children worldwide (10, 23, 135, 199, 233, 236). The three USH types are clinically differentiated by the age of onset and the mutated gene involved (23, 135, 236). USH3A is the slowest onset of the USH sub-types and is therefore the most promising target for treatment. Current treatments for USH3A are costly and limited only to hearing defects utilizing hearing and vision aids, cochlear implants being the most effective. In USH3A, hearing loss results from the loss of function of vestibular cochlear cells in the inner ear, whereas vision loss and progressive night blindness is caused by a loss of PR cells in the retina and is characterized clinically as retinitis pigmentosa (20, 107, 171, 172, 183, 185, 186, 189, 192). USH3A is caused by mutations in the *Clrn1* gene, which encodes a 232-amino acid four transmembrane domain protein of unknown function. Its pattern of endogenous expression in the retina remains unclear. It has been shown that Clrn1 contains an N48 glycosylation and PDZ domains which are likely responsible for proper protein localization and facilitation of its interaction with other USH proteins. The USH proteins are localized to photoreceptor IS, CC, ONL and PR/ bipolar cell synapses in the OPL, as well as to the kinocilium and stereocilia bundle of cochlear cells in the inner ear (3-6, 8-10, 14, 17, 23, 35, 53, 54, 68, 69, 88, 89, 93, 94, 105, 107, 114, 117, 131, 135, 138, 139, 142, 147-149, 152, 158, 169, 172, 178, 191-194, 198, 199, 204, 211, 217, 233, 237, 241, 242). The retinal location of *Clrn1*/Clrn1 remains controversial because previous localization data is conflicting depending on the

assay performed. (4, 87-89, 114, 182, 218, 241) A primary difficulty with regard to understanding USH3A function is that no current animal models fully recapitulate patient phenotypes. The genetically engineered models, N48K knock-in (KI) and *Clrn1* knock-out (KO) (Clrn1 $^{-/-}$) mice, described to date present with a hearing loss phenotype while their retinas appear morphologically and functionally normal based on histology, OCT, and ERG analysis (87-89, 218). In order to develop an effective treatment for USH3A, a preclinical animal model is required that more accurately mimics the patient phenotype because there is currently no restorative retinal therapy for Usher patients. Therefore, uncovering a retinal phenotype in available USH3A mouse models and determining the endogenous localization of *Clrn1*/Clrn1 in the retina are crucial for the development of clinical therapies. The aims of my study are to define an USH3A mouse retinal phenotype, identify the endogenous retinal location of Clrn1, and successfully rescue an identified retinal phenotype using AAV-mediated gene therapy.

Aim 1: Identify endogenous Clarin-1/CLARIN-1 expression in the retina.

- Hypothesis: *Clrn1*/Clrn1 is expressed in photoreceptor cells and its N48 glycosylation and PDZ binding domain are responsible for proper localization.
- Objective 1.1: Document *Clrn1*/Clrn1 retinal expression and localization in the presence or absence of photoreceptors.
- Objective 1.2: Identify endogenous Clrn1 localization by immunohistochemical (IHC) analysis employing new CLRN1 antibodies in mouse retinal tissue.
- Objective 1.3: Document Clrn1 subcellular localization when N48 glycosylation is absent.

Aim 2: Identify a retinal phenotype in N48K Knock-in (KI) (N48K) and Clarin-1 Knock-out (KO) (Clrn1 $^{-/-}$) mice.

- Hypothesis: There is a subtle but quantifiable visual phenotype in the USH3A mouse models.

- Objective 2.1: Perform light-driven protein translocation experiments in mice containing the *Clrn1* $^{-/-}$ KO or N48K KI mutation to characterize a retinal phenotype.

- Objective 2.2: Replicate the identified decreased b-wave phenotype in the new A/J mouse strain.

- Objective 2.3: Perform prolonged light exposure experiments and light damage experiments in *Clrn1* $^{-/-}$ KO or N48K KI mice to characterize a retinal phenotype and potentially induce degeneration compared to wild-type mice.

- Objective 2.4: Perform novel ERG methods using light exposure prior to ERG in order to characterize a retinal phenotype in *Clrn1* $^{-/-}$ KO or N48K KI mice.

Aim 3: Identify the optimal AAV gene construct, capsid serotype, and delivery method for Clarin-1 gene therapy treatment and assay for phenotypic rescue using AAV mediated gene therapy.

- Hypothesis: Clrn1 needs to be expressed at optimal levels by the correct cell type in order to develop a successful gene therapy treatment that can restore the previously defined phenotype through AAV-mediated gene therapy.

- Objective 3.1: Assess CLRN1 localization following AAV-injection containing human *CLRN1*.

- Objective 3.2: Optimize vector capsid, promoter, and titer for *CLRN1*/CLRN1 safe and effective AAV gene therapy treatment.

- Objective 3.3: Determine if exogenously-expressed *CLRN1*/CLRN1 can rescue the phenotypes previously described in Aim 2 *Clrn1* $^{-/-}$ KO or N48K KI mice.

CHAPTER 3
IDENTIFYING WHERE ENDOGENOUS CLARIN-1 RNA AND PROTEIN IS EXPRESSED IN THE RETINA

Background

It has been established that the majority of USH proteins localize to the CC and calyceal processes in PR cells and at the kinocilia and stereocilia bundle in cochlear hair cells (3, 147, 192, 198). As mentioned previously, many USH proteins contain PDZ domains, PDZ binding motifs, as well as transmembrane components, all of which have been proposed to link the USH interactome to the intracellular cytoskeletal network through macromolecular complexes (3, 135, 211). As of yet USH3A is the only USH protein that has not been definitively linked to the USH interactome.

USH3A is caused by mutations in the *Clrn1* gene which consists of 4 exons. There are 3 proposed protein-coding transcripts in the retina: isoform 1 containing exons 1, 3 and 4 which is the 232 aa isoform that is 26 kilo-Daltons (kDa) and is believed to be the primary variant, isoform 2 containing all exons 1-4 which is the 250 aa isoform, and isoform 3 containing exons 1 and 4, the smallest isoform at 180 aa (Ensemble: Isoform 1: Clrn1-201 ENSMUST00000051408.7, Isoform 2: Clrn1-202 ENSMUST00000055636.12, isoform 3 Clrn1-203 ENSMUST00000072551.6). It is unclear if all three isoforms are expressed in the retina or not, and if so, which retinal layers are expressing which isoform. Isoforms 1 and 2 are thought to contain four transmembrane domains and isoform 3 contains only two, with intracellular N- and C-terminal ends (4).The main variant codes for a tetraspanin transmembrane protein with an extracellular glycosylation residue on Asparagine (N)-48 (218). This transmembrane tetraspanin structure has been supported through recent 3D protein modeling utilizing multiple different software for protein domain analysis as well as I-TASSER for final

structure prediction (132). The most common patient mutation in the US is a loss of this N48 glycosylation, which is believed to render the protein non-functional and target it for degradation (114). Cell culture experiments looking at multiple mutations, including those in transmembrane-1, transmembrane-3, and the N48 loss of glycosylation (N48K), show that WT Clrn1 localizes to the plasma membrane and the mutant Clrn1 localizes almost completely with the ER (107, 114, 218). In addition to its glycosylation, Clrn1 also contains a PDZ binding domain on its intracellular C-terminal tail that may facilitate its interactions with other transmembrane proteins (100, 101, 146). *In vivo*, Clrn1 has been proposed to be associated with the ribbon synapses, CC, kinocilia, stereocilia bundle, and the cellular cytoskeleton in both PR and cochlear hair cells (87-89, 93, 182, 218, 241, 242). Functionally, Clrn1 was reported to be essential for the development, neuronal activation, and synaptic maturation of cochlear hair cells (87, 88, 241, 242). Because Clrn1's localization pattern and functional significance in cochlear hair cells is similar to other USH proteins, this suggests that Clrn1 also belongs to the USH protein network in both the hair cells and photoreceptors (3, 135, 198, 211, 241).

Due to conflicting results depending on the assay performed, the precise retinal localization of *Clrn1*/Clrn1 has not been conclusively established (53, 169, 182, 241). One group utilizing retinal transcriptome analysis reported *Clrn1* expression only in starburst amacrine cells (207). Dr. Flannery's group analyzed *Clrn1* mRNA expression in the retina by *in situ* hybridization, followed by laser-capture microdissection and RT-PCR. They reported that *Clrn1* mRNA was expressed throughout development and was absent at adulthood. cDNA analysis indicated that the transcript detected corresponded to isoform 1 (232 aa variant) and 3 (150 aa variant) and do not mention isoform 2 (250

aa variant) even though their RT-PCR gel shows a faint product for that isoform (Geller figure 1) (Figure 3-1) (87). *Clrn1* appears throughout the embryo, head, and brain during development as well as in the retina. They further observed *Clrn1* in multiple brain tissues, however, for all of these assays they used primers in exon 3 and 4, with no way to distinguish whether the isoform 2 (250 aa variant) is expressed in addition to isoform 1 (232 aa variant) because these primers would amplify both transcripts (Geller et al figure 1) (87). *In situ* hybridization showed mRNA expression in the INL and not in PR cells in WT fetal retinas, but no mRNA expression was observed in KO mice, and *Clrn1* expression declined to no transcript by adulthood (Geller figure 2) (87). Laser capture dissection showed *Clrn1* in the INL using isoform 1 primers (232 aa variant), and they suggest *Clrn1* is only expressed by retinal Müller glial cells (Geller figure 5) (87). This group also generated the first *Clrn1* KO mouse through loxP-Cre-excision of exon 1 containing part of the 5' UTR and the ATG start codon. A difficulty with this mouse model is the genotype for a *Clrn1* $^{-/-}$ is the lack of a PCR product, which creates the possibility that a heterozygote mouse could be mistakenly genotyped as a KO due to a failed PCR reaction (87). They further tested a novel antibody generated against human CLRN1 and saw identical staining in WT and KO retinas; however, they do not test this antibody in cochlear tissue. Another group looked at laser capture microdissection in the mouse cochlea and reported the highest level of *Clrn1* expression in the spiral ganglion cell region, similar to all the other USH proteins they tested (166).

In another study, Dr. Zallocchi and colleagues developed another novel CLRN1 human polyclonal antibody that recognized all CLRN1 isoforms and they report labeling at the stereocilia and synapses of inner hair cells and the CC and ribbon synapses in

PR cells (241). One difference between their methods and the methods of others was that they did not utilize any fixative prior to sectioning and staining which may help to preserve the antibody epitope better than if the samples are fixated prior to analysis. Dr. Zallocchi and colleagues provided a supplemental appendix demonstrating the specificity of their antibody by reporting no staining in their *Clrn1* $^{-/-}$ KO mouse model (53). When *Clrn1* expression was assessed via RT-PCR, they observed products only for what they reference as isoforms 2 (232aa variant) and 3 (180aa variant), which correspond to isoforms 1 (232 aa variant) and 3 (180aa variant) in Ensembl, respectively. They further showed that only one isoform (232 aa variant) was observed via western blotting. Their subcellular localization in both inner hair cells and photoreceptors coincides with the localization of all other USH proteins at the stereocilia, kinocilia, and ribbon synapses in the inner ear as well as the CC and calyceal processes in PR cells (198). Given these similarities, I hypothesized that *Clrn1*/Clrn1 is indeed expressed in PR cells and that the optimal therapeutic vectors should be targeted for PR cells in the retina. This will be discussed in Chapter 5.

Due to the phenotypic and biochemical inconsistencies with the current mouse models, a few groups have utilized zebrafish for a model organism to better recapitulate the retinal phenotypes of USH in patients. In zebrafish *Clrn1* has been observed from embryo through adulthood in both the cochlea and retina. Zebrafish *in situ* analysis shows *Clrn1* in hair and supporting cells in the ear and PR and INL cells in the retina (93, 169, 182). In zebrafish, Dr. Phillips and colleagues reported *in situ* hybridization of Clrn1 in sensorineuronal cells with weak expression in the brain, retina, and inner ear. In the retina, both ONL and INL cells contained *Clrn1* transcripts. Interestingly, Clrn1

INL staining was present at embryonic stages and restricted to amacrine cells in adult fish, similar to the Dr. Geller et al. paper; however ONL Clrn1 expression was present at all ages (182). They made a custom antibody for zebrafish Clrn1, targeting the 1st extracellular loop containing the N48 glycosylation. They transfected embryos with a *Clrn1*-HA tagged construct and looked for colocalization of an anti-HA antibody with their Clrn1 antibody. They showed Clrn1 localization at the synapses and apical cell body of inner hair cells with no staining in the stereocilia. In the retina, Clrn1 was expressed in the INL basal portion where amacrine cells reside as well as in the ONL and GCL. Furthermore, they saw significant Clrn1 expression at the OLM as well as the OPL and partial co-localization with Müller cells at the OLM and INL. In the adult retina they observed additional Clrn1 staining at cell-cell contacts between rod and cone PR cells (182). A second zebrafish study utilized a Novus Biologicals (NB)-rabbit-anti-human-CLRN1 antibody and they observed Clrn1 localization at the cochlear hair cell bundle where it colocalized with F-actin and they observed no Clrn1 antibody staining in the KO morpholinos (93). This is significant because it shows Clrn1 localization at the cochlear hair bundles and that their commercial antibody is specific for Clrn1. This also provides further evidence that Clrn1 has an overall localization pattern similar to all other USH proteins. The only complication with this study is that morpholino treated zebrafish retinas possessed a normal ERG response compared to WT fish (93).

A primary complication with studying USH3A mouse models is that the mice exhibit extensive hearing loss by 4 months of age but do not develop any previously defined retinal phenotype (87-89, 93). Additionally, *Clrn1* $^{-/-}$ KO mice display a characteristic circling behavior by 6 months of age. As mentioned above, some studies

claim *Clrn1*/Clrn1 is expressed in the inner retina, whereas others claim *Clrn1*/Clrn1 is in photoreceptor cells (53, 87, 88, 241). An additional complication is that the *Clrn1* $^{-/-}$ KO mice may potentially still express an isoform of *Clrn1*/Clrn1 because the previous antibody stained both WT and KO retinas (87, 88). There are 11 proposed *Clrn1* mRNA splice variants predicted to produce protein products, and there are three known Clrn1 isoforms thought to be expressed in the retina, but it is unclear which retinal layer or cell type is producing which isoform (4, 226). Due to the disagreements among the previously published data, it is critical to identify the endogenous retinal localization of *Clrn1*/Clrn1 in order to develop a successful gene therapy treatment for USH3A.

As noted above, *Clrn1* $^{-/-}$ KO and N48K KI mice were also generated on both the CBA/J and A/J backgrounds. CBA/J mice carry a mutation in phosphodiesterase PDE6B that causes a complete loss of photoreceptors by 3 months of age (rd1 mutation) (43). By utilizing these mice, I could determine if *Clrn1* is expressed in PR cells and which isoforms of Clrn1 are removed in *Clrn1* $^{-/-}$; rd1 $^{-/-}$ double KO mice.

The second strain of A/J mice additionally carry an Usher Syndrome Type 1D mutation in Cadherin 23 (Cdh23) that causes hearing loss, but no clear retinal phenotype (7, 26, 69, 70, 129, 138, 139, 142, 167, 201, 208, 243). Cdh23 was shown to interact with the Usher Syndrome Type 1B gene (USH1B) Myosin 7A, and is a glycosylated protein with a C-terminal PDZ-binding motif involved in mediating cell-cell contacts and calcium-dependent interactions (7, 10, 26, 69, 70, 129, 138, 139, 142, 201, 208). These mice were used to compare *Clrn1* $^{-/-}$; *Cdh23* $^{-/-}$ and *Clrn1* $^{+/+}$; *Cdh23* $^{-/-}$ mice in the context of a secondary USH mutation to potentially induce a retinal phenotype and perhaps identify potential interacting partners of Clrn1. Additionally, the

A/J strain has a smaller ERG amplitude than control C57BL/6J mice and they lose significant ERG amplitude over time (Figure 4-7, 4-8) (160, 217). A/J WT mice also undergo significant loss of ONL nuclei over time compared to C57BL/6J mice. This retinal degeneration in A/J mice suggests that their retinas 'age' much faster than other strains (160). This could potentially reveal an ERG phenotype due to the accelerated aging process. This will be discussed in Chapter 4. Overall, my experimental plan is aimed to determine whether *Clrn1*/Clrn1 is expressed in inner retina, outer retina, or both and identify potential interacting partners. I therefore documented mRNA and protein expression using RT-PCR, immunohistochemistry, and western blot analysis in all 3 mouse strains and the results are discussed below. Not all data was acquired for all strains because not all strains were available throughout the course of this work. However, the strain for each result is defined with each data set.

Methods

RT-PCR

The Dr. Flannery mixed albino C57BL/6J strain *Clrn1* $^{-/-}$ KO mice, the Dr. Imanishi A/J albino strain *Clrn1* $^{-/-}$ KO mice, and the Dr. Imanishi CBA/J strain *Clrn1* $^{-/-}$ KO mice were used for RT-PCR experiments (87, 88). Mice were euthanized with dual CO_2/cervical dislocation, retinas were dissected out, and RNA was isolated using a Trizol phenol chloroform method (Life Technologies, Trizol Reagent #15596026). Samples were processed according to the published protocol (https://tools.thermofisher.com/content/sfs/manuals/trizol_reagent.pdf) and all centrifuge spins were performed at 16,000 x g for 1 hour. RNA for RT-PCR was converted to cDNA using a Bio-Rad iScript cDNA Synthesis Kit (Bio-Rad #170-8891, http://www.bio-rad.com/webroot/web/pdf/lsr/literature/ 4106228C.pdf) at a maximum concentration of 1ug total RNA and RNA for

qRT-PCR experiments was processed using a Bio-Rad iScript Reverse Transcription Supermix for RT-qPCR (Bio-Rad #1708841, http://www.bio-rad.com/en-us/product/iscript-reverse-transcription-supermix-for-rt-qpcr) at a max concentration of 1ug total RNA. Primers for RT-PCRs were based on previously published data (Table 3-1) (87). Primer positions are defined in Figure 3-1A. All isoforms are based on NCBI-Ensembl accession numbers. Isoform 1 is exons 1, 3, and 4 (ENSMUST00000051408.7) the 232 aa isoform, Isoform 2 is exons 1-4 (ENSMUST00000055636.12) the 250 aa isoform, and Isoform 3 is exons 1 and 4 (ENSMUST00000072551.6) the 180 aa isoform and the predicted RT-PCR product sizes were obtained through alignment of the published primers to the NCBI reference sequences in Vector-NTI (Figure 3-1B).

Previously, Dr. Hauswirth's group has tested novel AAV2 serotype capsid mutations that allow for better transduction efficiency in the retina. I utilized the construct that had the best expression in PR cells in the retina, which was an AAV2 quadruple mutant. The AAV2 Quadruple mutant contains 4 tyrosine to phenylalanine mutations at residues Y-F 272, 444, 500, and 730 (AAV2-Quad). The AAV vector was produced and optimized as described previously (65, 71, 82, 83, 103, 128, 134, 179, 180, 197, 245). C57BL/6J mice along with A/J WT and *Clrn1* $^{-/-}$ KO mice were then injected subretinally with AAV2-Quad-Y-F-sc-smCBA-h*CLRN1*-HA at 8.43 x 10^{12} vg/ml (Table 5.1 construct 1) as described previously (128, 181, 182, 199). These mice were analyzed 1 month post-injection by RT-PCR as described above.

Immunohistochemistry

Mice were utilized from both strains described above and mice were housed as described above (87, 88, 217). C57BL/6J control mice were utilized for initial antigen retrieval and antibody staining optimization. All mice were housed in a 12 hour dim-

light/dark cycle and were euthanized as described above. Eyes were incubated in 4% paraformaldehyde (PFA) fixative for 1 hour prior to moving to a 1x phosphate buffered saline (PBS) solution. For paraffin sections, eyes were embedded using a paraffin processor (RMC Ventana Tissue Processor PTP 1530) and sectioned at a thickness of 4 um for all samples. For cryosections, eyes were incubated in 30% sucrose until saturated and then embedded in O.C.T. (Optimal Cutting Temperature) compound (Fisher Scientific Healthcare Tissue Plus O.C.T. compound 23-730-571) and sectioned on a Leica Cryostat (Leica CM 1900 Cryostat) at 12 um per section for all samples.

For paraffin immunostaining, antigen retrieval was optimized beginning with base protocols and combinations of protocols found in Fabio D'Amico et al, 2009 (57). The final optimized paraffin protocol is as follows: Prior to any treatment the slides were incubated in a dry incubator lying flat at 60^{o}C for 1 hour. The tissue sections were then de-paraffinized either with Histoclear II (National Diagnostics Inc. HS 202) or Xylenes (C8H10 X3P 3875 Fisher Scientific). Tissue sections were rehydrated with dilutions beginning with 100%, 95%, 90%, 80%, and 70% ethanol for 3 minutes each, followed by 1x PBS. Slides were then incubated with a Protinase K solution at a concentration of 10 mg/ml for 10 minutes at 37^{o}C then washed 3 times, followed by incubation in 0.5% Saponin for 20 min at room temperature and washed again 3 times in PBS. Slides were serum blocked with 1% bovine serum albumin (BSA) for 1 hour and incubated with primary antibody in 0.5% BSA overnight at RT. Primary antibodies are as follows: Novus Biologicals rabbit-anti-CLRN1 (NB-CLRN1) 1:2000 dilution (NBP69142), mouse-anti-Gamma Tubulin 1:1000 dilution (Thermo Scientific Pierce MA1-850), mouse-anti-arrestin-1 1:100 dilution (courtesy of Dr. WC Smith, C10C10) (73), mouse-anti-

rhodopsin 1:100 dilution (courtesy of Dr. WC Smith, B6-30) (2), and mouse-anti-GFP 1:100 dilution (Invitrogen A11121). The second day slides were washed 3 times in PBS and stained with the following secondary antibodies for 2 hours at a dilution of 1:400: goat-anti-rabbit 488 (A11008), goat anti-rabbit 594 (A11012), goat-anti-mouse 488 (A32723), goat-anti-mouse 594 (A11005), donkey-anti-rabbit 488 (A21206), donkey anti-rabbit 594 (A21207), donkey-anti-mouse 488 (A21202), and donkey-anti-mouse 594 (A21203). Secondary antibodies were acquired from Molecular Probes/Invitrogen, Eugene, OR. Lastly, slides were rinsed 3 times in 1x PBS and mounted with VectaShield containing DAPI (Vector Laboratories H1200). Sections were analyzed using a spinning disc confocal microscope at the University of Florida Cell and Tissue Analysis Core (Olympus DSU-IX81). Images were acquired with 10-15 confocal z-stacks and images were consecutively de-convolved and merged into a single projection image and each individual color channel was saved separately and merged.

Cryosections were stained with the following protocol: Tissue sections were air-dried at room temperature for 30 min prior to staining. Sections were consecutively incubated in PBS for 5 minutes, followed by incubation in 0.5% Saponin or Triton X-100 for 20 min at room temperature and washed again 3 times in PBS. Slides were then serum blocked with 1% BSA for 1 hour and then incubated with primary antibody in 0.5% BSA overnight at RT. Primary antibodies are as follows: NB-CLRN1 1:2000 dilution (NBP69142) and mouse-anti-rhodopsin 1:100 dilution (courtesy of Dr. WC Smith, B6-30) (2). The second day slides were washed 3 times in 1x PBS and stained with the following secondary antibodies for 2 hours at a dilution of 1:400: goat-anti-rabbit 488 (A11008) and goat-anti-mouse 594 (A11005) (Molecular Probes/Invitrogen,

Eugene, OR). Lastly, slides were rinsed 3 times in 1x PBS and mounted with VectaShield containing DAPI (Vector Laboratories H1200). Sections were analyzed using a spinning disc confocal microscope in the Cell and Tissue Analysis Core at the University of Florida (Olympus DSU-IX81). Images were acquired with 10-15 confocal z-stacks and images were consecutively de-convolved and merged into a single projection image and each individual color channel was saved separately and merged.

For the C57Bl/6J mice that were AAV treated for co-staining with the NB-CLRN antibody, the AAV vector was produced and optimized as described previously (65, 71, 82, 83, 103, 128, 134, 179, 180, 197, 245). These mice were then injected subretinally with AAV2-Quad-Y-F-sc-smCBA-h*CLRN1*-Venus at 1.54 x 10^{12} vg/ml (Table 5.1 construct 3) or intravitreally with AAV2-Quad-Y-F-sc-smCBA-h*CLRN1*-Venus at 1.54 x 10^{12} vg/ml (Table 5.1 construct 4) that both contain a Venus-GFP protein analog with the previously described methods (179, 180). Mice were euthanized, and sections were obtained and analyzed 1 month post-injection by paraffin immunohistochemistry as described above. Sections were stained with primary antibodies: NB-CLRN1 1:2000 dilution (NBP69142) and mouse-anti-GFP 1:100 dilution (Invitrogen A11121). Secondary antibodies were goat anti-rabbit 594 (A11012) and goat-anti-mouse 488 (A32723) (Molecular Probes/Invitrogen, Eugene, OR). Lastly, slides were rinsed 3 times in 1x PBS and mounted with VectaShield containing DAPI (Vector Laboratories H1200). Sections were analyzed using a spinning disc confocal microscope through the Cell and Tissue Analysis Core at the University of Florida (Olympus DSU-IX81). Images were acquired with 10-15 confocal z-stacks and images were de-convolved and merged into a single projection image and each color channel was saved separately and merged.

Western Blot Analysis

Mice from both strains described above were housed and euthanized as described above (87, 88, 217). C57BL/6J control mice were utilized for initial antibody staining optimization. Eyes were dissected as eye-cups, retinas, and remaining ocular tissue. Whole eyes were removed from the mouse, eye cups and retina dissections were performed by cutting off the cornea and removing the lens. Retinal dissections were then separated from the other ocular tissues by placing a slit between the retina and choroid tissue, slowly separating the two layers. The NB-CLRN1 antibody was tested on all tissues and eye-cups were used for the majority of experiments. Samples were sonicated in 200 ul of homogenization buffer for 5 seconds (30mmol/l Tris-HCl, 10mmol/l EGTA, 5 mmol/l EDTA, 1% Triton X-100, 250 mmol/l sucrose and 1 mmol/l phenylmethylsulfonyl fluoride, pH 7.5) and stored on ice. Samples were centrifuged at 16,000 g for 1 min to precipitate out debris and loaded in a 4-20% SDS-PAGE gradient gel (Bio-Rad Mini-PROTEAN TGX precast gel #456-1094) in a running buffer (25mM TrisBase, 192 mM Glycine, and 1% SDS) for 1 hour at 200 volts 0.08 amps and 30 watts of current. Gels were transferred in a wet transfer system to a 0.45 um pore sized PVDF membrane (Immobilion-FL IPFL00010) for 1 hour in a transfer buffer (25mM TrisBase, 192 mM Glycine, and 10% methanol) at 200 volts, 0.2 amps, and 40 watts. Membranes were washed in 50% Odyssey blocking buffer in PBS for 1 hour (Li-Cor 927-40000) followed by 3 washes in PBS with 0.1% Tween-20 and incubated at room temperature overnight with the primary antibody. The primary antibodies are as follows: NB-CLRN1 1:2000 (NBP69142), mouse-anti-rhodopsin 1:200 (courtesy Dr. WC Smith, B6-30) (2), mouse-anti-arrestin-1 (courtesy Dr. WC Smith, C10C10) (73) mouse anti-gamma tubulin Thermo Scientific Pierce MA1-850). The second day membranes were

washed 3 times in 1x PBS with 0.1% Tween-20 and incubated with the secondary antibodies in a blocking buffer mix for two hours (5 ml PBS with 0.1% Tween-20, 1 ml Odyssey blocking buffer, and 10 ul 20% SDS). Secondary antibodies were diluted at 1:10,000 and were as follows: goat-anti-mouse IRDye 800CW (Li-Cor926-32210) and goat-anti-rabbit IRDye 680LT (Li-Cor 926-68021). Membranes were finally rinsed 3 times with 1x PBS with 0.1% Tween-20 and imaged on an Odyssey imaging system.

For the new A/J *Clrn1* $^{-/-}$; *Cdh23* $^{-/-}$ double KO and A/J *Clrn1* $^{+/+}$; *Cdh23* $^{-/-}$ WT mice that were treated for co-staining with the NB-CLRN antibody, the AAV vector was produced and optimized as described previously (65, 71, 82, 83, 103, 128, 134, 179, 180, 197, 245). These mice were then injected subretinally with AAV2-Quad-Y-F-sc-smCBA-h*CLRN1*-HA at 8.43 x 10^{12} vg/ml (Table 5.1 construct 1) that contained a hemagglutinin (HA)-tag sequence as described previously (179, 180). These mice were euthanized, and eyecup dissections were obtained and analyzed 1 month post-injection as described above. Western blots were performed as described above with primary antibodies: NB-CLRN1 1:2000 dilution (NBP69142) and mouse-anti-HA 1:200 dilution (3F10, Roche Diagnostics, Indianapolis, IN). Secondary antibodies were diluted at 1:10,000 and were as follows: goat-anti-mouse IRDye 800CW (Li-Cor926-32210) and goat-anti-rabbit IRDye 680LT (Li-Cor 926-68021). Membranes were finally rinsed 3 times with 1x PBS with 0.1% Tween-20 and imaged on an Odyssey imaging system.

Results

Clarin-1 mRNA Isoform-Specific Expression

Initial RT-PCR experiments were performed utilizing the previously published primers from Dr. Geller and colleagues in 2009, with intracellular actin as the positive control (Figure 3-1 E, E') (87). Figure 3-1 A shows the general schematic of primer

location. Figure 3-1 B, B', and B" shows which exons are expressed in each isoform of *Clrn1*/Clrn1. I first tested primers F1-R1 in exons 3 and 4 which picks up both isoforms 1 and 2 (Figure 3-C) In C57BL/6J control mice there was a clear RT-PCR product for *Clrn1* at the expected size of 273 bp which would correlate to isoform 1. When CBA/J *Clrn1* $^{+/+}$ WT rd1 $^{-/-}$ KO mice were assessed, there was an RT-PCR product at the expected size similar to the C57Bl/6J mice, indicating that isoform 1 is produced in the inner retina because the rd1 $^{-/-}$ strain of mice are completely lacking PR cells at 2 months of age (Figure 3.1C) (43, 126, 177). When the CBA/J double *Clrn1* $^{-/-}$ KO, rd1 $^{-/-}$ KO mice were assessed, they did not show any transcript present for the same PCR reaction, indicating that isoform 1 is absent in these mice (Figure 3-1C). This is significant because *Clrn1* $^{-/-}$ KO mice lacking PR cells do not produce any isoform 1 *Clrn1* mRNA from the inner retina, but *Clrn1* WT mice without PR cells do. This indicates that isoform 1 is most likely expressed by the inner retinal cells. When I further tested isoform 2-specific primers F2-R4, there is only a product for the un-injected C57BL/6J mice indicating that isoform 2 is most likely the isoform that is expressed in PR cells because it is not present in either the CBA/J *Clrn1* $^{+/+}$ WT rd1 $^{-/-}$ KO or CBA/J double *Clrn1* $^{-/-}$ KO, rd1 $^{-/-}$ KO mice (Figure 3-1D).

The right eyes of the C57BL/6J mice were injected subretinally with AAV2-Quad-Y-F-sc-smCBA-h*CLRN1*-HA (Table 5-1 construct 1), and there did seem to be an increased amount of isoform 1 in the injected vs un-injected eyes of C57BL/6J mice indicating that I am also detecting the injected construct as well as the endogenous *Clrn1* transcript (Figure 3-1C). When I tested primers F2-R4, which should only pick up isoform 2, I only detect the expected fragment 300 bp in the un-injected C57Bl/6J eyes,

but not in the AAV-treated eyes (Figure 3-D). This indicates that isoform 2 is absent in both *Clrn1* $^{-/-}$; rd1 $^{-/-}$ and *Clrn* $^{+/+}$; rd1 $^{-/-}$ mice and that isoform 2 is most likely expressed by PR cells because it is absent from both *Clrn1* WT and KO mice when on the rd1 background (Figure 3-D). The only mice that show a significant presence of isoform 2 from this first group were the C57BL/6J controls with a correct band at 300 bp.

I next tested the published primers on the new A/J *Clrn1* $^{-/-}$; *Cdh23* $^{-/-}$ double KO and A/J *Clrn1* $^{+/+}$; *Cdh23* $^{-/-}$ WT mice that were treated in one eye with subretinally with AAV2-Quad-Y-F-sc-smCBA-h*CLRN1*-HA (Table 5-1 construct 1), (Table-5-1 construct 1). With primers F3-R1 I detected the expression of isoform 1 at 326 bp in the WT A/J Clrn1 $^{+/+}$; *Cdh23* $^{-/-}$ mouse un-injected retinas. A significant finding is that when comparing the injected to the un-injected KO A/J *Clrn1* $^{-/-}$; *Cdh23* $^{-/-}$ mice, the untreated eyes do not have any isoform 1 expression at 326 bp, but the treated retinas show expression of isoform 1 with the F3-R1 primers as expected (Figure 3-F). This further supports the conclusion that isoform 2 is most likely expressed by PR cells while isoform 1, and perhaps 3, are expressed in the INL.

Endogenous Clarin-1 Protein Localization Using Immunohistochemistry

For immunohistochemistry, mice were sacrificed and paraffin samples were processed as described above. Antigen retrieval was optimized in C57BL/6J mice first and endogenous Clrn1 was detected using an anti-human rabbit polyclonal CLRN1 primary antibody, Novus-Biolgicals-CLRN1 (NB-CLRN1). I saw Clrn1 staining at the CC of PR cells in the retina (Figure 3-2 A', A"'). When I tested the WT A/J *Clrn1* $^{+/+}$; *Cdh23* $^{-/-}$ and KO A/J *Clrn1* $^{-/-}$; *Cdh23* $^{-/-}$ mice I saw NB-CLRN1 staining at the CC of PR cells and some staining within the ONL in the WT mice (Figure 3-2 B', B"', C', C"'). In contrast, although the A/J *Clrn1* $^{-/-}$; *Cdh23* $^{-/-}$ mice show some staining within the ONL, there

seems to be an absence of staining at the CC in PR cells. (Figure 3-2 C', C"') This is promising given that there is a difference in *Clrn1* $^{-/-}$ KO vs WT mice in the A/J; *Cdh23* $^{-/-}$ strain. Comparison of C57Bl/6, A/J *Clrn1* $^{+/+}$; *Cdh23* $^{-/-}$, and *Clrn1* $^{-/-}$; *Cdh23* $^{-/-}$ mouse tissue indicates Clrn1 is present, but localizes specifically to the CC alone only in C57Bl/6 mice. A/J *Clrn1* $^{+/+}$; *Cdh23* $^{-/-}$ mice that show localization in the CC and outer nuclear layer (ONL) and *Clrn1* $^{-/-}$; *Cdh23* $^{-/-}$ mice show little expression. Cryosections were processed as described above. In C57BL/6J mice, cryo-preserved sections showed NB-CLRN1 localization throughout the entire PR cell, concentrated at the IS and OPL, similar to that in A/J *Clrn1* $^{+/+}$; *Cdh23* $^{-/-}$ mice in paraffin sections (Figure3-3). The difference in paraffin vs cryo-staining is most likely due to the different treatment methods prior to staining. The paraffin processed samples undergo much harsher processing methods that the cryo processed samples because the tissues undergo a series of dehydration steps before being immersed in Xylene and embedded. The tissues are then re-treated with xylene before several rehydration steps as mentioned above. This can act to mask certain antigens or alter some antigen specificity compared to the cryo-processed tissue that are not exposed to these treatments.

When analyzing NB-CLRN1 staining in A/J *Clrn1* $^{+/+}$; *Cdh23* $^{-/-}$ N48K KI mice, NB-CLRN1 localized only to the distal tips of the OS of PR cells (Figure 3-4). In previous cell culture experiments, the mutant N48K KI Clrn1 failed to traffic to the plasma membrane and (114). Due to the high levels of protein synthesis in PR cells, it is possible that N48K KI Clrn1 is trafficked to the RPE cells for degradation rather than being degraded by the PR cell. In PR cells there are several mechanisms that regulate protein homeostasis including ubiquitination enzymes, heat-shock proteins, and ER

stress response proteins (13). Interestingly, Clrn1 has been shown to interact with several of these proteins including HSP70, HSPA5, calnexin, and cation-independent mannose-6-phosphate receptor that were identified by Tian et al (218). Since then, there have been no further studies looking at the functional interactions of Clrn1 with any of the 54 identified interacting partners. It is possible that in the presence of the N48K mutation, cell stress pathways stimulate protein degradation in order to maintain cellular homeostasis. Given the OS/RPE localization of N48K KI Clrn1, this may be what stimulates retinal degeneration in patients over time because PR and RPE cells cannot keep up with the amount of mutant protein being made in PRs.

I further validated the localization of NB-CLRN1 at the CC of PR cells by co-staining with both NB-CLRN1 and gamma-tubulin, a basal body marker, which stains adjacent to the CC in PR cells. I saw staining of gamma-tubulin with NB-CLRN1 indicating that Clrn1 is indeed localized at the CC in PR cells (Figure 3-5). I further validated whether the NB-CLRN1 antibody recognized Clrn1 protein by colocalizing NB-CLRN1 with injected AAV constructs expressing the 232 aa isoform of human Clrn1 cDNA. C57BL/6J mice were treated withAAV2-Quad-Y-F-sc-smCBA-h*CLRN1*-Venus at 1.54 x 10^{12} vg/ml either subretinally or intravitreally (Table 5-1 construct 3 or 4) and sections were immunostained with NB-CLRN1 and CLRN1-Venus (GFP analog). Subretinally injected *CLRN1*/CLRN1 localized at the RPE and PR cells and intravitreally injected *CLRN1*/CLRN1 localized throughout the whole retina as I had seen previously (Figure 3-6 A', B'; Figure 5-1 A, B) (72). For both injections, the AAV-*CLRN1*/CLRN1 protein colocalized with the NB-CLRN1 staining (Figure 3-6 A"', B"'). NB-CLRN1 also stained for endogenous Clrn1 protein expression given the localization at the CC in the

intravitreally treated retinas as seen previously (Figure 3-2 A, A"', B, B"'; Figure 3-6 A", B"). Overall, it appears that the NB-CLRN1 antibody recognizes Clrn1/CLRN1 based on the colocalization of AAV-CLRN1-Venus with the NB-CLRN1 antibody.

Endogenous Clarin-1 Protein Localization Using Western Blot

Tissue samples were processed and western blots were performed as described above with C57BL/6J mice being used for initial NB-CLRN1 antibody optimization. For the initial western blot data, the expected 26 KDa band was seen for both the retina and eye cup dissections (Figure 3-7A, A'). This product is absent from the RPE/choroid dissection samples suggesting that this Clrn1 protein product is only expressed in the retina. These samples appear to be from clean dissections without retinal contamination as evidenced by the lack of arrestin-1 in these samples (Figure 3-7 A). This confirms that the 26 kDa protein is only expressed in retinal tissue because it is present in the retina and whole eyecup samples but not the RPE/choroid samples. I further validated these dissected samples by co-staining for arrestin-1 and rhodopsin along with NB-CLRN1 in both C57BL/6J and A/J WT mice (Figure 3-8 A, B). Arrestin-1 only appears in the retinal and eye-cup dissections, suggesting they are pure dissections containing only retina tissue (Figure 3-8 A). In the secondary antibody-only negative controls, there appears to be no cross-reactivity with the anti-rabbit secondary that would recognize NB-CLRN1. I do see cross-reactivity for the anti-mouse secondary that recognize arrestin-1 and rhodopsin (Figure 3-8 C). I believe that this is coming from the anti-IgG epitopes present in the choroidal vasculature that are only present in the RPE/choroid and whole eye-cup dissections since these bands only present in those sample lanes.

I further tested the NB-CLRN1 antibody in AAV-expressed *CLRN1*/CLRN1 vector injected eyes vs un-injected eyes. A/J WT *Clrn1* $^{+/+}$; *Cdh23* $^{-/-}$ and KO *Clrn1* $^{-/-}$; *Cdh23* $^{-/-}$

mice were injected subretinally with AAV2-Quad-Y-F-sc-smCBA-h*CLRN1*-HA (Table 5.1 construct 1). When comparing the injected vs un-injected eyecups, the expected 26 KDa band was seen for all mice which would correspond to a monomer protein product (Figure 3-7 B, B'). Additionally, I have clear co-localization of NB-CLRN1 with the anti-HA antibody that recognizes this vector expressed CLRN1 protein (Figure 3-7 B, B'). Overall, it seems that the NB-CLRN1 antibody does recognize Clrn1/CLRN1 both as endogenous and an AAV-expressed protein. Given that there are additional bands that do not run at the expected size for Clrn1 it is likely that there may be some non-specific staining for other proteins in the retina. A potential way to decipher this would be to analyze these samples on a coomassie blue stained gel, excise out the protein fragments and send both for mass-spectrometry analysis in order to identify the exact protein(s) running in each band. Possible ways to test this hypothesis would be to generate a *Clrn1*-Crisper-Cas9 KO mouse that would delete the entire *Clrn1* locus and therefore should have no Clrn1 expression from any isoform. Alternatively, a *Clrn1*/Clrn1 KI mouse with an N-terminal or C-terminal HA-tag under endogenous promoter control of *Clrn1* could be made. This should allow for anti-HA staining of endogenously expressed Clrn1 and should therefore be able to clearly demonstrate the endogenous expression of Clrn1 without any artifact from non-specific targets with the NB-CLRN1 antibody in immunohistochemistry and western blot analyses.

Table 3-1. Previously published *Clarin-1* RT-PCR primers

Primer Oligo Name	Primer Sequence 5'-3'
Clrn1 F1 Forward	GGTCCAAGCCATCCCCGTA
Clrn1 F2 Forward	TCATGCCAAGCCAGCAGAAGAAG
Clrn1 F3 Forward	AGGCAATGTGGGTTAGGAGCAAG
Clrn1 R1 Reverse	TGTTCTGTAGGCATAGGTCCCTTC
Clrn1 R4 Reverse	CTCTCCTTTGTCCTCATACAGAGAGTACC
Clrn1 R5 Reverse	AGCCCCAGTGGTCCATGAAGAG
Actin F1 Forward	ACCAACTGGGACGACATGGAGAA
Actin R1 Reverse	CATGGCTGGGGTGTTGAAGGT

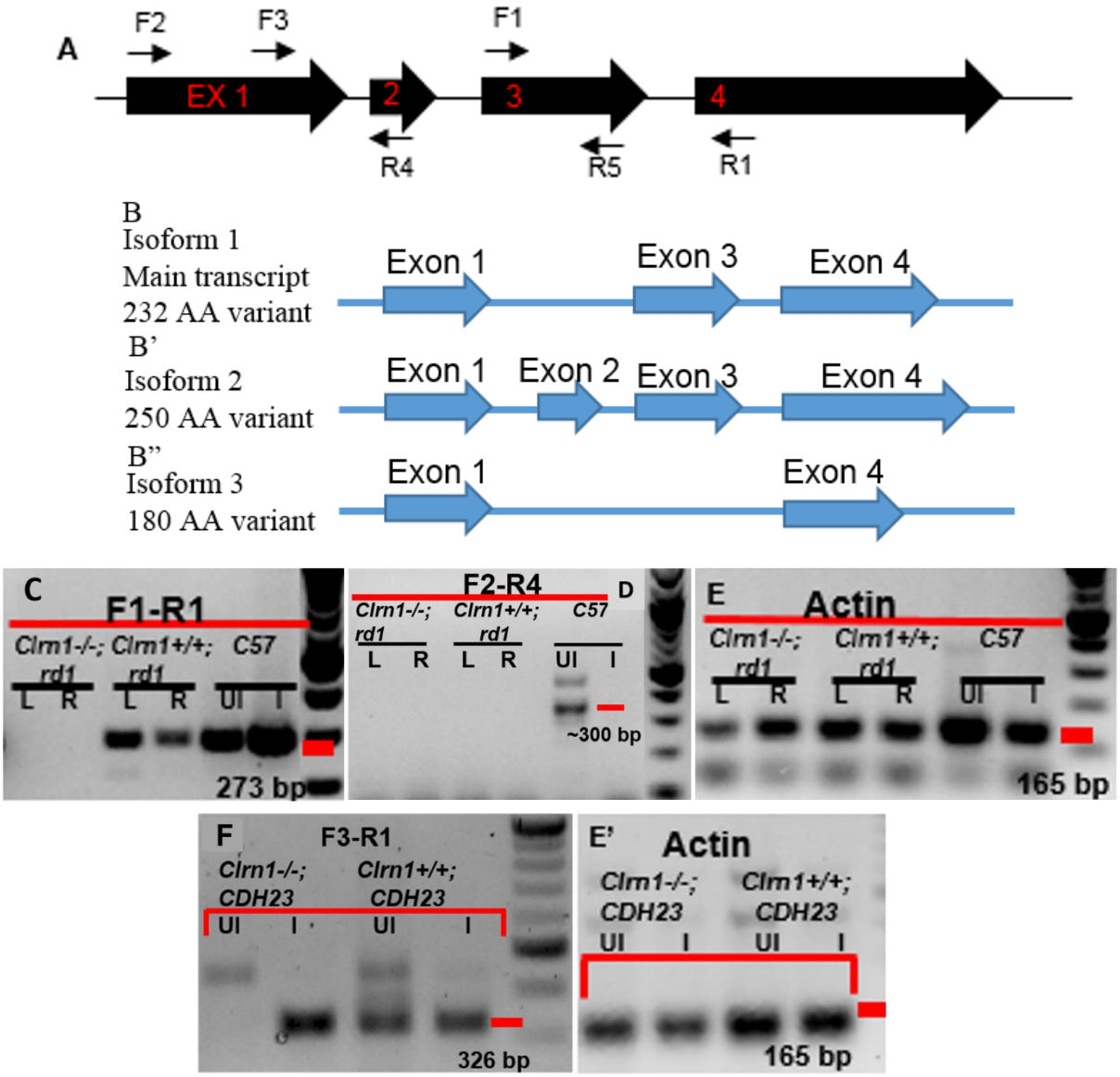

Figure 3-1. RT-PCR and *Clarin-1* isoform expression. A): Schematic of *Clrn1* RT-PCR with primer locations, arrows represent published primers (87). B, B', B") Clrn1 three main protein isoforms. C-E) CBA/J mice (*Clrn1* $^{-/-}$, rd1 $^{-/-}$ double KO vs *Clrn1* $^{+/+}$; rd1 $^{-/-}$ KO, left eye (L) vs right eye (R), C57 control, un-injected (UI) vs injected (I) with AAV8-Y733F-CBA-h*CLRN1*-HA subretinally. C) F1-R1 expected size for isoform 1 273 bp, isoform 3 should not be present. D) F2-R4 should only pick up isoform 2 at approximately 300 bp. E) Actin control should be 165 bp. F, E') A/J mice (*Clrn1* $^{-/-}$; *Cdh23* $^{-/-}$ double KO vs *Clrn1* $^{+/+}$; *Cdh23* $^{-/-}$ KO, un-injected (UI) vs injected (I) AAV2-smCBA-h*CLRN1*-HA subretinally. F) F3-R1 expected size for isoform 1 326 bp is seen in both the injected retinas. E') Actin control should be 165 bp.

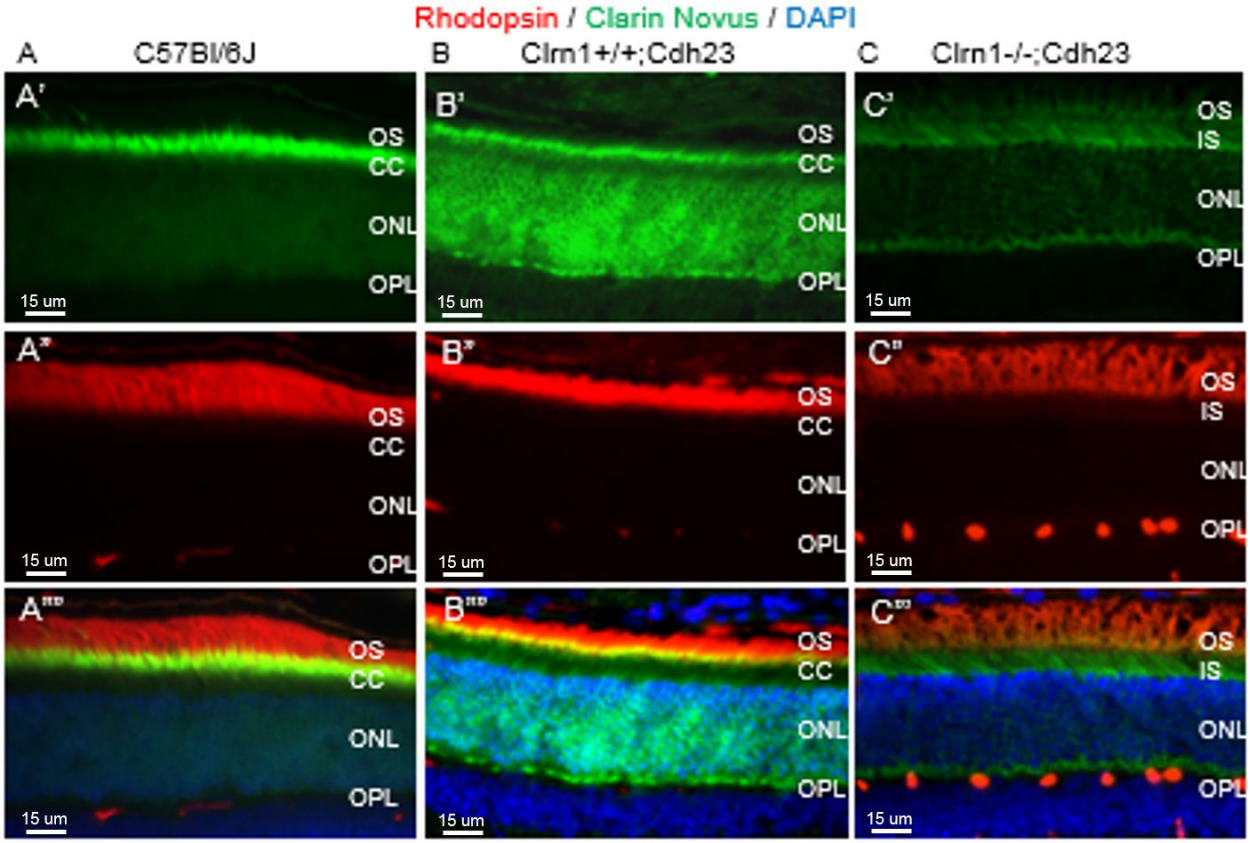

Figure 3-2. Novus Biologicals-CLARIN-1 antibody staining for immunohistochemistry. NB-CLRN1 localizes to CC in A) C57Bl/6J B) *Clrn* $^{+/+}$, *Cdh23* $^{-/-}$ WT mice but not in C) *Clrn1* $^{-/-}$. *Cdh23* $^{-/-}$ KO mice A', B', C') Goat-488-anti-rabbit-NB-CLRN1. A", B", C") Goat-594-anti-mouse- rhodopsin. A"', B"', C"') Merged 488-594-DAPI.

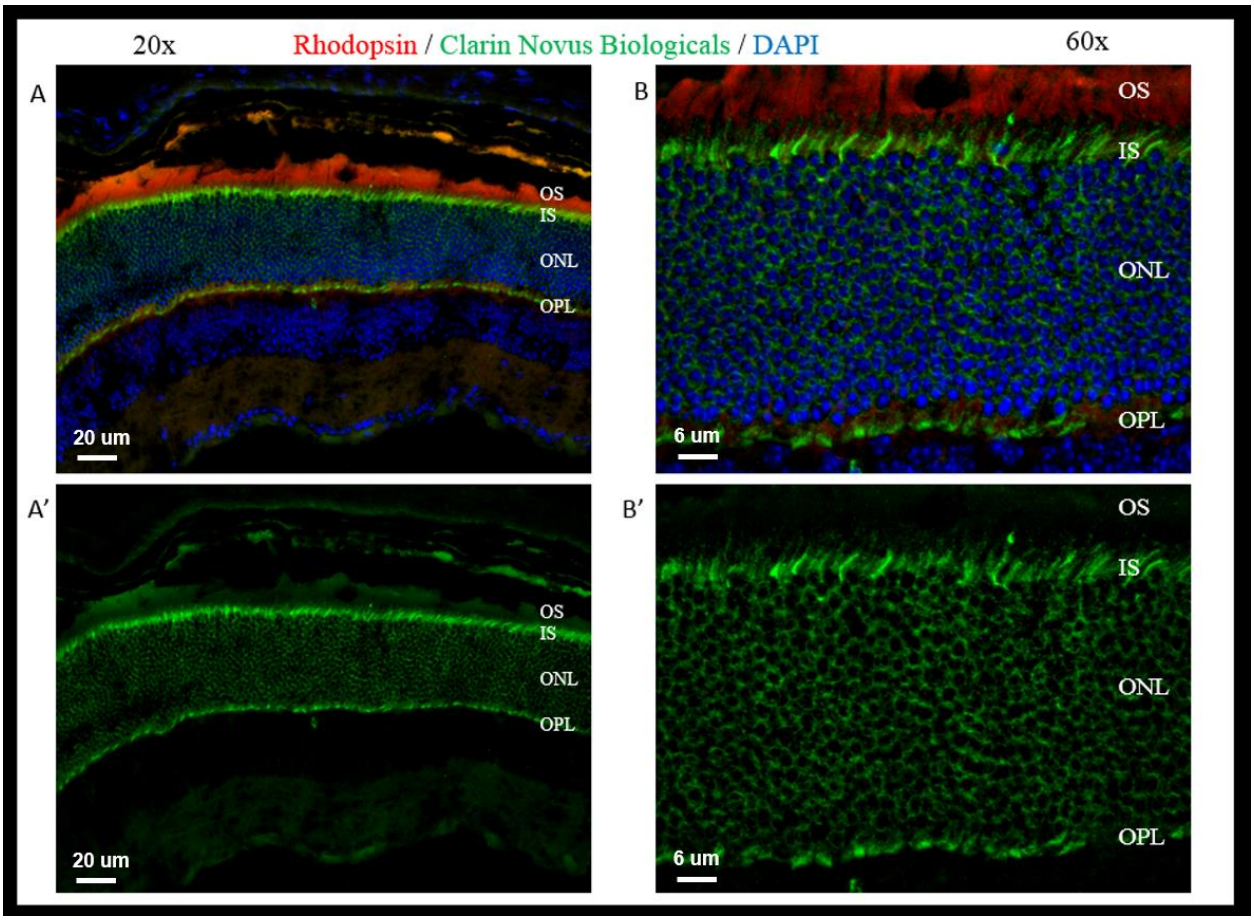

Figure 3-3. Cryo-preserved C57BL/6J Novus Biologicals-CLARIN-1 staining. A, A') 20x magnification of C57BL/6J mice. NB-CLRN1 is localized throughout the entire PR cell, particularly at the IS and OPL. B, B') 60x magnification of C57BL/6J mice. A, B) Merged goat-594-anti-mouse- rhodopsin, goat-488-anti-rabbit-NB-CLRN1, merged with DAPI-358. A', B') NB-CLRN1 staining alone goat-488-anti-rabbit-NB-CLRN1.

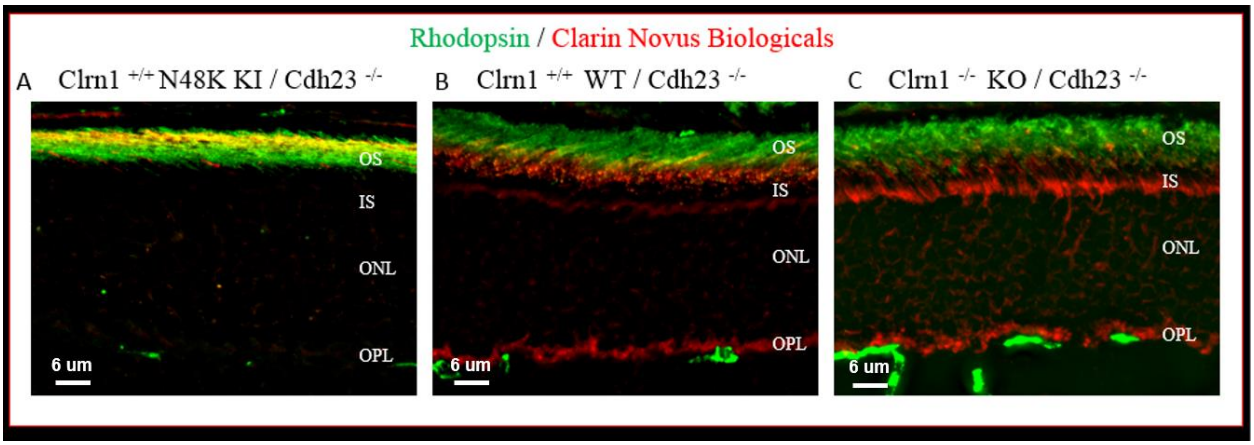

Figure 3-4. Novus Biologicals-CLARIN-1 localization in WT vs Clarin-1 KO, and N48K KI A/J mice. A) NB-CLRN1 localizes at the distal tips of the OS in N48K KI mice, possibly within the RPE microvilli. Merged donkey-488-anti-mouse-rhodopsin, donkey-594-anti-rabbit-NB-CLRN1. Compared to B) WT and C) Clrn1 $^{-/-}$ KO A/J mice.

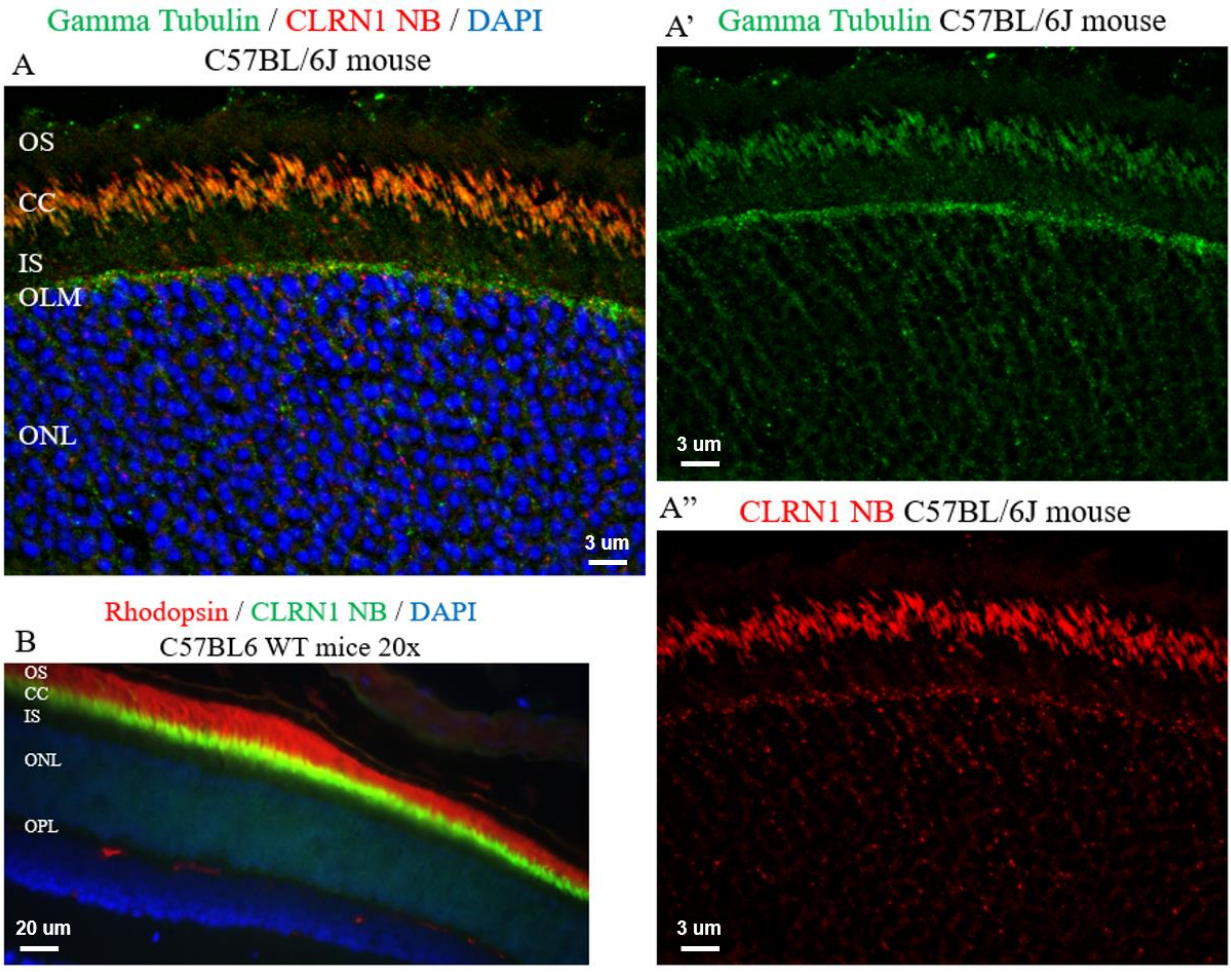

Figure 3-5. Novus Biologicals-CLARIN-1 colocalization with gamma tubulin. A) NB-CLRN1 localizes at CC with partial overlap of gamma-tubulin (cilia basal body marker) in C57BL/6J mice. A') gamma-tubulin localization at the basal bodies in PR cells. A") NB-CLRN1 at the CC of PR cells. B) Reference image for NB-CLRN1 localization at the CC in C57Bl/6J mice. A) Goat-594-anti-rabbit-NB-CLRN1, Goat-488-anti-mouse-gamma tubulin, DAPI-358, DAPI-358. A') Goat-488-anti-mouse-gamma tubulin. A") Goat-594-anti-rabbit-NB-CLRN1. B) Donkey-488-anti-rabbit-NB-CLRN1, Donkey-594-anti-mouse- rhodopsin, DAPI-358.

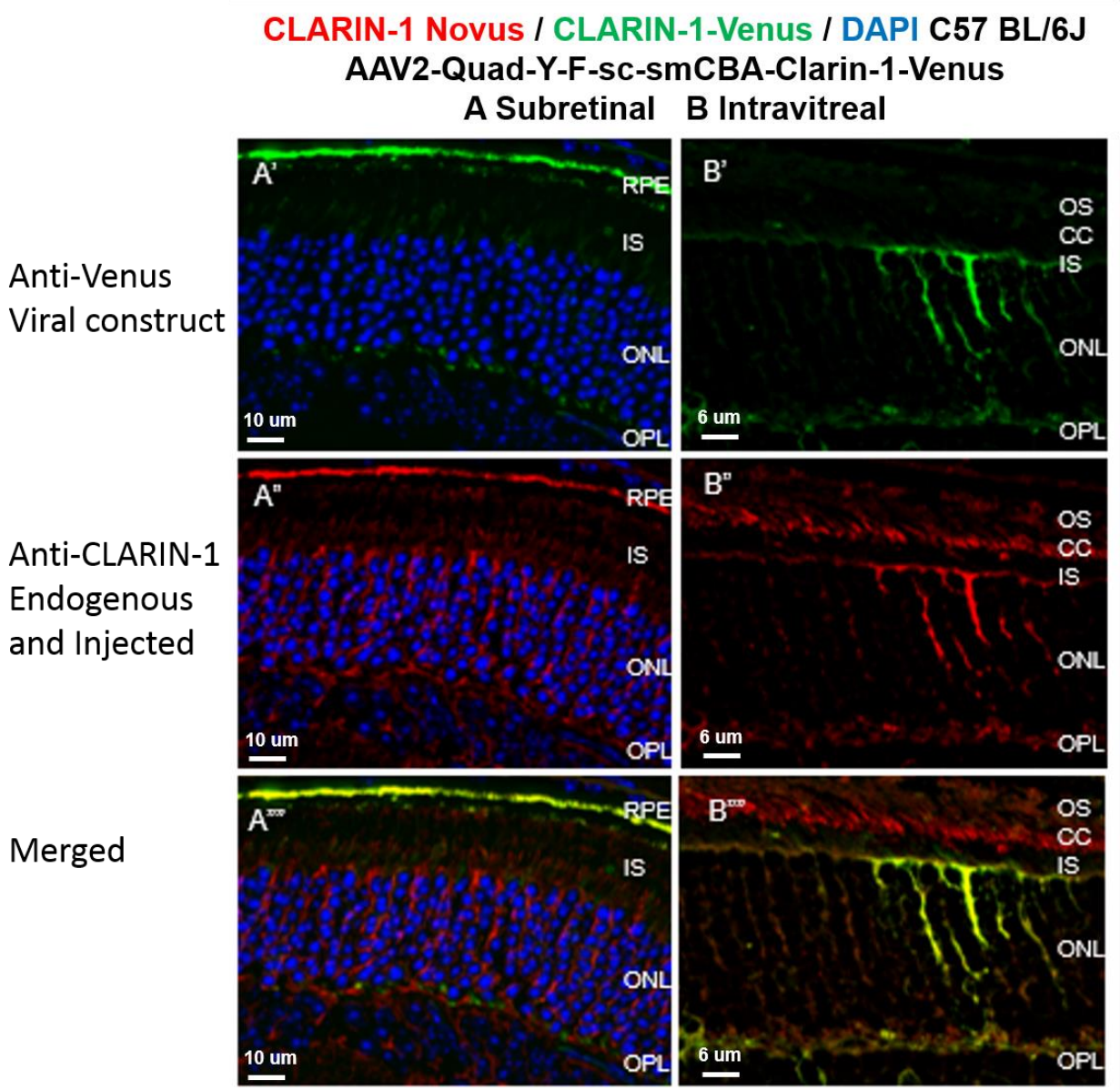

Figure 3-6. Subretinal and intravitreal AAV-injected *CLARIN-1* colocalization with Novus Biologicals-CLARIN-1 antibody. A) Subretinal injection AAV2-Quad-Y-F-smCBA-h*CLRN1*-Venus (GFP analog). B) Intravitreal injection AAV2-Quad-Y-F-smCBA-h*CLRN1*-Venus (GFP analog). A', B') Donkey-488-anti-mouse-GFP (Venus-analog). A", B") Donkey-594-anti-rabbit-NB-CLRN1. A"', B"') merged with DAPI-358, complete co-localization is observed with GFP and some endogenous NB-CLRN1 staining is observed in the connecting cilium of photoreceptors.

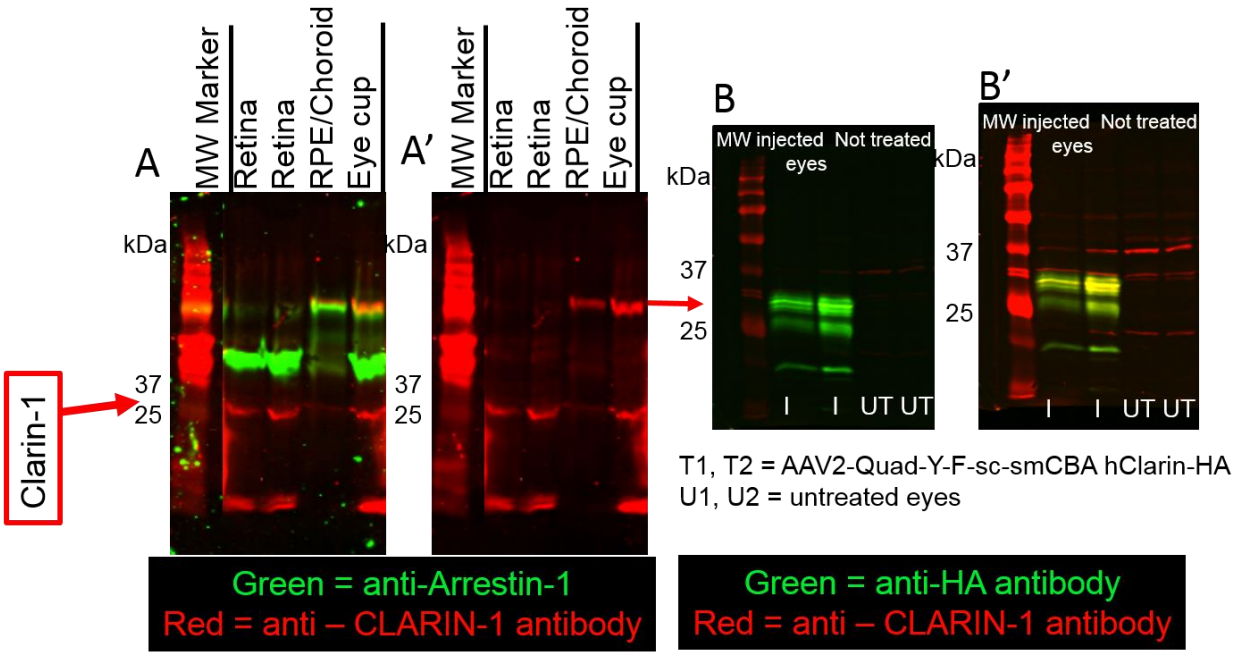

Figure 3-7. Novus Biologicals-CLARIN-1 western blot analysis. A) Western blot analysis of different dissection methods staining for arrestin-1 and NB-CLRN1. A') NB-CLRN1 staining alone. Retina dissections show the expected Clrn1 band at 26 kDa and arrestin-1 at 50 kDa. RPE/choroid dissections have minimal to no arrestin-1 present at 50 kDa indication that they do not contain much if any retinal tissue. The RPE/choroid dissections also do not contain any Clrn1 at the predicted 26 kDa size. Eye cup dissections containing both the retina and RPE/choroid tissues have both the 26 kDa and 100 kDa bands further indicating that the 26 kDa band for Clrn1 is only present in the retinal tissue and the larger 100 kDa fragment is coming from the RPE/choroid tissue. B) Western blot analysis of injected vs un-injected retina eyecups. B') color enhanced image of B with a longer exposure time. Eyes were treated subretinally with AAV2-Quad-Y-F-sc-smCBA-h*CLRN1*-HA and blots were stained for anti-HA in green and anti-CLRN1 in red.

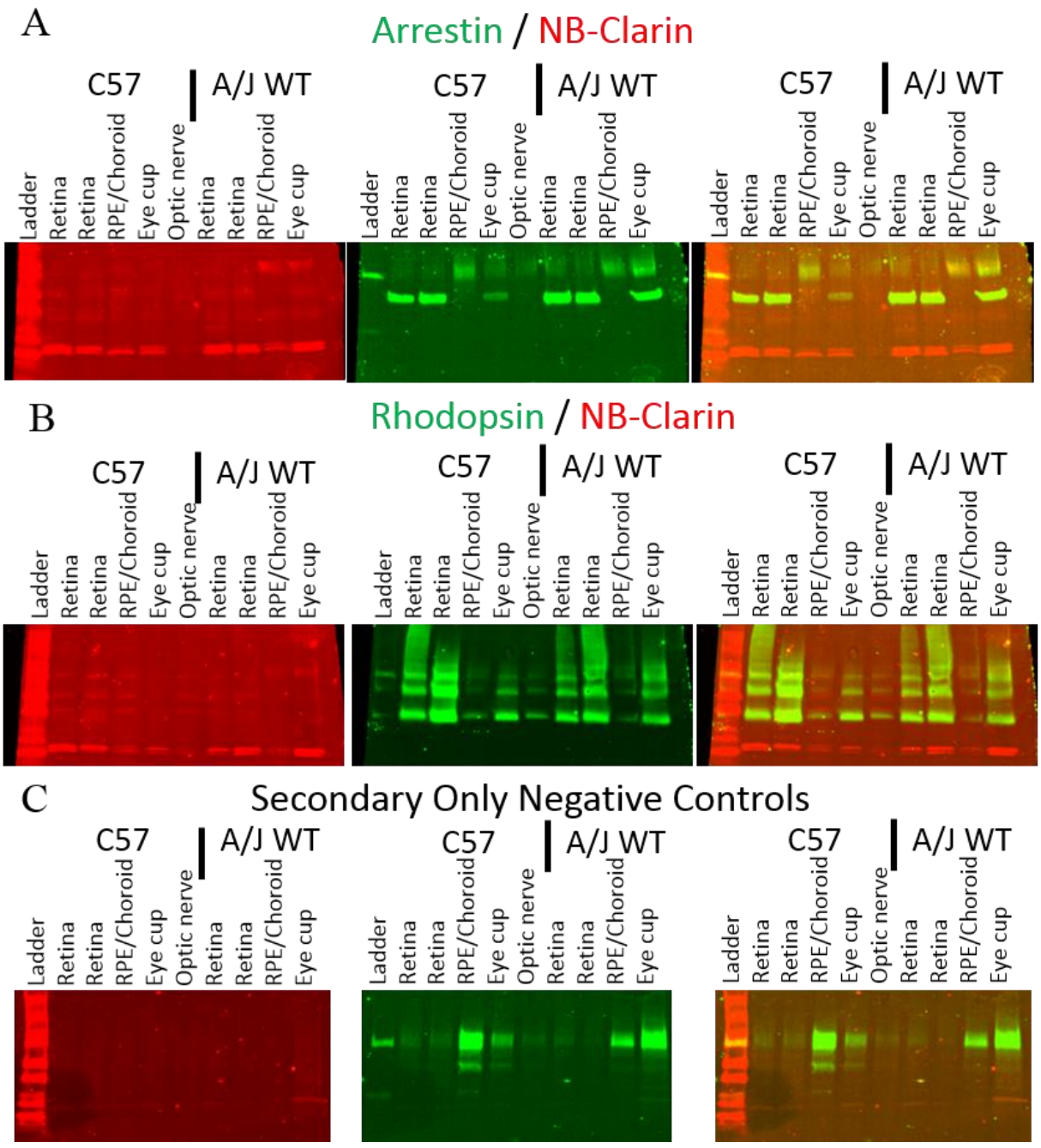

Figure 3-8. Arrestin-1, rhodopsin, and secondary-only control western blots. A) Arrestin-1 is only present in retinal samples. B) Rhodopsin is present in all samples, but the majority is in retinal samples. C) Secondary only controls show no staining for anti-rabbit (CLRN1) and IgG staining for anti-mouse (arrestin-1, rhodopsin).

CHAPTER 4
IDENTIFYING A RETINAL PHENOTYPE IN CLARIN-1 KNOCK-OUT (KO) (Clrn1 $^{-/-}$) AND N48K KNOCK-IN (KI) MICE*

Background

As stated previously, in dark-adapted PR cells, the Gα protein transducin is localized in the OS disc membranes and is associated with the trimer of Gβ and Gγ complex and arrestin-1 is localized to the rod PR IS and OPL synapses. Upon exposure to light, transducin moves from the OS to the IS and OPL whereas arrestin-1 will move from the OPL and IS to the OS where it will bind to phosphorylated rhodopsin (79). The majority of transducin will move from the OS to IS within 2 minutes of light exposure and the majority of arrestin-1 will translocate to the OS within 8 minutes of light exposure (37, 79). There is an ongoing debate as to whether these proteins travel through diffusion or through active transport with molecular motors along the actin and tubulin cytoskeletal filaments (36-39, 95, 97, 98, 162-164, 210). Dr. Wolfrum, as well as others, have assessed arrestin-1 and transducin's ability to utilize cytoskeletal filaments in a dark-adapted vs light-adapted retina. In the light they believe arrestin-1 and transducin do not require filaments; however, in the dark, arrestin-1 and transducin travel along cytoskeletal filaments in order to return to their normal dark-adapted state (39, 190).

Dr. Cosgrove's group previously showed that the *shaker1* (MYO7A) USH1B and the *whirler* (whirlin) USH2D mice have a delay in transducin translocation upon exposure to light (176, 219). MYO7A mice also display a slightly attenuated ERG response for both a- and b-waves, but prior to this study no retinal degeneration had

* Reprinted with permission from Dinculescu A and Stupay RM et al. AAV-Mediated Clarin-1 Expression in the Mouse Retina: Implications for USH3A Gene Therapy. PLoS One 2016.11(2):e0148874.

been observed. The level of light intensity required for transducin activation was much brighter than WT controls. They further demonstrated that mice exposed to continuous bright light of 2500 lux, and mice housed in mid-level light at an intensity of 1500 lux, develop retinal degeneration in approximately 6 months; however they do not degenerate when the mice are housed at a low light intensity of 200 lux (176). Dr. Cosgrove's group was also able to demonstrate that lentiviral delivery of WT MYO7A can rescue this transducin translocation phenotype as well as the light induced retinal degeneration (240). Similarly, they also showed a transducin translocation defect in whirlin mutant mice along with a requirement for brighter levels of light to induce complete transducin translocation. Whirlin mice develop a retinal degeneration phenotype when exposed to 1500 lux for a continuous period of time, and also have miss-localized rhodopsin protein in the IS of PR cells (219). Given this translocation phenotype in other USH mouse models, I hypothesized that there may be a similar translocation phenotype, retinal degeneration after bright light exposure, attenuated ERG, or a potential additional ERG phenotypes in my USH3A mouse models.

As noted previously, a primary complication with studying USH3A is that the current mouse models do not show a retinal phenotype but do present with significant hearing loss and inner hair cell death by 4 months of age (87-90, 93). An additional complication with the original *Clrn1* $^{-/-}$ KO and N48K KI mouse models is that each was generated on different genetic backgrounds which means that any phenotype identified may have confounding variables due to the genetic background of the mouse strain. Additionally, the original *Clrn1* $^{-/-}$ KO mice are albinos and the N48K KI mice are pigmented adding another layer of complexity to comparing any phenotype of

translocation and/or light-induced degeneration between *Clrn1* $^{-/-}$ KO and N48K KI mice. Particularly with the hypothesis of a light exposure phenotype, pigmented mice are traditionally less sensitive to light and require much higher levels of light to induce degeneration compared to albinos. This is one benefit to switching to the A/J strain.

One complication is that the A/J mice develop more pronounced age-related retinal degeneration than other strains. This PR cell death is due to an upregulation of inflammatory factors and a decrease in neuroprotective factors and these mice show changes in their RPE prior to PR cell death (160). A/J mice have significant thinning of the ONL and a noticeable decline in cone PR number at 8 months old. Consequentially, there was a decrease in scotopic and photopic ERGs at 8 months of age. This PR cell death is independent of light exposure since WT A/J mice raised in the dark also undergo PR degeneration (160). Upon fundus exam, A/J mice have an increase in auto-fluorescence at 8 months of age and have evidence of inflammation and immune cell activation originating from the RPE. Additionally, 8 month old mice show an increase in RPE cell size and multinucleated cells, and they also fail to regenerate 11-cis retinal over time (160). Additionally, this strain of mice also carry other background mutations that cause the mice to age at an accelerated rate and they have a higher incidence of cancer and mitochondrial defects. These mice also have RPE defects and undergo retinal degeneration over time with an attenuated ERG at 12 months of age (160).

Methods

Arrestin-1 and Transducin Translocation Assay

Mice from both the C57Bl/6J mixed albino and the A/J strain described above were housed as described above (87, 88, 217). All mice were housed in a 12 hour dim-light/dark cycle prior to translocation experiments. Mice were dilated with Atropine

Sulfate Ophthalmic Solution 1% (Akorn Inc, Lake Forest IL USA, NDC 17478-215-05) a long acting dilator prior to being dark adapted overnight. The following day mice were dilated again with Phenylephrine Hydrochloride Ophthalmic Solution 2.5% (Paragon BioTeck Inc, Portland OR, USA, NDC 42702-102.15) prior to translocation experiments. One mouse of each genotype was moved into a clear plastic box and exposed to 1000 lux of light for 1 hour, and the mice were then euthanized as stated previously. Eyes were enucleated and placed in a 4% PFA fixative solution for 1 hour prior to moving to a 1x PBS solution. All eyes were processed for paraffin sections as described above. Immunostaining was performed as described previously with the exceptions of not baking the slides at 60^{o}C prior to staining and having a Protinase K digestion step. Primary antibodies were as follows: mouse-anti-arrestin-1 1:100 dilution (courtesy of Dr. WC Smith, C10C10) (73), mouse-anti-rhodopsin 1:100 dilution (courtesy of Dr. WC Smith, B6-30) (2), and rabbit-anti-transducin 1:1000 dilution (rabbit polyclonal Santa Cruz Biotechnology sc-389). Secondary antibodies were as follows at 1:400 dilution: goat-anti-rabbit 488 (A11008), goat anti-rabbit 594 (A11012), goat-anti-mouse 488 (A32723), goat-anti-mouse 594 (A11005), donkey-anti-rabbit 488 (A21206), donkey anti-rabbit 594 (A21207), donkey-anti-mouse 488 (A21202), and donkey-anti-mouse 594 (A21203). All secondary antibodies were acquired from Molecular Probes/ Invitrogen, Eugene, OR. Slides were mounted and imaged and analyzed as described above using a spinning disc confocal microscope through the Cell and Tissue Analysis Core at the University of Florida (Olympus DSU-IX81). Images were acquired with 10-15 confocal z-stacks and images were consecutively de-convolved and merged into a single projection image and each color channel was saved separately and merged.

Fluorescence intensity plots were made with ImageJ software (National Institutes of Health). Densitometric plots were obtained across the PR cell layer and the Plot Profile program was used to calculate arrestin-1 and transducin staining intensity across the PR cell layer. Nuclear staining with DAPI defined the ONL. For this analysis three random regions across the retina were selected for WT, KO, and KI mice. The fluorescent signal in the OPL was defined as a percentage of total fluorescence across the entire PR cell layer. The statistical difference was calculated via an unpaired t-test using GraphPad software and error bars calculated as the mean ± standard error of mean (SEM) and was considered to be statistically significant at $p<0.05$ or greater.

GFAP Expression and Olfaction Assays to Test for Alternative Phenotypes

Immunohistochemistry was performed on paraffin retinal sections to look for any upregulation in glial fibrillary acidic protein (GFAP) expression in WT vs KO mice. Slides were mounted and imaged as described above using KO mice from the C57BL/6J mixed albino strain. GFAP is an intermediate filament protein that is upregulated in Müller glial cells in response to retinal injury or degeneration (77). Eye-cups were processed and stained as described above with an anti-GFAP antibody (Thermo Fisher mouse antibody ASTRO6, #MA5-12023) and Vecta-Shield with DAPI.

For olfactory assays, mice were anesthetized and sacrificed and olfactory and respiratory epithelium and olfactory bulb samples were processed in collaboration with Dr. Jeffrey Martens' group at UF. Experimental protocols are described in their previous studies (153, 232). Olfactory lysates were obtained from WT A/J and N48K KI mice and RT-PCR analysis was done with the previously published primers (87). Samples were dissected and RT-PCR was performed as described above.

Electroretinography

For the LKC system, an electrode was placed on the surface of the cornea and a reference electrode was placed in the skin at the surface of the skull between the ears. A third grounding electrode was placed in the tail to establish a baseline measurement. The mice were set up on a mobile platform then moved into an upright Ganzfeld dome that generated a uniform light field for the procedure (EM Win UTAS LKC Technologies Gaithersburg, MD). For the Espion system, a contact electrode was placed on the surface of the eye, the reference electrode was placed in the cheek of the mouse, and the ground electrode was placed in the tail. The mice were setup on a stationary platform and a moveable Ganzfeld dome was lowered on top of the mice prior to the procedure (40). Both systems contain a platform heating pad to keep the mice at a stable body temperature during the experiment. Both systems were utilized through the course of this work, but unless otherwise noted, only the LKC data is presented here.

For scotopic ERG, mice were dark adapted overnight for 12 hours prior to ERG. The mice were dilated the day before using Atropine Sulfate Ophthalmic Solution 1% (Akorn Inc, Lake Forest IL USA, NDC 17478-215-05) a long acting dilator. Prior to ERG the mice were then dilated again using Phenylephrine Hydrochloride Ophthalmic Solution 2.5% (Paragon BioTeck Inc, Portland OR, USA, NDC 42702-102.15). Mice were then anesthetized using a mixture of ketamine (72 mg/kg) (Ketaset: Ketamine HCl injection, USP, Zoetis Inc, Kalamazoo MI, USA, NADA 043-304) and xylazine (4 mg/kg) (LLOYD Shenandoah IA USA, NADA 139-236) by intraperitoneal injection with a volume of 4 ul per gram of weight. Then the mice were setup on the platform and, prior to electrode placement, either Gonak Hypermellose Opthalmic Demulcent Solution 2.5% (Akorn Inc, Lake Forest IL, USA NDC 17478-064-12), Serile eye wash (Altaire

Pharmaceuticals Inc, Aquebouge NY USA, NDC 59390-175-35), or GenTeal Lubricant Eye Drops (Alcon Laboratories Inc, Fort Worth TX USA NDC 0078-0518-16) was applied to the surface of the cornea to keep the eyes hydrated throughout the procedure. The mice were then placed in the Ganzfeld dome and exposed to 3 light intensities of -20 dB, -10 dB, and 0 dB (corresponding to 0.02, 0.2 and 2 scot-cd·sec·m^{-2} stimuli). After ERG the mice were provided anesthesia reversal using a solution of Antisedan Orion Pharma Corporation Finland, Zoetis Inc, Kalamazoo MI USA NADA 141-033) (63, 72, 175, 184). Scotopic a-wave, b-wave, and OPs were compared between control C57BL/6J, A/J WT, and KO mice to validate the previously published ERG phenotype. The a-wave was measured from the highest amplitude immediately after the light stimulus to the lowest amplitude afterward prior to the increase in amplitude for the b-wave. The b-wave was measured from the lowest amplitude used for the a-wave to the highest amplitude after the OPs. The OPs are the oscillations along the increasing amplitude of the b-wave and there can be a range of up to 5 OPs. OP1 is measured from the lowest amplitude used for the a-wave to the next highest amplitude prior to the next trough. OP2 begins at the first trough to the next highest amplitude. OP3 is measured similarly from the next trough to the next highest peak.

For a photopic ERG, mice were first light adapted, and mice were prepared as described above. In order to select the optimal time, mice were light adapted in the Ganzfeld dome for 2, 4, 6, 8, and 10 minutes and then the highest light intensity for a cone response was tested to determine a plateau of maximal response and then all intensities were recorded. Cone response is recorded at 4 light intensities of -3 dB, 3 dB, 6 dB, and 10 dB (25 phot-cd·sec·m^{-2} maximum intensity). After the procedure, mice

were provided anesthesia reversal as described above (63, 72, 175, 184). Photopic cone ERGs were compared between C57BL/6J, A/J WT, and KO mice.

For the dual-flash ERG recovery responses, mice were dark adapted overnight, then fully bleached to suppress rod responses using the Espion ERG system, then a scotopic ERG was recorded at 1 cd.s/m^2 which is equivalent to the 0 Db intensity on the LKC system. After the initial flash post light adaptation, the mice were tested at varying time points post light exposure to measure how rapidly the mice were able to recover a scotopic ERG response. This protocol is defined in Table 4-1 and was only assessed on the initial C57BL/6J mixed albino mice. Due to the amount of time required to set up the mice on the Espion system compared to the LKC system, I was unable to reproduce the protocol on the new A/J strain because the A/J mice are extremely sensitive to the anesthesia and cannot be anesthetized for the 1 hour required for the experiment.

For ERG analysis post 1000 lux light adaption, mice were dark adapted overnight, exposed to 1000 lux of light for 1 hour, and then a scotopic ERG was measured immediately after light exposure. Maximum scotopic a- and b-wave ERG recordings were analyzed for WT, Clrn1 $^{-/-}$ KO and N48K KI A/J strain mice, the amplitudes were averaged between left and right eyes from the same mouse, and then averaged together for each genotype. The results were analyzed by a Student's t test using GraphPad statistical software (GraphPad Prism 6.0, GraphPad Software, San Diego, CA). ERG responses were considered statistically significant at $p<0.05$ *, <0.01 **, and <0.001 *** and all ERG data are represented as the mean ± SEM.

Spectral Domain Optical Coherence Tomography

SD-OCT was used to assay for retinal degeneration post-light damage as follows. Mice were anesthetized and eyes were dilated and kept hydrated during the

procedure as described above. Mice were arranged on the Bioptigen platform and focusing scans were used to align the retina with the optic nerve at the center of the image. Two more scans were obtained peripheral to the optic nerve, both nasally and temporally. SD-OCT parameters for all scans were the same for all mice. Rectangular volume scans were obtained with an A/B scan ratio of 1000, 5 frames per B-scan at 100 B-scans and 80 lines of inactive A-scans per B-scan ratio taken at 1 volume with a square field of 1.4 mm length and 1.4 mm width and a horizontal offset of 0.1 mm. After the procedure, mice were woken up as described above (19). Images were analyzed with InVivo Vue Bioptigen software and ONL thickness was measured using Bioptigen Diver software with a 9x9 spider plot. ONL thickness was measured both manually and using the auto-segmenting program, and values were compared. The ONL thickness was measured and calculated using Diver software calipers through the Bioptigen OCT system placed at the OPL synapses and the OLM at the top of the ONL and plotted in GraphPad software and a two way ANOVA (Analysis of Variance) test was performed to assess whether changes in ONL thickness was statistically significant.

Light Damage

Mice were housed in the animal facility as described above. Prior to light damage mice were analyzed by ERG and SD-OCT as described above for a light damage control. During light damage experiments, the previously published protocols were adapted (99, 223, 224). The mice were dark adapted the day before and two mice were placed in each cage, one of each genotype, with minimal bedding and food placed on the bottom of the cage to allow for minimal blockage of light. Mouse cages were housed on a standard ACS (animal care services) rack with LED lights, emitting 5500K of light, arranged under the cage lids. These lights are adjustable to achieve the desired light

intensity. Light intensity was calibrated using a traceable dual-range light meter (Sper Scientific 840006 Light Meter Lux). Timing of light exposure was also controlled by an electric timer. Mice were placed in the rack at 6 pm and light damage was performed for 4 hours until 10 pm at specified light intensities. One week post-light damage mice were analyzed using SD-OCT and ERG, and the ONL thickness and scotopic ERG responses were measured, calculated, and analyzed as described above.

For the initial A/J light intensity optimization, light intensities of 1300, 1500, 2000, or 5000 lux were used to optimize the light damage conditions for the maximum ONL degeneration in WT mice. At all light intensities tested, SD-OCT was performed 1 week post light damage, ONL thickness was analyzed using a two way ANOVA (Analysis of Variance) to assess if changes in ONL thickness was statistically significant after light damage. Scotopic ERG responses were assessed for all mice pre- and post-light damage at all intensities and a- and b-wave amplitudes were measured as described above. A Student's T-test was performed and the ERG response was considered statistically significant at $P<0.05$ *, <0.01 **, and <0.001 ***. The 2000 lux intensity was chosen to assess for light damage in the *Clrn1* $^{-/-}$ KO and N48K KI mice and light damage was performed as stated above. SD-OCT and ERG were performed pre- and post-light damage to measure ONL thickness and retinal function as mentioned above.

Results

Light-Driven Protein Translocation to Characterize a Retinal Phenotype

Upon dark-adaptation, both the mixed albino C57BL/6J WT and *Clrn1* $^{-/-}$ KO mice have proper localization of transducin in the OS and arrestin-1 in the IS, ONL and OPL (Figure 4-1). Upon exposure to 1000 lux of light for 1 hour, both the WT and *Clrn1* $^{-/-}$ KO mice have normal transducin movement (Figure 4-1 C, C'). Fluorescence quantification

is plotted in Figure 4-1 B, B'. However, after 1 hour of light exposure at 1000 lux both the *Clrn1* $^{-/-}$ KO and N48K KI mice show a significant delay in arrestin-1 translocation from the OPL and IS to the OS and this delay is statistically significant for both the *Clrn1* $^{-/-}$ KO and N48K KI mice on the mixed C57BL/6J albino mice (Figure 4-2 B, B', C, C'). This is in contrast to USH1B and USH2D mouse models that have a delay in transducin translocation rather than arrestin-1 (176, 219, 220). This translocation phenotype was also reproducible in the new A/J *Clrn1* $^{-/-}$ KO and N48K KI mice compared to WT. It is unclear what the biological significance of this arrestin-1 delay is, given that there is no PR degeneration or loss of ERG response over time. Previous studies have looked at arrestin-1 KO mice and they see a prolonged photoresponse in mice completely lacking arrestin-1. These mice also do not have ONL degeneration, but they do have slightly disorganized OSs and a highly altered recovery phase of rhodopsin (235). I therefore also tested for a similar delay in rod PR cell recovery response but there was no significant difference between the WT and N48K KI mice (Figure 4-10).

GFAP Expression in WT vs KO Mice

As mentioned above, GFAP is an intermediate filament protein that is upregulated by Muller glial cells in response to retinal injury or degeneration (77). When comparing the mixed albino C57BL/6J WT and *Clrn1* $^{-/-}$ KO mice there did appear to be some slight upregulation in some *Clrn1* $^{-/-}$ KO mice, however this was not consistent across a larger pool of samples (Figure 4-3). The samples were all processed according to the same protocol at the same time. This was shown in other previous studies (87).

Olfactory Structure and Clarin1 Expression in Olfactory Cells

A collaboration was arranged with the Dr. Jeffrey Martens' lab at UF to assess *Clrn1*/Clrn1 expression in olfactory tissue. As noted above, olfactory epithelium,

respiratory epithelium, and olfactory bulb tissue was acquired, sectioned, and stained in addition to mRNA isolation from olfactory tissue for RT-PCR analysis. First I compared the cilia formation in both olfactory and respiratory epithelium looking at acetylated tubulin and there did not appear to be any differences in either tissue from WT or N48K KI mice. I next looked at whether there was normal olfactory signaling present in the WT vs N48K KI A/J mice by assessing the presence and amount of tyrosine hydroxylase activity. There appeared to be normal localization in the juxtaglomerular cells that innervate the olfactory glomeruli (Figure 4-4 B, B', C, C'). Overall there did not appear to be any olfactory phenotype, which was disappointing because previous studies have looked at the other USH proteins in olfaction, both in animal models and patients and they saw significant decrease in olfactory signaling as well as decreased beat frequency in nasal cilia (12, 120, 196). Next I looked at transcript analysis of *Clrn1* in olfactory lysates. Utilizing the previously published primers that were used above, I saw isoform-specific products for isoform 2 with primers F2-R4 indicating this isoform is expressed in olfactory epithelium. I also saw much fainter products for F2-R5 which detects isoforms 1 and 2, as well as a product for F3-R1 which detects all three isoforms (Figure 4-5 A). Overall, this indicates that *Clrn1* is expressed in olfactory tissue and correlates with other USH proteins being expressed there as well.

Validation of the Previously Published Novel ERG Phenotype

First I compared the A/J strain ERGs for the WT and *Clrn1* $^{-/-}$ KO mice to my previous control C57BL/6J mice in order to understand any differences that may hinder future studies. Like the previously published data on the A/J strain (160), the A/J mice do have significantly smaller a- and b-wave ERG amplitudes compared to the C57BL/6J mice. It appears that the cones are most affected in the A/J strain because all light

intensities for the pure cone response were all significantly reduced and the only a- and b-wave intensity that was significantly decreased was at the 0 Db flash intensity which is the brightest rod response condition and does detect some cone response (Figure 4-7 A, B). Furthermore, the A/J cone ERGs were significantly decreased at all three intensities compared to the C57BL/6J controls (Figure 4-6 C). I also examined OPs in the A/J mice. In the pure rod response ERG there is a difference between the A/J WT and *Clrn1* $^{-/-}$ KO mice (Figure 4-6 D). This may be significant because the OPs are a result of the inner retinal response after synaptic transmission from PR cells. There is no conclusive agreement in the published data that supports which cell types in the inner retina are producing the OPs, but they are generally believed to originate from either amacrine cells, horizontal cells, or the on/off rod cone bipolar cell pathways (209). If OPs do in fact originate in amacrine cells, this would be significant because they are reduced in the *Clrn1* $^{-/-}$ KO mice. I further confirmed the ERG difference previously published in the WT vs *Clrn1* $^{-/-}$ KO A/J mice (217).

As described above, Dr. Imanishi generated a *Clrn1* $^{-/-}$ KO and N48K KI strain on an A/J background that possess an aging mutation allowing for more rapid retinal degeneration over time. The goal was to identify an additional retinal phenotype for the *Clrn1* $^{-/-}$ KO and N48K KI mice. He showed that at 3 and 6 months old the *Clrn1* $^{-/-}$ KO mice have a reduced ERG by approximately 30%, however by 9 months of age the WT mice also have a reduced ERG response similar to *Clrn1* $^{-/-}$ KO levels but there did not appear to be any difference in the WT vs N48K KI mice (217). I validated this difference in ERG amplitudes for the WT vs *Clrn1* $^{-/-}$ KO mice and saw a similar trend, however the KI mice did not have a significant decrease compared to WT at older ages (Figure 4-7).

Abnormal Retained Electroretinogram in N48K Mice

Given the delay in arrestin-1 movement upon exposure to light and the reduced OPs potentially due to problems in the inner retina, I tested for any physiological significance that could be observed i*n vivo*. I performed scotopic ERGs on WT, *Clrn1* $^{-/-}$ KO, and N48K KI A/J mice after the translocation experiment with 1 hour of light exposure at 1000 lux. I found that at the brightest scotopic response of 0 Db, there was a significant difference in that the N48K KI mice still produced a b-wave ERG response (Figure 4-8). I am unsure as to what this response is telling us about a potential mechanism of retinal degeneration over time and how it is relevant to the biological and physiological processes that are occurring. There are a few potential theories that may be playing a role. 1: The N48K KI mice fail to completely suppress rhodopsin signaling as efficiently as WT mice and they therefore still respond to light, which makes sense in terms of the arrestin-1 delay phenotype. 2: N48K KI mice have prolonged synaptic signaling, which also could be related to the arrestin-1 phenotype with it remaining bound to the OPL. 3: N48K KI mice are able to recover rhodopsin signaling more rapidly than WT mice. 4: N48K KI mouse cones respond to lower levels of light compared to WT mice so they are more responsive in the mesopic light range. And finally, 5: N48K KI mice have abnormal communication between the on/off rod-cone bipolar cell signaling processes or their feedback mechanisms with horizontal cells.

Given the complex nature of the cell types in the INL, it is difficult to determine which potential pathway is causative, and it very well may be a combination of several mechanisms. I have considered possibly using synaptic inhibitors to block any potential recovery or collaborating with groups that can perform single cell recordings *ex vivo*.

One other method I did attempt is a dual-flash ERG recovery response, which would possibly show a more detailed difference in ERG recovery over time.

Dual-Flash ERG Recovery Response

For the dual-flash ERG recovery, the flash protocol is defined in Table 4-1 as well as described above. I assessed WT vs N48K KI mixed C57BL/6J albino mice at time-points up to 45 minutes and I did not observe any statistical significance between the WT and KI mice (Figure 4-9). This would perhaps eliminate any dim cone response since the light intensity used was a mesopic mixed rod-cone intensity, however this was performed on the Espion ERG system and not the LKC system as for the previous translocation ERG experiment and this may introduce some variability between the two experiments. The lack of a dual-flash ERG recovery phenotype may also eliminate any abnormal on/off rod-cone bipolar cell signaling because the rods were completely bleached after the extended light exposure, and there was no significant difference in the rods ability to slowly respond to light over time. I was unable to test this on the new A/J strain mice because they are highly sensitive to the anesthesia and are unable to remain anesthetized for the required 1 hour in order to run the experiment.

Light Damage in WT, KO, and KI Mice

Because I found a delay in arrestin-1 translocation upon light exposure, I wished to see if I could induce retinal degeneration after bright light exposure through the use of light damage (223, 224). In order to test if my mice were susceptible to light damage, I first assessed WT mice at a range of light intensities from 1300, 1500, 2000, and 5000 lux as described above. At all light intensities tested using a two-way ANOVA there was significant degeneration post-light damage in the WT mice (Figure 4-10 A, Table 4-2). The most significant damage occurred at 5000 lux, which was expected (Figure 4-10 B,

Table 4-2). At 2000 lux the WT mice did have statistically significant degeneration, particularly in the superior retina, however, they still had a normal scotopic ERG response for both the a- and b-waves and only had a significantly reduced ERG at 5000 lux (Figure 4-10 C, C', D, D', Table 4-2). I therefore chose to analyze the *Clrn1* $^{-/-}$ KO and N48K KI mice at 2000 lux for ONL thickness and scotopic ERG response. After light damage, only the superior retina showed slight degeneration in the *Clrn1* $^{-/-}$ KO mice and the N48K KI mice had significant degeneration furthest from the optic nerve both in the superior and inferior retina (4-11 A, B) (Table 4-3). Interestingly, similarly to the WT mice, the *Clrn1* $^{-/-}$ KO mice did not show any reduction in scotopic ERG amplitude post light damage for either the a- or b-waves (Figure 4-11 C, C'). This may not be the most reliable results because the *Clrn1* $^{-/-}$ KO mice already have a reduced b-wave at 6 months old and they would therefore not necessarily show any significant difference since their ERG responses are already reduced without an treatment (Figure 4-11 C').

When I assayed for light damage on the N48K KI mice, I saw a significant decrease in scotopic ERG amplitudes for both the a- and b-waves for all light intensities (Figure 4-11 D, D'). This is intriguing because unlike the WT and *Clrn1* $^{-/-}$ KO mice, the N48K KI mice are the only ones that display any significant loss of function following light damage. This can provide us with an additional phenotype to utilize in order to validate our AAV gene therapy vectors for an effective therapeutic treatment.

Given there is a significant decrease in N48K KI ERG after light damage and a maintained ERG after bright light exposure, there may be an underlying mechanism that is affected by both light conditions. The combination of these two experiments may be able to explain why patients do not lose vision initially, but go blind over a prolonged

period of time. This suggests the rate of vision loss may be related to the amount and level of light exposure over time. Perhaps initially PR cells can handle a minimal amount of light induced stress, but there is a limit above which continued stress to the PR-RPE visual system leads to PR degeneration. I can further test the Clrn1 $^{-/-}$ KO and N48K KI mice for pre-conditioning prior to light damage which would be to expose the mice to a low level of light for one week prior to light damage to see if the loss of ONL thickness and ERG function can be reduced. This would allow me to assess whether the N48K KI mice have any abnormal neuroprotective features compared to the WT and Clrn1 $^{-/-}$ KO mice because they have a significantly reduced ERG response after light damage.

One complication with the A/J mouse strain is that they were shown to have abnormal RPE function and undergo retinal degeneration as they age. Therefore the strain itself may possibly be more susceptible to light damage due to background RPE complications. The A/J mice have extensive inflammatory changes as they age with an increase of immune cell infiltrates in the retina which can have an impact on the rate of retinal degeneration due to light damage. Dr. Palczewski's group showed in RPE flat-mounts that the majority of RPE cells were multi-nucleated with an abnormally large cell size, indicating that the RPE cells were unhealthy and undergoing senescence (160).

Table 4-1. Dual-flash ERG recovery response

Steps	Flash Intensity ($cd.s/m^2$)	Interval Between Two Flashes	Adaptation Time
1	1	0 ms	30 s
2	1	25 ms	30 s
3	1	50 ms	30 s
4	1	100 ms	30 s
5	1	250 ms	30 s
6	1	500 ms	30 s
7	1	750 ms	30 s
8	1	1 s	30 s
9	1	2 s	30 s
10	1	4 s	30 s
11	1	16 s	30 s

N = 5 at 3 months old for all genotypes

Table 4-2. Two-way ANOVA for WT light damage range of intensities

Distance from Optic Nerve (um)	Light Damage Brightness Intensity 1300 lux	1500 lux	2000 lux	5000 lux
-600 um	ns	p < 0.05 *	ns	p < 0.0001 ****
-450 um	ns	ns	ns	p < 0.0001 ****
-300 um	ns	p < 0.01 **	p < 0.05 *	p < 0.0001 ****
-150 um	p < 0.05 *	p < 0.0001 ****	p < 0.0001 ****	p < 0.0001 ****
0 um	ns	ns	ns	ns
150 um	p < 0.05 *	p < 0.0001 ****	p < 0.0001 ****	p < 0.0001 ****
300 um	p < 0.05 *	p < 0.01 **	p < 0.0001 ****	p < 0.0001 ****
450 um	ns	p < 0.01 **	p < 0.0001 ****	p < 0.0001 ****
600 um	p < 0.001 ***	p < 0.0001 ****	p < 0.0001 ****	p < 0.0001 ****

N = 4 for all light intensities

Table 4-3. Two-way ANOVA in *Clarin-1* KO and N48K KI mice, 2000 lux light damage

Distance from Optic Nerve (um)	Clrn1 -/- KO	N48K KI
-600 um	ns	p < 0.001 ***
-450 um	ns	p < 0.0001 ****
-300 um	ns	p < 0.001 ***
-150 um	ns	ns
0 um	ns	ns
150 um	ns	ns
300 um	p < 0.05 *	p < 0.01 **
450 um	p < 0.001 ***	p < 0.01 **
600 um	ns	p < 0.0001 ****

N = 10 for all light intensities

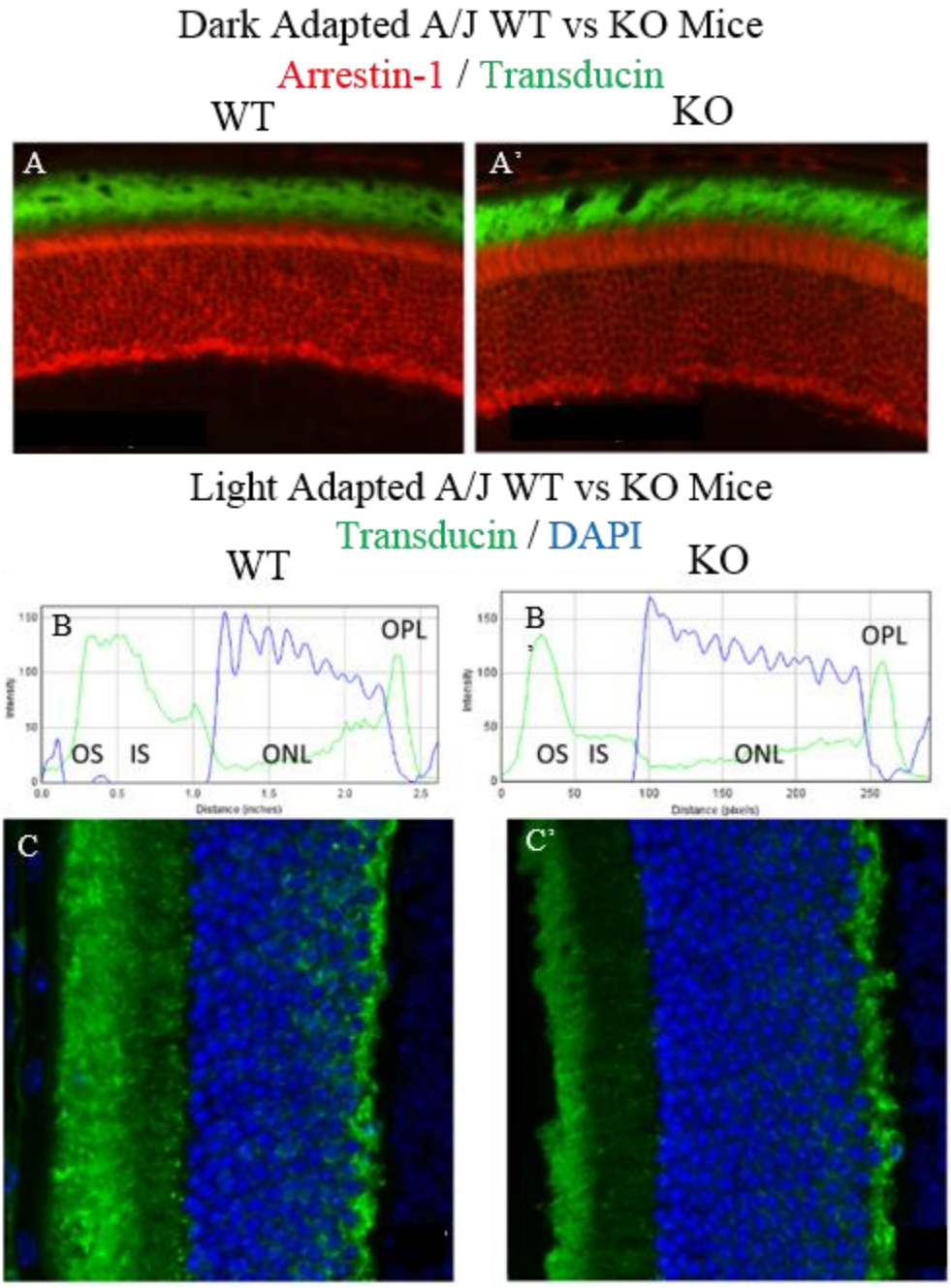

Figure 4-1. Normal localization of arrestin-1 and transducin. A, A') Normal dark-adapted localization of arrestin-1 and transducin in WT and *Clrn1* $^{-/-}$ KO A/J mice. Goat-488-anti-rabbit-transducin and Goat-594-anti-mouse-arrestin-1. B, B') Fluorescence intensity plots of transducin in WT vs *Clrn1* $^{-/-}$ KO A/J mice after 1 hour light exposure at 1000 lux. Goat-488-anti-rabbit-transducin and DAPI-358 VectaShield. C, C') Representative immunohistochemistry of light-adapted transducin localization in WT vs *Clrn1* $^{-/-}$ KO A/J mice. Goat-488-anti-rabbit-transducin and DAPI-358-vectashield.

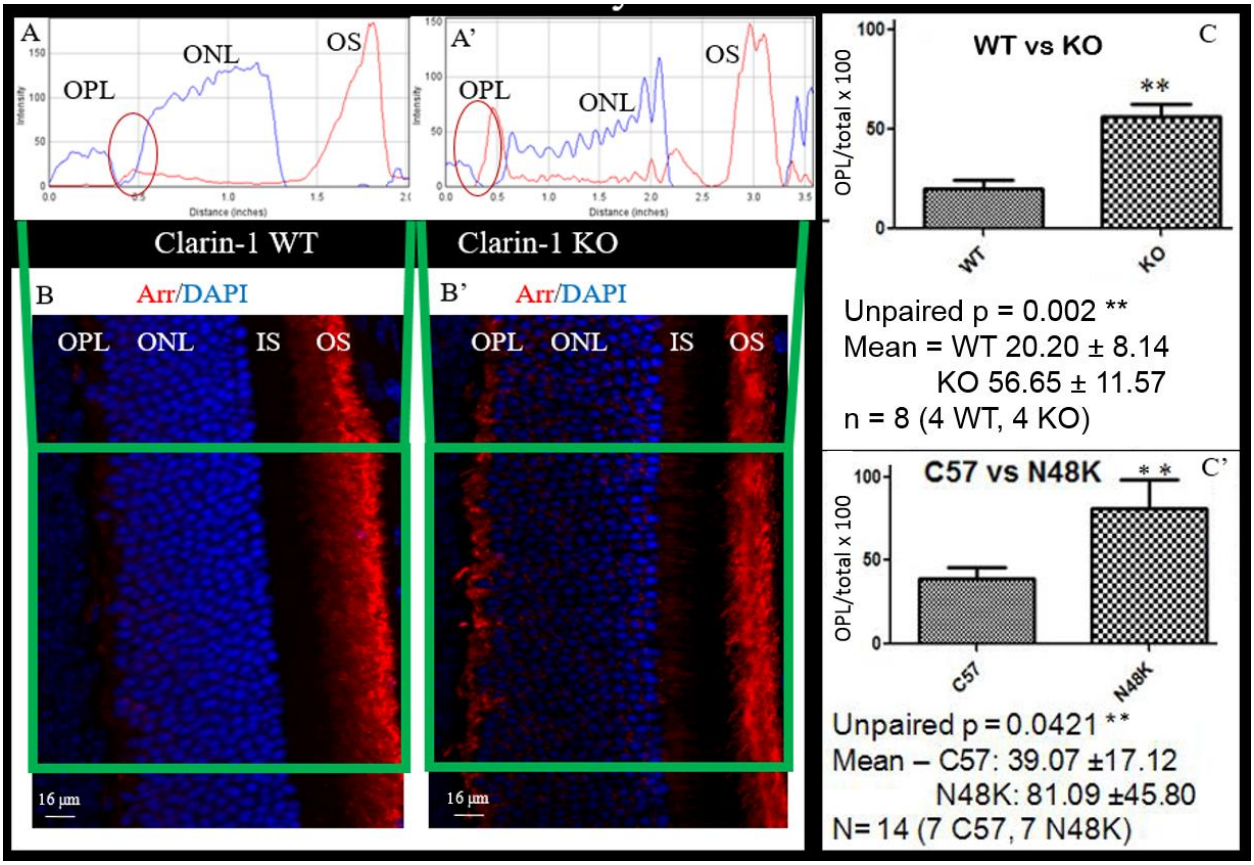

Figure 4-2. Immunofluorescence and quantification of arrestin-1 in light-adapted *Clarin-1* KO and WT retinal sections. A, A') Corresponding profiles of fluorescent signal intensity scanned across the photoreceptor layer. There is a significant amount of increased arrestin-1 signal in the OPL of *Clrn1* $^{-/-}$ KO mice (A') compared to WT OPL (A). B, B') Immunohistochemistry of arrestin-1 distribution after light exposure translocation. Nuclei are stained blue with DAPI. B) WT immunohistochemistry. B') *Clrn1* $^{-/-}$ KO immunohistochemistry. C) Bar graph showing the relative signal intensities of arrestin-1 in the OPL of Clrn1 $^{-/-}$ KO and WT mice, expressed as a percentage of the total signal intensity in the photoreceptor layer, shown for both *Clrn1* $^{-/-}$ KO and N48K KI mice (**p<0.01). C') Bar graph showing the relative signal intensities of arrestin-1 in the OPL of N48K KI and WT mice, expressed as a percentage of the total signal intensity in the photoreceptor layer, shown for both *Clrn1* $^{-/-}$ KO and N48K KI mice (**p<0.01). Similar staining was seen for both the mixed C57BL/6J albino strain and the A/J strain.

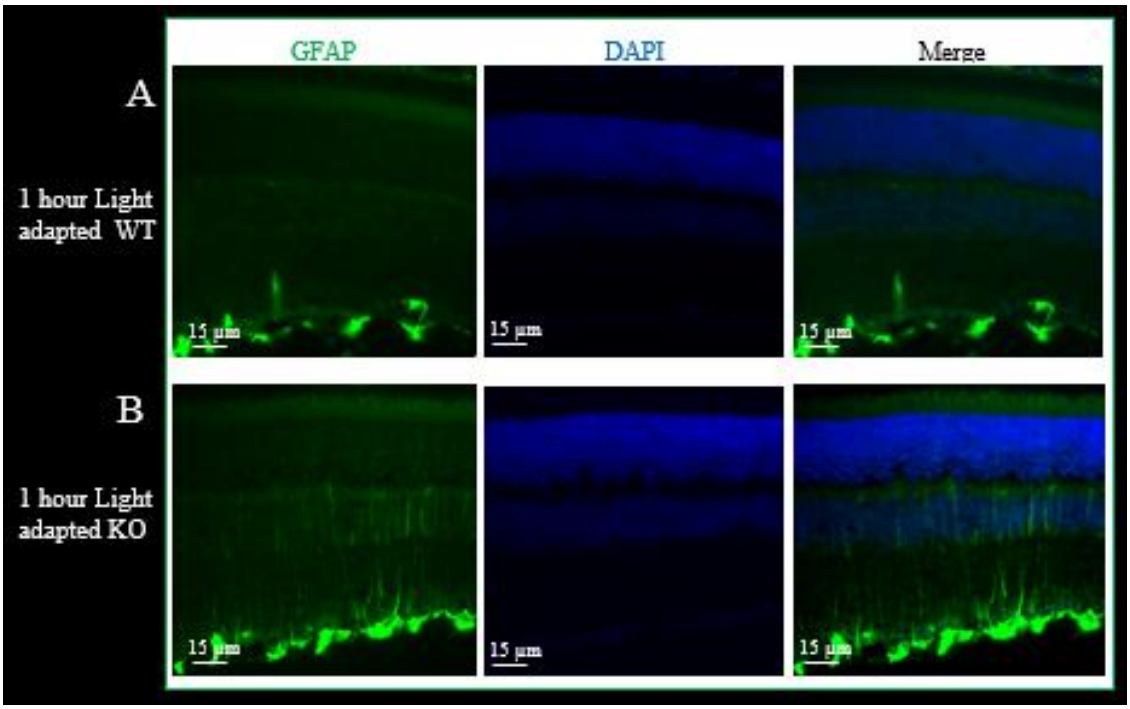

Figure 4-3. GFAP expression in WT vs *Clarin-1* KO C57BL/6J mixed albino mice. A) Representative WT staining of GFAP. The staining appears to have relatively minimal GFAP expression. B) Representative *Clrn1* $^{-/-}$ KO staining of GFAP. The staining appears to be relatively similar to the WT mice with perhaps a slight upregulation of GFAP expression, but it is not significantly higher across multiple samples.

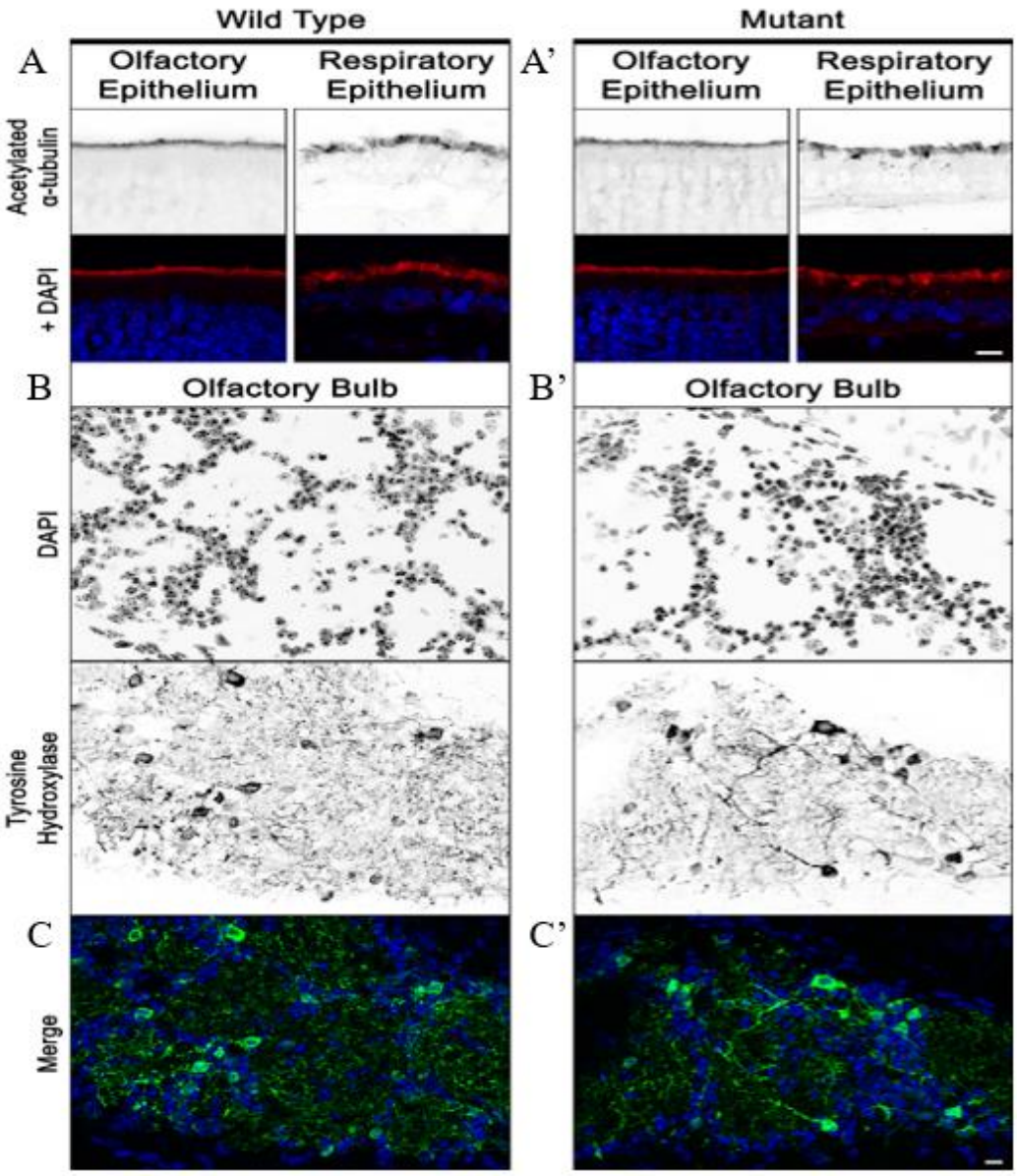

Figure 4-4. Normal olfactory structure in both WT and N48K KI A/J mice. A) WT olfactory and respiratory epithelium. A') N48K KI olfactory and respiratory epithelium. Disruption of CLRN1 does not affect cilia formation in the nasal cavity. Representative confocal images of olfactory and respiratory epithelium from 7 month-old control and mutant mice stained with the ciliary axoneme marker acetylated α-tubulin. Scale, 10 μm. B) WT olfactory signaling. B') N48K KI olfactory signaling. There is normal active olfactory signaling in CLRN1 WT and N48K KI mice. Representative confocal images of olfactory bulb glomeruli from WT and N48K KI mice stained with tyrosine hydroxylase. Tyrosine hydroxylase is present in juxtaglomerular cells innervating glomeruli of control and CLRN1 mutants, indicative of active olfactory signaling. Scale, 10 μm. C, C') Merged images of DAPI and tyrosine hydroxylase.

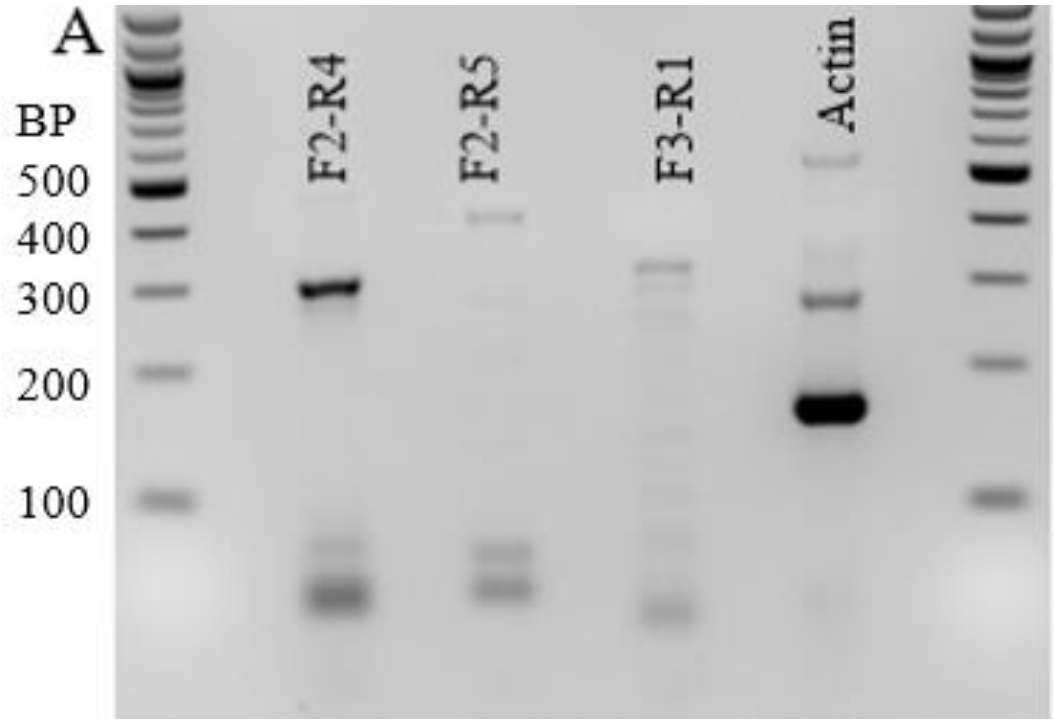

Figure 4-5. RT-PCR of WT A/J olfactory epithelial tissue lysates. A) There is a PCR product for all three primer sets from olfactory epithelial lysates. F2-R4 can pick up the 250 AA isoform of *Clrn1*. F2-R5 can pick up isoform 1 and 2, and F3-R1 can pick up all three isoforms.

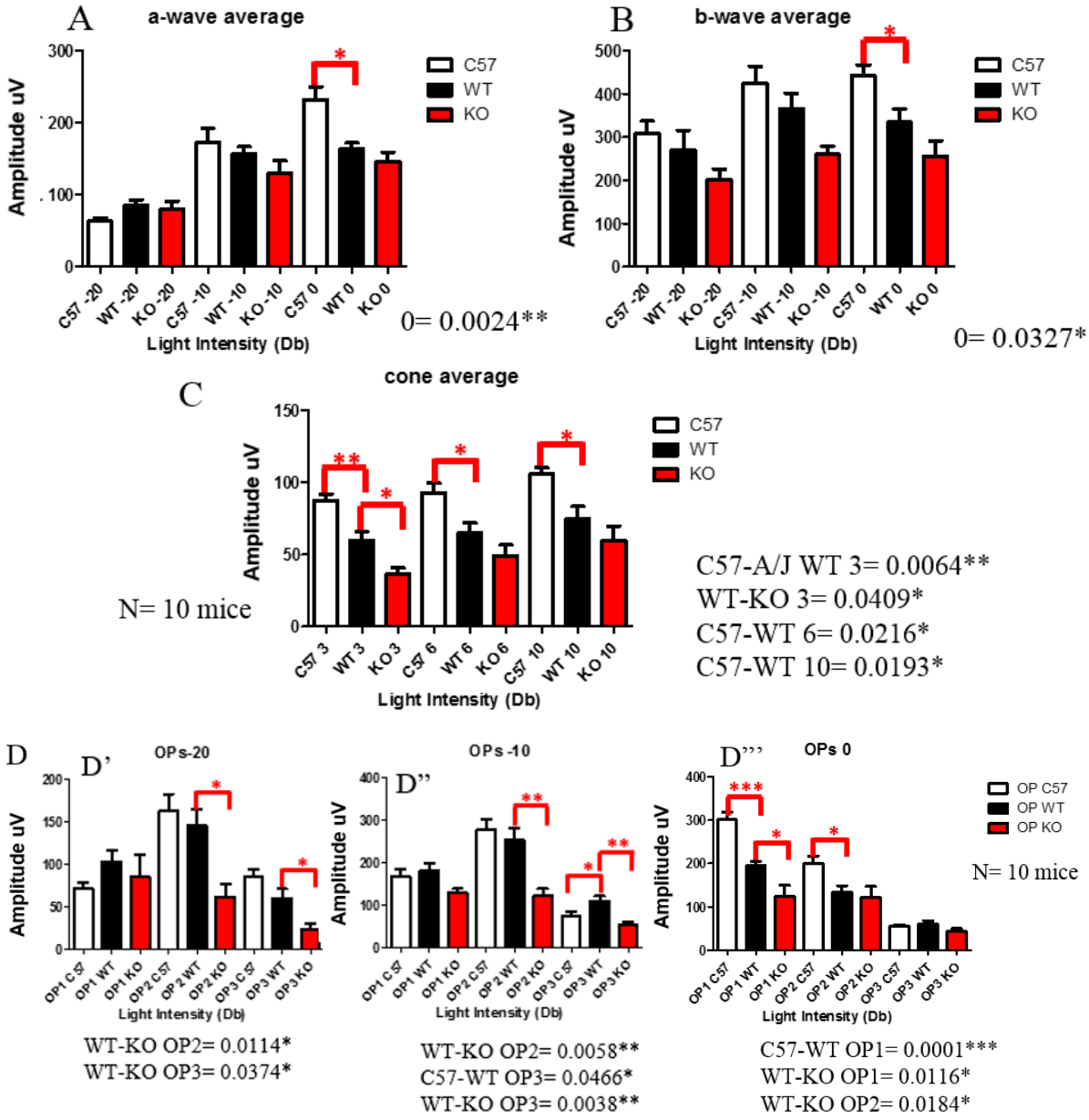

Figure 4-6. ERG difference in C57BL/6J vs WT and *Clarin-1* KO A/J mice. White bars are C57BL/6J mice, black bars are WT A/J mice, and red bars are *Clrn1* $^{-/-}$ KO A/J mice. A) a-wave ERG, 0 Db is significantly decreased in A/J mice. B) b-wave ERG, 0 Db is significantly decreased in A/J mice. C) Cone ERG, all light intensities are decreased in A/J vs C57BL/6J mice and 0 Db is decreased in A/J WT vs *Clrn1* $^{-/-}$ KO mice. D) Oscillatory potentials in C57BL/6J vs A/J mice. Only the 0 Db OP1 is decreased in C57BL/6J vs A/J mice and all light intensities have reduced OPs in WT vs *Clrn1* $^{-/-}$ KO A/J mice.

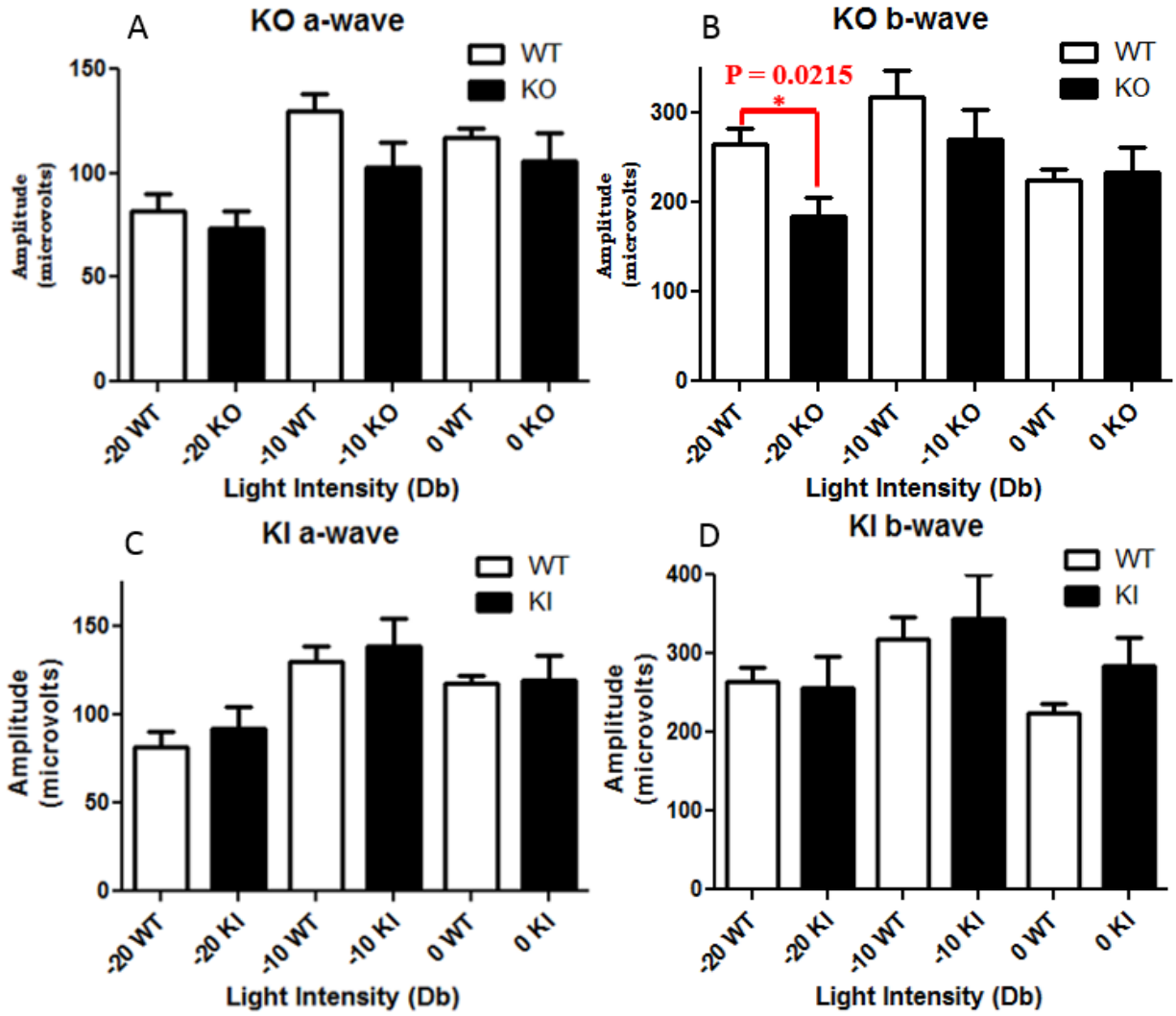

Figure 4-7. Validation of the ERG phenotype in A/J *Clarin-1* KO mice. A) WT vs *Clrn1* $^{-/-}$ KO normal scotopic a-wave ERG response. B) WT vs *Clrn1* $^{-/-}$ KO abnormal scotopic b-wave ERG response. C) WT vs N48K KI normal scotopic a-wave ERG response. D) WT vs N48K KI normal scotopic b-wave ERG response.

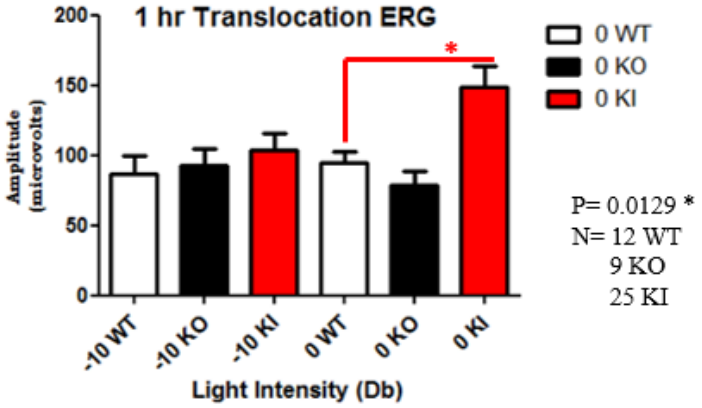

Figure 4-8. ERG phenotype post 1 hour light exposure in the N48K KI mice. After 1 hour of light exposure at 1000 lux, the N48K KI mice are still able to generate an ERG response at a 0 Db light intensity.

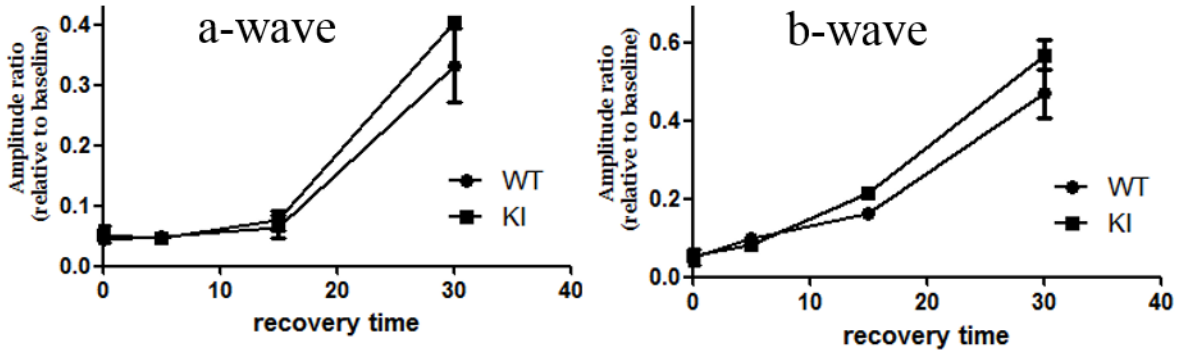

N=3 at 4 months old

Figure 4-9. Dual flash ERG recovery response in the N48K KI mice. a- and b-wave recovery ERG response after light exposure. There is no significant difference in either a- or b-wave ERG between WT and N48K KI mice.

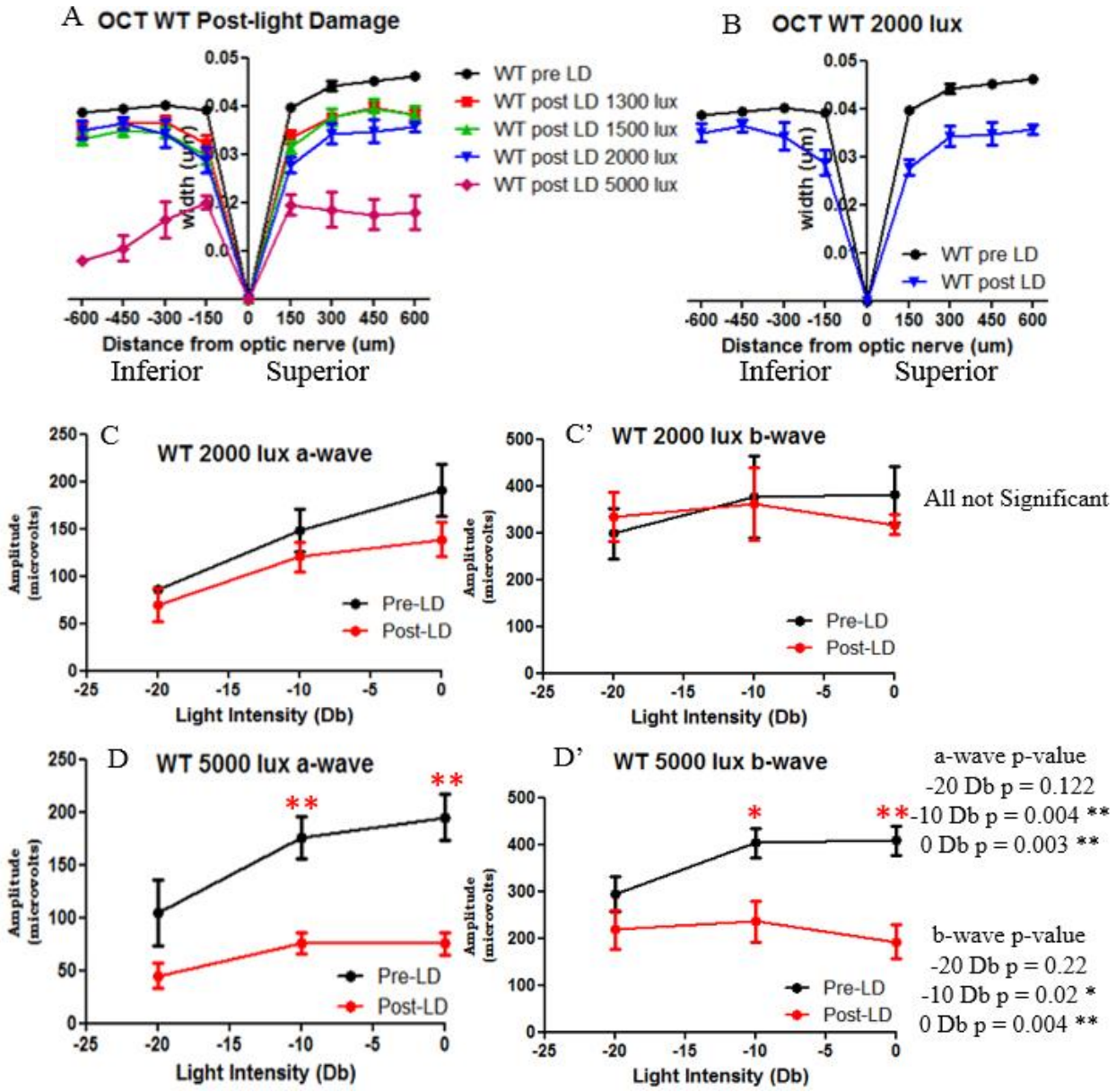

Figure 4-10. Light damage optimization in WT A/J mice. A) Comparison of light damage in A/J WT mice at varying light intensities using SD-OCT. There is minimal difference in loss of PR cells between untreated controls, 1300, 1500, or 2000 lux intensities of light. The only extreme difference is between WT untreated vs 5000 lux of light. B) Comparison of untreated control vs 2000 lux treated WT mice. C) WT scotopic a-wave and C') b-wave ERG after 2000 lux light damage, there is no significant decrease in ERG amplitude after 4 hours of light exposure at 2000 lux. D) WT scotopic a-wave and D') b-wave ERG after 5000 lux light damage, there is a significant decrease in ERG amplitude after 4 hours of light exposure at 5000 lux.

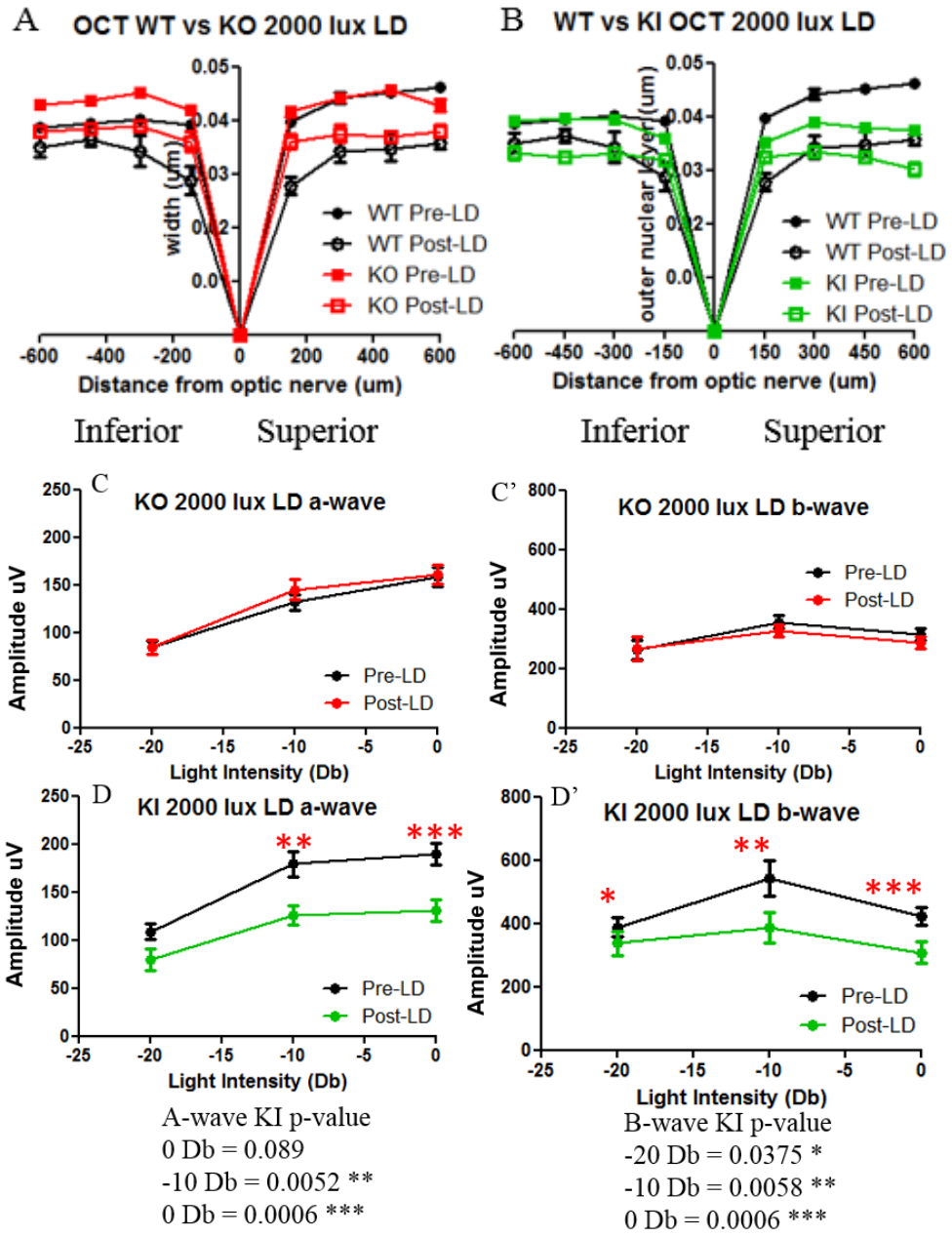

Figure 4-11. SD-OCT and ERG in *Clarin-1* KO vs N48K KI A/J mice pre- vs post-light damage. A) *Clrn1* $^{-/-}$ KO and B) N48K KI ONL thickness pre- and post-light damage at 2000 lux. There is a significant decrease in both genotypes post-light damage, mostly in the superior retina for the *Clrn1* $^{-/-}$ KO mice and farthest from the optic nerve in both the superior and inferior retina in the N48K KI mice. C, C') *Clrn1* $^{-/-}$ KO a- and b-wave ERG. There is no significant difference between pre- vs post-light damage. B, B') N48K KI a-wave ERG. There is a significant difference between pre- vs post-light damage for -10 and 0 Db. C, C') N48K KI b-wave ERG. There is a significant difference between pre- vs post-light damage for all scotopic light intensities.

CHAPTER 5
ASSAYING FOR PHENOTYPIC RESCUE USING AAV-MEDIATED GENE THERAPY*

Background

In order to develop a successful gene therapy treatment, the serotype, capsid mutation(s), promoter, and cDNA, targeted to the desired cell type, need to be optimized in order to avoid toxicity and achieve optimal expression levels. This can be highly variable based on the promoter, gene of interest, and fluorescent tags within the AAV plasmid. There is further variability of many different AAV capsid serotypes and additional capsid mutations allowing for greater cell specificity and transduction efficiency in the retina. All of these are elements that need to be considered in order to design a successful gene therapy treatment for USH3A. Previously, Dr. Cosgrove showed delays in transducin movement upon exposure to light in Myo7A and whirlin mice compared to WT controls, and they further showed that lentiviral delivery of WT MYO7A can rescue the transducin translocation phenotype (176, 219, 240). Given that my data is similar to Dr. Cosgrove's, I hypothesized that I could also rescue the arrestin-1 translocation phenotype using an AAV-mediated delivery of *CLRN1* to the retina.

Adeno-Associated virus

AAV is the most prevalent method of viral gene therapy to date and has also had the most clinical success to date, particularly in the retina. AAV is a non-pathogenic parvovirus that can infect both dividing and non-dividing cells. AAV has the smallest packaging capacity of all the viral vectors with a maximum DNA size of only about 5kb. The AAV genome is a linear single strand of DNA that consists of two reading frames

* Reprinted with permission from Dinculescu A and Stupay RM et al. AAV-Mediated Clarin-1 Expression in the Mouse Retina: Implications for USH3A Gene Therapy. PLoS One 2016.11(2):e0148874.

containing the replication and capsid coding genes. There are 3 transcriptional initiation sites that control expression for 4 replication proteins. There are 3 capsid proteins that are composed of two smaller proteins (VP1 and VP2) and one larger protein (VP3). These capsid proteins are in a ratio of 1:1:10, with VP3 being the most abundant. Flanking these sequences are the inverted terminal repeat sequences that are necessary for replication and packaging (66, 108). The AAV constructs employed for gene therapy have all of the replication and capsid genes removed so that all that remains are the inverted terminal repeat sequences for packaging, in addition to a promoter, enhancers, gene of interest, and a polyadenylation addition sequence that are inserted between the inverted terminal repeats (108). For my AAV gene therapy, there are two primary backbones that I have utilized, a pTR vector and a self-complimentary (sc) vector. The pTR vector is a single stranded vector that requires the cellular machinery for second strand DNA synthesis and therefore expresses the gene of interest relatively slowly at lower levels initially. The sc vector is able to fold onto itself resulting in a double stranded DNA molecule immediately upon cellular infection. This allows for rapid transcription and expression of the gene (cDNA) of interest (66).

Serotypes and Modifications

Multiple different capsid serotypes have been identified, as well as multiple different capsid-serotype-specific mutations that have optimized the AAV vectors for better cell type-specific infection. There have also been many studies looking at the success of AAV-mediated gene therapy in the retina and the optimization of targeting specific cell types with different capsid mutants. The initial studies in the 1990's looked at a simple AAV2 capsid serotype injected into the subretinal space. Using a rod opsin promoter driving a synthetic GFP protein, they saw exclusive expression in PR cells

with 20% pan-retinal expression and 100% expression at the site of injection (83). They further validated that their recombinant AAV viral preps were free of Adenovirus and WT AAV (83). Subsequent retinal gene therapy studies in the early 2000's examined cell-type specific infection after subretinal and intravitreal injection as well as long term expression, stability, and toxicity (71, 104, 108, 222). These studies initiated the development of successful gene replacement therapies for several animal models of retinitis pigmentosa. The AAV2 capsid utilizes several charged surface residues that are responsible for AAV2 binding to its heparin sulfate receptor and allows for entry into the cell. One complication with the AAV2 capsid is that on the capsid surface there are many tyrosine residues that can be phosphorylated and therefore target the viral particle for ubiquitination and degradation within the cell (179). Site specific mutation of these tyrosine residues, specifically in the VP3 region of the capsid surface, allow for AAV vectors to avoid degradation and achieve higher transduction efficiency (128, 179, 197).

The initial capsid mutations studied were single point mutations in the tyrosine residues on the AAV capsid surface for the AAV2, 8 and 9 serotypes (180). Further studies looked at the efficacy of combining multiple capsid mutations in different combinations of tyrosine to phenylalanine both after subretinal and intravitreal delivery. They showed that multiple combinations of tyrosine-phenylalanine (Y-F) mutants displayed pan-retinal expression of an AAV2-GFP injected virus (179, 180). Upon immunohistochemistry analysis, there was differential expression with each capsid mutation from only PR cells to expression in all retinal cell types after subretinal delivery. In contrast, after intravitreal delivery, the majority of viral expression was present in retinal ganglion cells for all capsid mutations analyzed, with only two

appearing to successfully target PR cells after an intravitreal delivery (179, 180). A subsequent study examined un-modified or modified capsid mutants for serotypes AAV1, 2, 5, and 8 in RPE cell and 661W cone cell retinal cultures to assess for which additional mutations may be optimal (197). Vector expressed protein was detected by FACS sorting for both cell lines and it was found that the addition of Y-F mutations increased the transduction efficiency (197). These capsid mutations were further tested *in vivo* to test which mutations would be optimal for intravitreal injection in order to avoid any surgical damage from subretinal injection. Additional threonine to valine (T-V) mutations were examined as well. It was found that the previously identified AAV2-Quadruple mutant with an additional T-V mutation at aa 491 worked the best for intravitreal injection and produced the highest level of transduced PR cells across the retina (128). This vector is described in the Methods below. Similar studies have been done looking at systemic delivery to the retina using various AAV9 capsid mutations in dogs (33, 34, 60-62). For this study however, the two mutants I have focused on are the AAV2 Quad Y-F and AAV2-Quad-T491V vectors in addition to WT AAV2 capsid.

Methods

Clrn1 $^{-/-}$ KO and N48K KI mice were generated as described above (87, 88, 217). Animals were housed and maintained as noted previously. The AAV viral vectors were generated and purified as previously reported and viral titers was measured by real time-PCR (103, 115, 245). All viruses that were tested here are listed in table 5-1 with their capsid serotype and mutations, vector construct, and viral titer listed. The AAV2 Quadruple mutant contains 4 tyrosine to phenylalanine mutations at residues Y-F 272, 444, 500, and 730 (AAV2-Quad). The second mutant utilized was the AAV2-Quad capsid with an additional tyrosine to valine mutation at aa 491 (AAV2-Quad-T491V).

Either a ubiquitous smCBA (small chicken β-actin) or a PR specific GRK1 (G-protein receptor kinase 1) promoter was used for all experiments. For direct vector product visualization, either a C-terminal Venus-tagged human CLRN-1 (CLRN1-Venus, from Dr. Imanishi at Case Western University) or a hemagglutinin (HA)-tagged CLRN1 was used for all experiments. Both subretinal and intravitreal injections were performed as previously described (179, 180). Briefly, a 30.5 gauge needle was used to pierce the nasal side of the cornea and a Hamilton syringe with a 33 gauge needle was used to inject the virus into the eye. Subretinal injections used a blunt-tip needle to deposit the virus into the subretinal space between the RPE and PR cells, and intravitreal injections used a 45^{o} beveled tip needle to deposit the virus into the vitreous space. All eyes were injected with 1 ul of viral vector and the associated vector genome copies/ ml are defined in table 5-1 for each. Right eyes were injected and left eyes remained un-injected. C57BL/6J mice were tested with buffer alone in the right eye to assess any damage resulting from the injection procedure. Intravitreal and subretinal vectors at a 1: 1000 dilution of CBA and GRK *CLRN1* were also tested in right eyes against and buffer alone in left eyes further minimize any variability due to injection damage (data not shown). For vector toxicity assays, right eyes received dilutions of one microliter of either a full strength titer of approximately 10^{13} vector genome/ml (vg/mL) or serially diluted vectors of 10^{12}, 10^{11}, or 10^{10} vg/mL in the right eye. All treated mouse eyes were first documented for PR function by ERG and for retinal structure by OCT at 4 months post-injection with several were analyzed up to 1 year post-injection. Later experiments were also analyzed by OCT at 1 week post-injection to verify there was no injection damage prior to ERG analysis. At 1 month CLRN1-Venus and CLRN1-HA were visible

by immunohistochemistry using an anti-GFP or anti-HA antibodies (3F10, Roche Diagnostics, Indianapolis, IN). ERG, OCT, translocation, and immunohistochemistry experiments were performed as described above. Differences in maximum a- and b-wave amplitudes between injected and un-injected eyes were analyzed by the Student t test (GraphPad Prism 6.0, GraphPad Software, San Diego, CA), and were considered statistically significant if $p<0.05$ or less. All ERG amplitudes are presented as mean ± SEM. All tissue samples were processed and stained as described above.

Results

AAV-Delivered Clarin-1 Retinal Localization

I first wanted to assess AAV-CLRN1 localization in a subretinal vs intravitreal vector delivery to see which cell types express AAV injected CLRN1. For subretinal injection, vector construct 3, Table 5-1 was delivered subretinally to WT C57BL/6J mice, retinal sections were obtained at 1-month post-injection, and sections were imaged on a spinning disc confocal microscope as described above (72). Sc-smCBA-CLRN1-Venus localization was seen primarily in PR cells but also in RPE cells (Figure 5-1 A) with significant CLRN1-Venus expression throughout the PR cell body, particularly in the IS and some punctate staining at the CC. For intravitreal injections, vector construct 4, Table 5-1 was delivered intravitreally to WT C57BL/6J mice and analyzed the same as subretinal injections. CLRN1-Venus expression was seen in all retinal cell types except for RPE cells with the majority of AAV-CLRN1 expression in the inner retina and GCL. There appeared to be significant expression in Müller cells, particularly in their apical microvilli adjacent to the OLM (Figure 5-1 B) (72) with limited expression in PR cells, unlike the subretinal injection expression. Given that we believe Clrn1 is expressed in PR cells, it seems the optimal delivery method would be a subretinal injection, however,

a complication with this method is the risk of potential damage from injection due to the obligate retinal detachment. The previous human clinical trials have seen this post-injection, particularly if the injection is delivered close to the fovea (46-49, 102, 117). Because mice lack a fovea, this is not an issue for these preliminary studies.

Although the CLRN1-Venus construct allowed me to see where virally expressed protein was localized, a Venus-tagged construct is inappropriate for a gene therapy treatment in the clinic. Therefore, I designed an AAV construct replacing the Venus tag with an HA tag (Construct 1 Table 5-1). Ideally no additional tags should be on the injected construct in order to take the vector into the clinic, but prior to this study there was not an optimal antibody that could recognize endogenous or injected Clrn1/CLRN1 in the retina. By using an HA-tag I can assess if there is any toxicity when there is no interference with the PDZ binding domain. Additionally, now that I have identified an antibody that recognizes Clrn1 in WT, Clrn1 $^{-/-}$ KO, and N48K KI mice, I can generate an AAV construct without any tags so that it can be optimized for the clinic.

When I tested this new HA-tagged vector subretinally, I see similar significant expression in PR and RPE cells (Figure 5-2 A, B). Interestingly, there appeared to be significant cell death near the injection site, where the viral bleb was administered, and this cell toxicity was reduced towards the periphery of the retina (Figure 5-2 B, C). This suggests that the full viral titer is toxic to the retina using an HA-tagged CLRN1 construct. This is most likely because Clrn1 is normally expressed at very low levels in the retina, thus excess CLRN1 is likely toxic. I believe that the reason why I do not see this toxicity with a subretinally delivered CLRN1-Venus construct is that there is a PDZ-binding domain on the CT tail of CLRN1 and this is where both tags were placed. The

Venus tag is very large and most likely masks the binding ability of the PDZ domain, whereas the HA tag is very small, only 10 aa, and therefore leaves the PDZ binding domain open to interactions. This would lead to copious amounts of functional CLRN1 protein in the cell and most likely leads to the observed toxic effect. In addition to the large amounts of CLRN1 protein, CBA-CLRN1-HA is also expressed in the RPE cells, where Clrn1 is not normally expressed, and this may be a contributing factor to the toxicity because Clrn1 is a transmembrane protein and its membrane localization may interfere with the normal function of the RPE microvilli. Given that I cannot utilize the Venus-tagged construct for a gene therapy treatment, and that the HA-tagged construct is extremely toxic, I needed to optimize the HA-construct in order to minimize the toxicity or optimize an intravitreal delivery vector to target PR cells.

Optimized AAV Vector Capsid, Promoter, and Titer for Safe and Effective Gene Therapy

Initially, constructs 7 and 8 Table 5-1 were tested in C57BL/6J WT control mice following subretinal or intravitreal injection, to assess whether the toxicity could be reduced using a less potent AAV serotype, a simple AAV2 capsid. Although I did see expression via a subretinal injection, there was almost no expression at all with the intravitreal injection. Therefore, I chose to optimize for minimal toxicity using the original HA-tagged vector, construct 1 Table 5-1. As noted above, using a full viral titer of 8.43 x 10^{12} vg/ml, I saw significant PR cell loss via immunohistochemistry as well as a significant loss of PR cell function via ERG analysis (Figure 5-3 A, A'). I then assessed reduced viral titers sequentially to a 1:1000 dilution at 8.43 x 10^{9} vg/ml. The only dilution that did not show significant cell death or loss of function was the 1:1000 dilution dose (Figure 5-3 B', B) (Figure 5-4) (72). I next compared PR cell function by ERG analysis

after a full titer subretinal injection and a full titer intravitreal injection. Similar to the 1:1000 subretinal injection, intravitreal injection did not show any functional loss in ERG amplitude in injected vs un-injected eyes (Figure 5-5 A, B). Using immunohistochemistry for CLRN1-HA in the intravitreally treated mice, there seemed to be ample expression in all retinal cell types as seen previously, but it appears to preferentially target Müller cells and RGCs (Figure 5-5 C, C', C") (72). This is a complication because I believe that Clrn1 should be expressed in PR cells and they do not appear to be targeted via an intravitreal injection with the CBA promoter. Because of this, I wanted to first optimize for toxicity and optimize for intravitreal delivery to target PR cells.

Given the initial constructs are under a ubiquitous CBA promoter, I also wanted to see if the subretinal toxicity could be mediated by using a photoreceptor-specific GRK1 promoter, with construct 10 Table 5-1 injected in WT C57BL/6J mice. I also tested construct 11 Table 5-1 intravitreally to assess if I can both target PR cells specifically and avoid toxicity from the subretinal injection. First, using OCT analysis, I assessed the amount of PR cell loss *in vivo* prior to ERG functional analysis. Using a full titer virus, there was a significant loss of PR cells in the retina at the injection site, and cell loss was not observed in the half of the retina not receiving vector. However, there was extensive thickening of the ILM and nerve fiber layer (Figure 5-6 A, A'). At 3 months post-injection, there was significant degeneration in the retinal periphery at a 1:10 dilution of 2.1×10^{11} vg/ml, which correlated with the injection site (Figure 5-6 B, B'). I did not see any significant degeneration at a 1:100 dilution at 3 months post-injection, but there was thickening of the ILM and nerve fiber layer and there was no significant retinal damage in the mice that were treated intravitreally (Figure 5-6 C, C').

I next assessed functional loss via ERG analysis in all subretinal dilutions as well as for intravitreal injections. Given the extensive retinal degeneration with full titer injections, they were excluded from ERG analysis. Similar to the CBA promoter constructs, the full titer, as well as a 1:10 dilution at 2.1 x 10^{11} vg/ml of subretinal GRK1-*CLRN1*-HA vector exhibited a significant loss of function by ERG analysis of both the a- and b-wave amplitudes compared to un-injected eyes (Figure 5-7 A, B). When I tested the same AAV2-Quad-Y-F-GRK1-*CLRN1*-HA vector using an intravitreal injection I saw no significant reduction in either the a- or b-wave amplitudes (Figure 5-7 C). I still have significant CLRN1-HA expression even at a subretinal 1:1000 vector dilution, suggesting there is sufficient CLRN1 expression even at low vector dose levels. Given these results, it seems that a 1:1000 dilution is optimal for either the CBA or GRK1 promoter vectors (Figure 5-8 A, A', A"). At 8 months post-treatment there is still significant GRK1-CLRN1-HA expression in PR cells and there is no significant cell loss.

When I assess the scotopic ERG response at 10 months of age, however, there is a significant loss of ERG amplitude for all light intensities both for the a- and b-wave responses (Figure 5-8 B, C). This indicates that there is still some toxicity over time with the 1:1000 dilution of subretinal GRK1-CLRN1-HA in control C57BL/6J mice. Unfortunately, even though intravitreal GRK1-CLRN1-HA injected retinas do not degenerate or have a decrease in ERG response, I was unable to detect CLRN1-HA using immunohistochemistry in these retinas. This may be due to low levels of protein being expressed through the intravitreal vector delivery route because the intravitreal vector at this dose cannot penetrate to PR cells efficiently enough to detect expression. I additionally tested a novel AAV2 serotype that contains an additional mutation that

changes a threonine to a valine and has been shown to allow greater transduction efficiency across the retina (AAV2-Quad-Y-F-T491V) (27, 28, 128, 197). Even with the additional modification to the viral capsid, I am still unable to detect any anti-CLRN1-HA staining post-injection and it remains unclear why this is the case. Moving forward in terms of a gene therapy treatment, it seems that either the CBA intravitreal route or the 1:1000 CBA or GRK subretinal route are the best current options.

Gene Therapy Rescue of Clarin1 Retinal Phenotypes

Given my studies on identifying an optimal AAV CLRN1 vector design for gene therapy, I first tested the AAV2-Quad-Y-F-smCBA-*CLRN1*-HA construct after an intravitreal injection and looked at the arrestin-1 translocation phenotype 1 month post-injection in the original mixed C57BL/6J albino mouse strain. I performed the translocation assay as described in Chapter 4 and mice were analyzed as described previously (Figure 4-2) (72). Looking at the initial immunohistochemistry analysis, there did appear to be some decrease in arrestin-1 miss-localization after light exposure in the N48K KI mice, however this was not very consistent across samples (Figure 5-9 A, A'). This was quantified in the fluorescence intensity plots as previously described and the overall ratio of OS/OPL x100 was calculated for all mice (Figure 5-9 B, B') (71). After averaging all mice assayed for all genotypes, surprisingly the N48K KI mice no longer had a significantly higher amount of arrestin-1 in the OPL compared to WT mice. However, the percentage of arrestin-1 in the OPL is not significantly different from the untreated N48K KI retinas (Figure 5-9 C). There is also the problem of antigen masking because there is so much viral expression in the OPL post-injection, which makes it possible that I am not picking up all of the arrestin-1 protein because the antibody

cannot bind. When I compare the WT to the Clrn1 $^{-/-}$ KO mice, there did not appear to be any potential rescue of the arrestin-1 translocation phenotype (Figure 5-9 D).

I next assessed the potential to rescue the reduced b-wave ERG phenotype in the new A/J strain of mice. Because only the *Clrn1* $^{-/-}$ KO mice showed a reduced ERG phenotype, I only tested those mice for phenotypic rescue. I tested construct 2 Table 5-1 after intravitreal injections and measured scotopic ERGs for WT and *Clrn1* $^{-/-}$ KO mice at 2 months and 4 months post-injection. At two months post-injection, there was no significant difference between the treated vs untreated *Clrn1* $^{-/-}$ KO mice, however, there was a significant difference between WT and *Clrn1* $^{-/-}$ KO untreated mice as seen previously (Figure 4-7) (217). At 4 months post-injection, there was a significant difference between the WT and *Clrn1* $^{-/-}$ KO untreated eyes. I also saw a significant increase in ERG response in the treated vs untreated *Clrn1* $^{-/-}$ KO mice at 4 months of age (Figure 5-10). This suggests a potentially successful gene therapy in that there is a maintained ERG response after AAV gene therapy treatment in the *Clrn1* $^{-/-}$ KO mice as they age. Given the additional light damage and maintained translocation ERG phenotypes, there is a potential to use those assays for treatment in the N48K KI mice.

Table 5-1. AAV constructs

Construct	Plasmid	Serotype	Titer	Volume	Injection
1	Sc-smCBA-h*CLRN1*-HA	AAV2 Quad Y-F	$8.43x10^{12}$	1 ul	Subretinal
2	Sc-smCBA-h*CLRN1*-HA	AAV2 Quad Y-F	$8.43x10^{12}$	1 ul	Intravitreal
3	sc-smCBA-h*CLRN1*-Venus	AAV2 Quad Y-F	$1.54x10^{12}$	1 ul	Subretinal
4	sc-smCBA-h*CLRN1*-Venus	AAV2 Quad Y-F	$1.54x10^{12}$	1 ul	Intravitreal
5	sc-smCBA-h*CLRN1*-HA	AAV2 Quad Y-F	$1.68x10^{12}$	1 ul	Subretinal
6	sc-smCBA-h*CLRN1*-HA	AAV2 Quad Y-F	$1.68x10^{12}$	1 ul	Intravitreal
7	sc-smCBA-h*CLRN1*-HA	AAV2	$2.27x10^{12}$	1 ul	Subretinal
8	sc-smCBA-h*CLRN1*-HA	AAV2	$2.27x10^{12}$	1 ul	Intravitreal
9	sc-smCBA-h*CLRN1*-HA	AAV8 Y733F	$1.23x10^{13}$	1 ul	Subretinal
10	pTR-GRK1-h*CLRN1*-HA	AAV2 Quad	$2.1x10^{12}$	1 ul	Subretinal
11	pTR-GRK1-h*CLRN1*-HA	AAV2 Quad	$2.1x10^{12}$	1 ul	Intravitreal
12	pTR-GRK1-h*CLRN1*-HA	AAV2 Quad Y-F-T491V	$2.31x10^{13}$	1 ul	Intravitreal

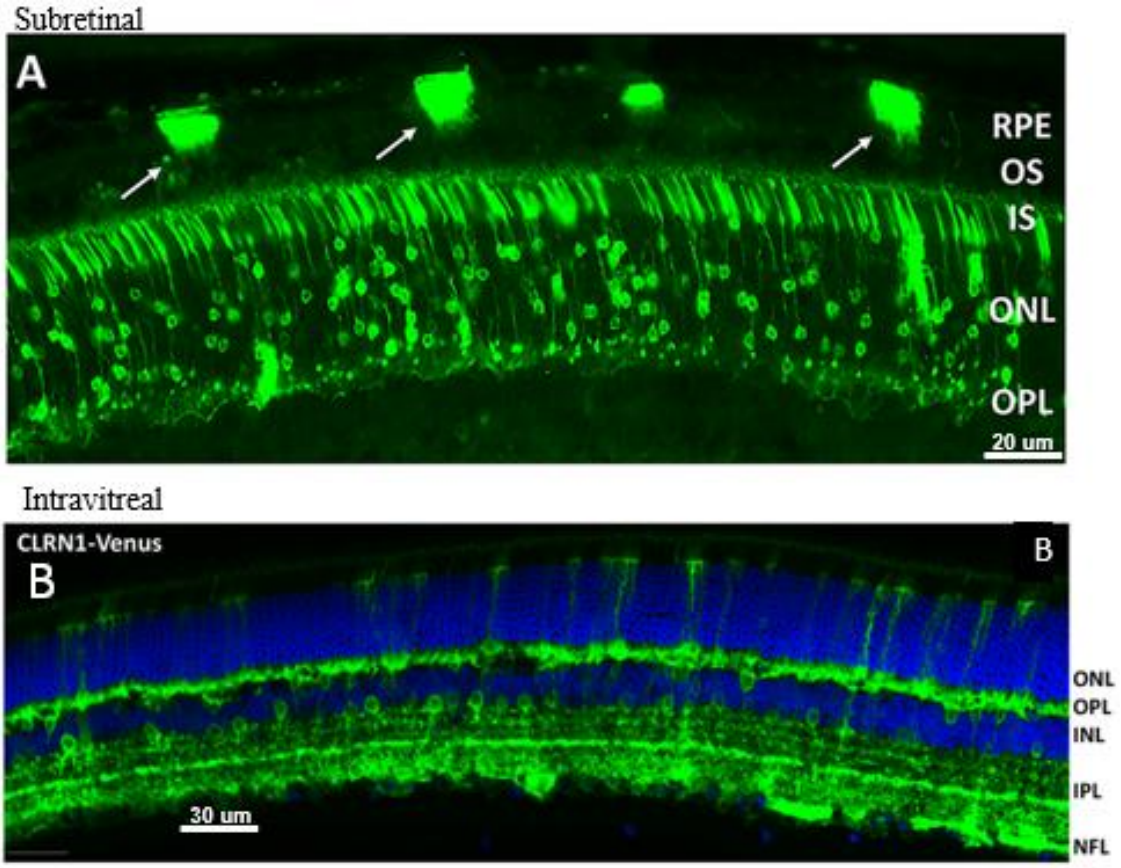

Figure 5-1. Localization of vector-expressed CLARIN-1-Venus following subretinal and intravitreal delivery. A) CLRN1-Venus fusion fluorescence was detected on the apical side of RPE cell membranes (arrows), and in PR IS, ONL and OPL. Scale bar: 20 µm. There is strong CLRN1-Venus fluorescence in specific regions within photoreceptor cells: IS, cell body membrane and OPL. Nuclei are stained blue with DAPI. B) Representative image of retinal cross-section showing CLRN1-Venus fusion fluorescence. Strong expression is seen at the OPL, the stratified dendrites within the IPL, and inner retinal neurons. CLRN1-Venus expression is shown by intense fluorescence at the Müller cells and their apical processes at the OLM Scale bar: 30 µm.

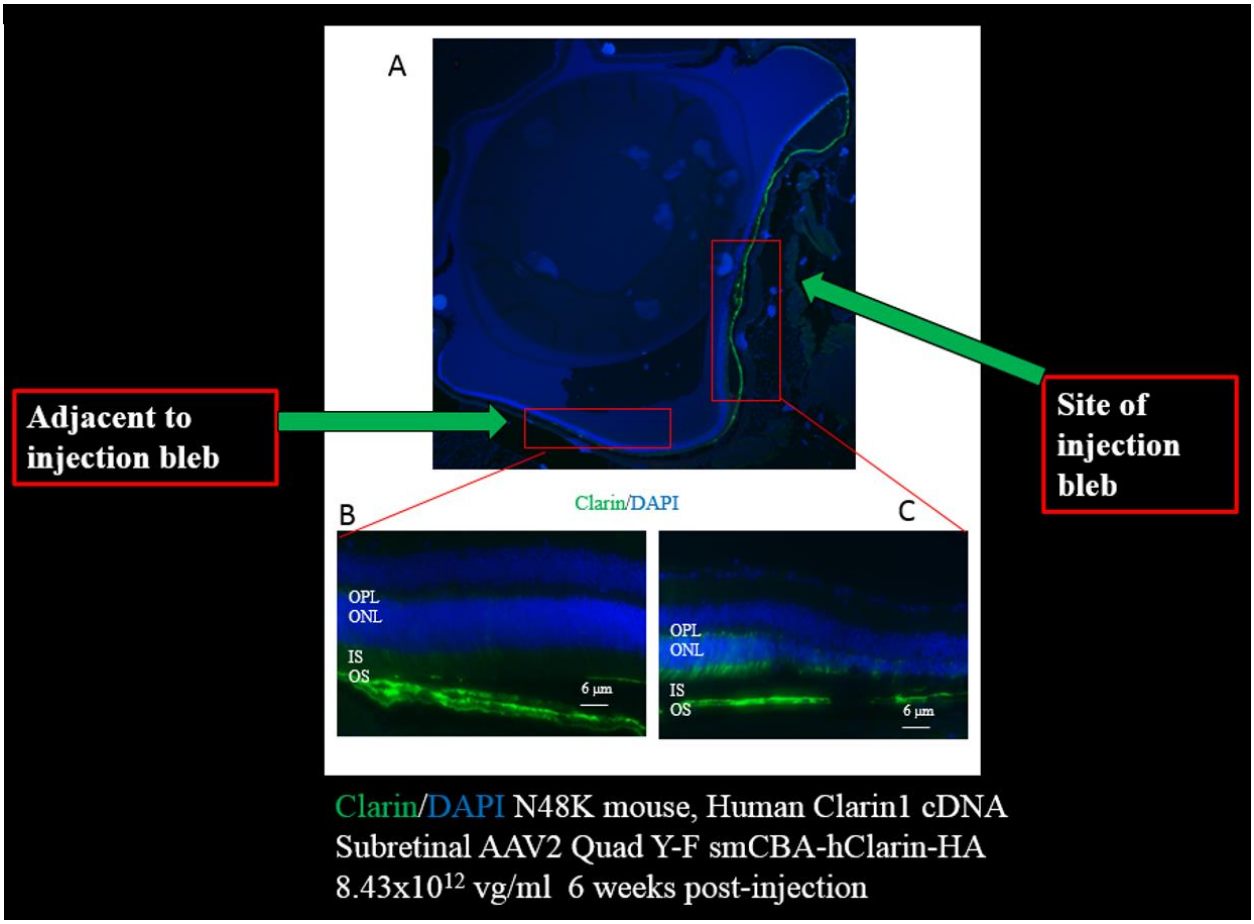

Figure 5-2. Toxicity and photoreceptor cell death post-subretinal injection of *CLARIN-1*. A) A cross-section of a whole eye showing pan-retinal expression of AAV-delivered CLRN1 (green). C57BL/6J mice were injected subretinally with an AAV2-Quad-Y-F-sc-sm-CBA-h*CLRN1*-HA virus at a full titer of $8.43x10^{12}$ vg/ml and showed at 6 weeks post-injection. B) Retinal section adjacent to injection site, there is minimal PR cell death peripheral to the injection site. C) Retinal section at the site of injection, there is significant PR cell death. Localization of vector-expressed CLRN1-HA protein by immunostaining with an anti-HA antibody (40X magnification).

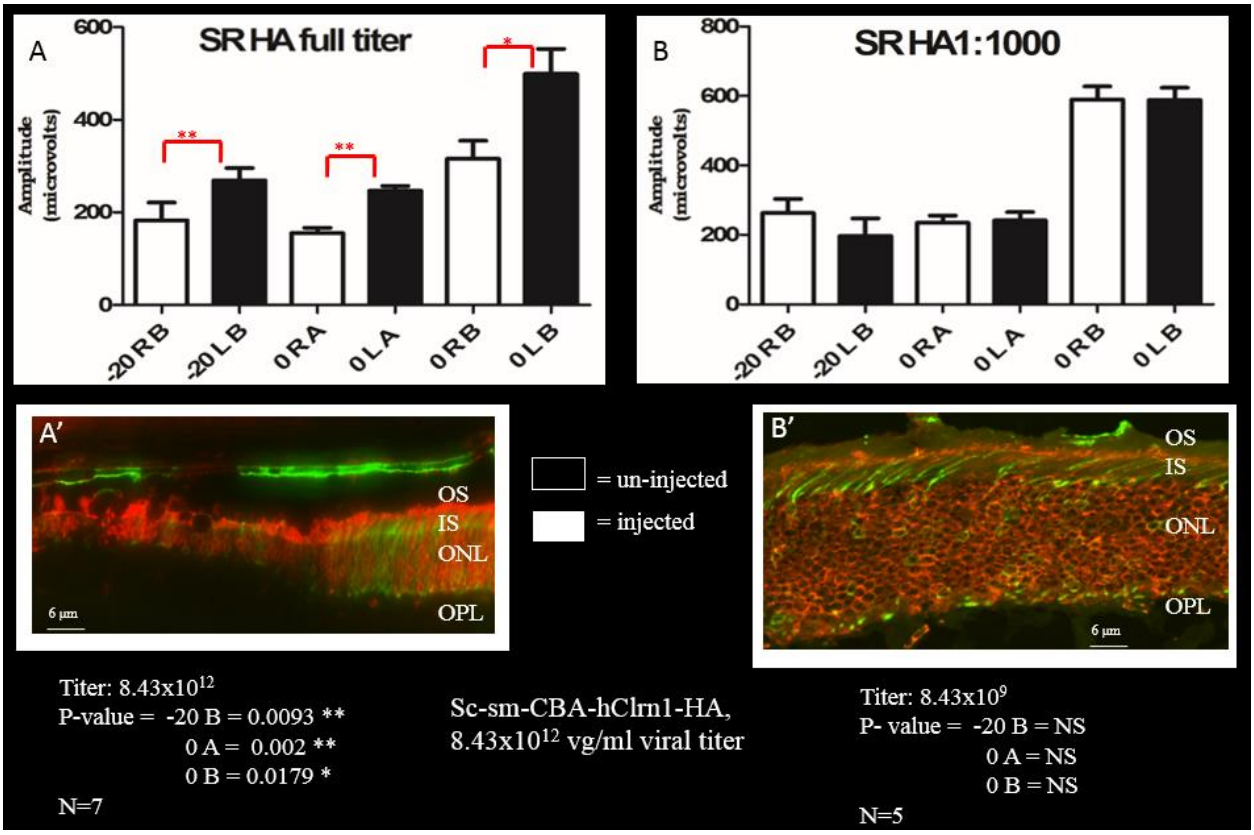

Figure 5-3. Photoreceptor cell death and retinal morphology in full titer vs 1:1000 dilution of subretinally delivered *CLARIN-1*. A) Average ERG amplitudes of 7 mice injected subretinally with a full titer of AAV2-Quad-Y-F-sc-sm-CBA-h*CLRN1*-HA at a viral titer of $8.43x10^{12}$ vg/ml. Black bars are un-injected left eyes and white bars are injected right eyes. The full titer shows a significant decrease in ERG amplitude at all scotopic light intensities. A') Immunohistochemistry staining for anti-HA-CLRN1 (green) and anti- arrestin-1 (red). Retinal cross-sections show significant retinal damage and PR cell death at the site of injection. B) Average ERG amplitudes of 5 mice injected subretinally with a 1:1000 dilution of AAV2-Quad-Y-F-sc-sm-CBA-h*CLRN*1-HA at a viral titer of $8.43x10^{9}$ vg/ml. Black bars are un-injected left eyes and white bars are injected right eyes. The 1:1000 dilution titer shows no significant decrease in ERG amplitude at all scotopic light intensities. B') Immunohistochemistry staining for anti-HA CLRN1 (green) and anti- arrestin-1 (red). Retinal cross-sections show significant preservation of retinal morphology and minimal PR cell death at the site of injection.

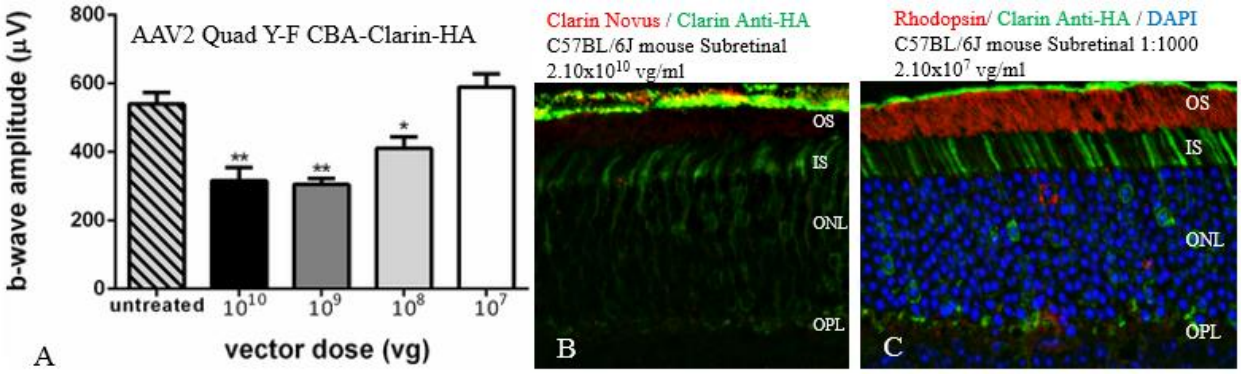

Figure 5-4. Evaluation of retinal function and retinal morphology in CLARIN-1-HA injected mice following subretinal delivery. A). Bar graphs show the average maximum ERG b-wave amplitudes in scotopic, dark-adapted conditions of un-injected wild-type control eyes, compared to AAV-injected eyes that received decreasing doses of AAV-CLRN1-HA vector (2 months post-injection). Max b-wave amplitudes in AAV-injected eyes were dose dependent, and were significantly lower than un-injected controls at 10^{10}, 10^{9}, and 10^{8} vg (* $p<0.05$, ** $p<0.001$). B). Localization of CLRN1-HA protein following subretinal delivery of the AAV2-Quad-Y-F-sc-smCBA-h*CLRN1*-HA vector. CLRN1-HA fluorescence (green) was detected by immunohistochemistry in photoreceptor IS region, ONL and OPL, and was absent from the outer segments (labelled with a rhodopsin antibody, red). The eyes received diluted vector (10^{7} vg).

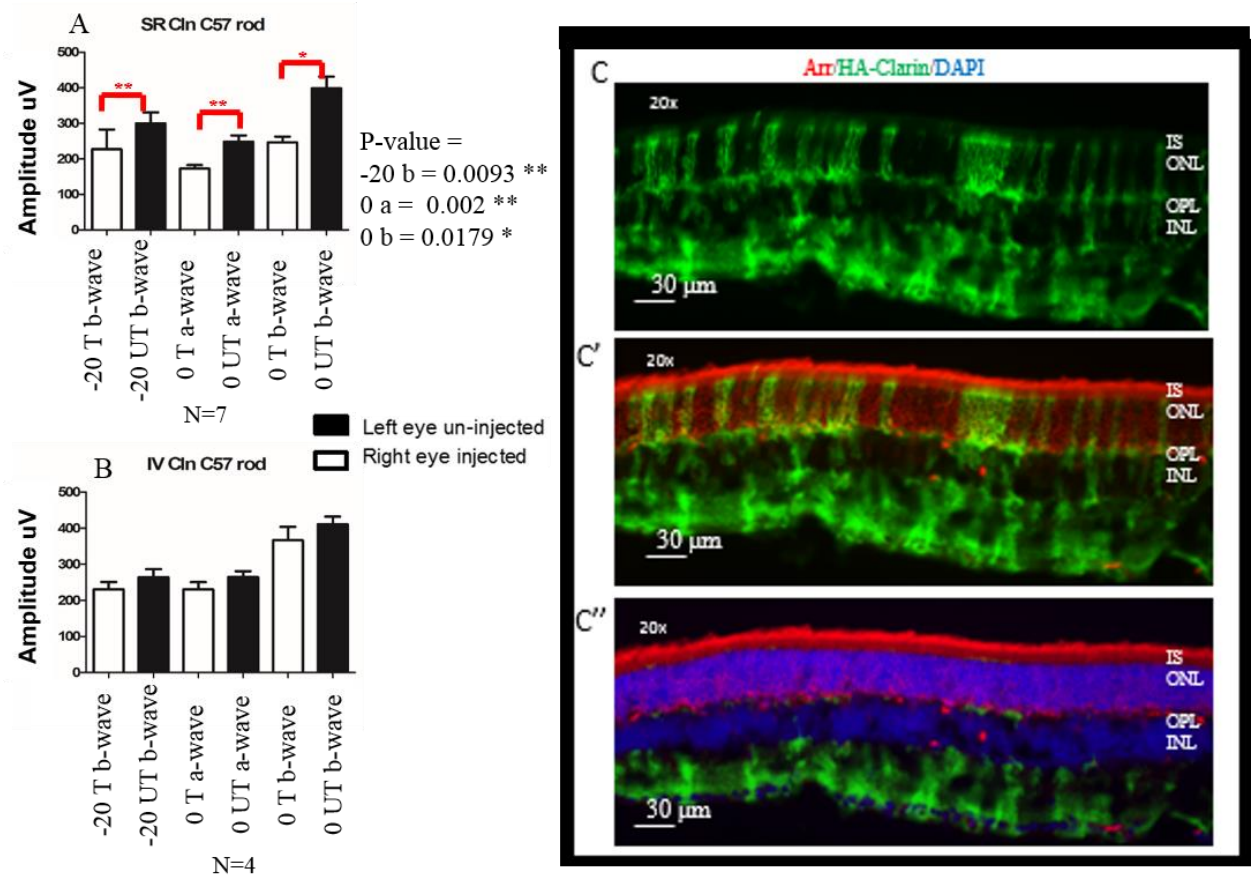

Figure 5-5. ERG and Immunohistochemistry analysis of subretinal vs intravitreal AAV2-Quad-Y-F-smCBA-h*CLARIN-1*-HA in C57BL/6J mice 6 weeks post-injection. All mice are control C57BL/6J strain measured 1 month post-injection. Black bars are un-injected eyes and white bars are injected eyes. A) Subretinal injected AAV2-Quad-Y-F-sc-smCBA-h*CLRN1*-HA. ERGs for all scotopic light intensities are significantly decreased in injected vs un-injected eyes for both the a- and b-waves. P-values= *<0.05. **<0.01. B) Intravitreally injected AAV2-Quad-Y-F-smBA-h*CLRN1*-HA. ERGs are not significantly decreased in injected vs un-injected eyes for all light intensities. C) Immunohistochemistry staining for anti-HA-CLRN1 (green). There is significant expression in the GCL and INL. There also seems to be significant expression in Müller cells, with some possible expression in PR cells. C') arrestin-1 (red) staining for PR cells merged with CLRN1-HA (green). C") arrestin-1 (red), Clrn-HA (green), and DAPI (blue) co-staining, merged.

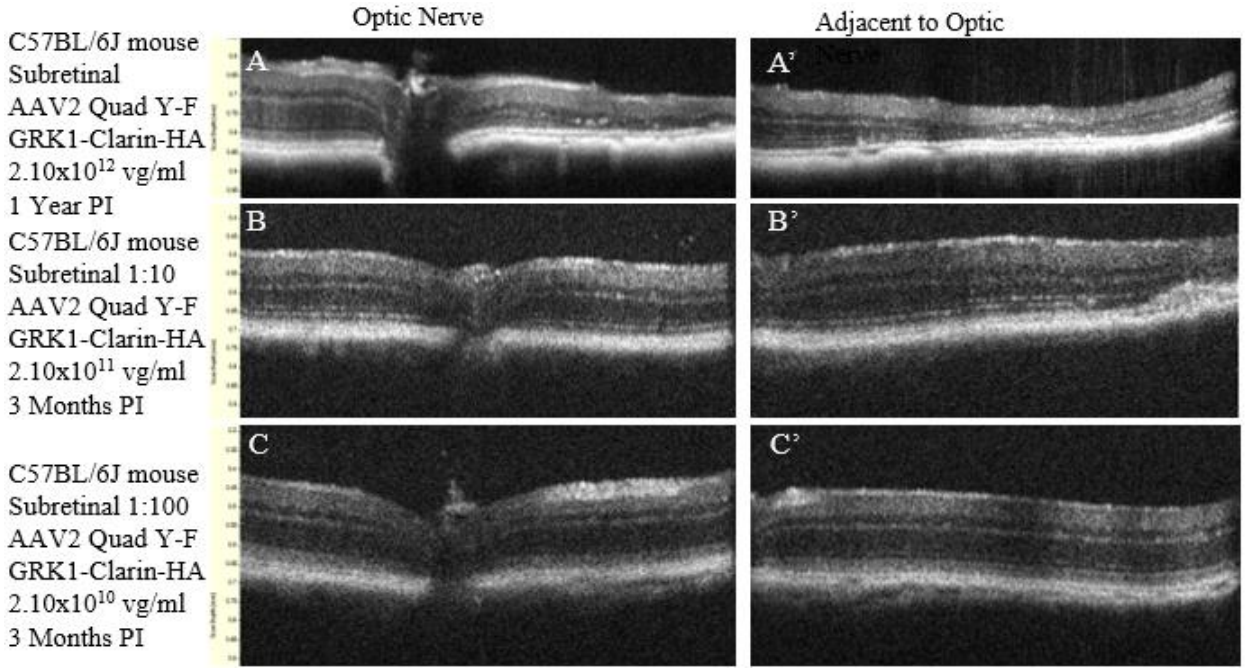

Figure 5-6. SD-OCT of subretinally injected AAV2-Quad-Y-F-pTR-GRK-1-h*CLARIN-1*-HA. All mice tested were C57BL/6J controls injected subretinally with AAV2-Quad-Y-F-pTR-GRK1-h*CLRN1*-HA. A) Full titer of $2.10x10^{12}$ vg/ml 1 year post-injection taken at the optic nerve. A') Image A taken adjacent to the optic nerve. B) 1:10 dilution of $2.10x10^{11}$ vg/ml. 3 months post-injection taken at the optic nerve B') Image B taken adjacent to the optic nerve C) 1:100 dilution of $2.10x10^{10}$ vg/ml. 3 months post-injection taken at the optic nerve C') C image taken adjacent to the optic nerve.

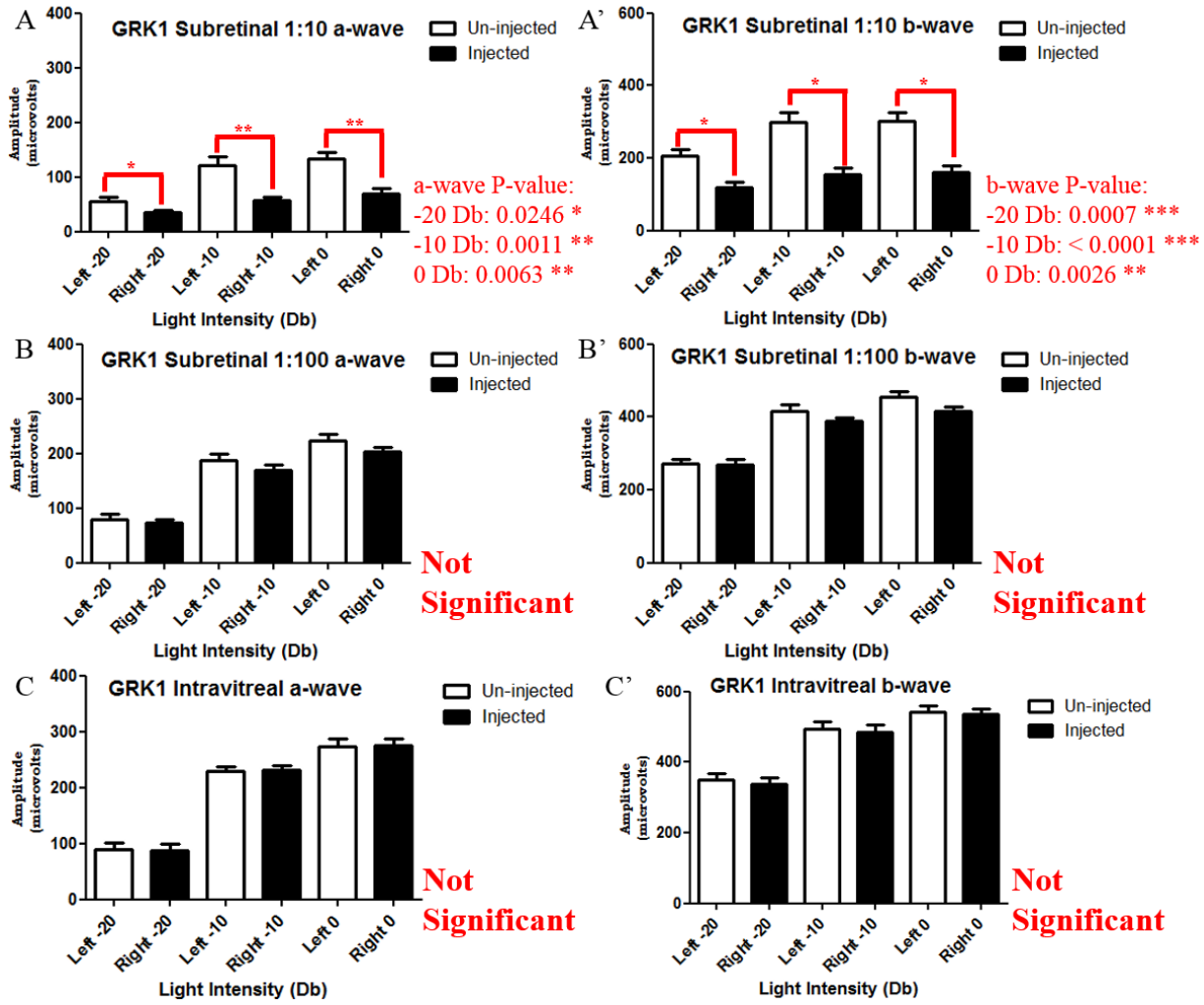

Figure 5-7. ERG analysis of subretinal vs intravitreal AAV2 Quand-Y-F-pTR-GRK1-h*CLARIN-1*-HA 3 months post-injection. White bars are un-injected and black bars are injected eyes. A) Subretinal 1:10 dilution a-wave ERG. All light intensities are significantly decreased in injected versus un-injected eyes, p-values= *<0.05, **<0.01. B) Subretinal 1:10 dilution b-wave ERG. All light intensities are significantly decreased in injected versus un-injected eyes, p-values= *<0.05, **<0.01, ***<0.001. C) Intravitreal full titer a-wave ERG. All intensities are not significantly different between injected and un-injected eyes. D) Intravitreal full titer b-wave ERG. All intensities are not significantly different between injected and un-injected eyes.

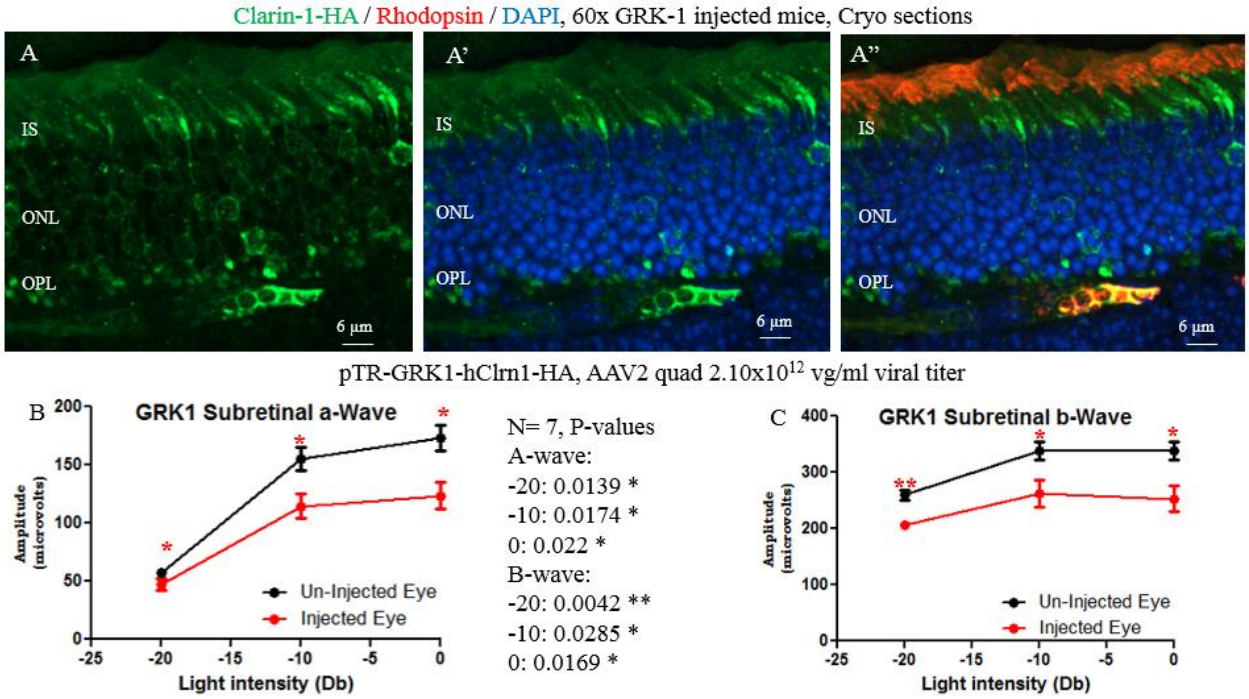

Figure 5-8. Evaluation of retinal function and GRK1-h*CLARIN-1*-HA expression following subretinal delivery. A). Localization of CLRN1-HA protein following subretinal delivery of the AAV2-Quad-pTR-GRK1-h*CLRN1*-HA vector. CLRN1-HA fluorescence (green) was detected by immunohistochemistry in photoreceptor IS region, ONL and OPL, and was absent from the outer segments. A') Co-staining with CLRN1 and DAPI. A") Co-staining with CLRN1, DAPI, and rhodopsin for OS marker. The eyes received a diluted vector at a dilution of 1:1000. At 10 months pf age there did not appear to be any reduction in ONL thickness. B) a-wave ERG at 10 months post-injection. C) b-wave ERG at 10 months post-injection. Over time there is a significant loss in scotopic ERG amplitude for both a- and b-waves over time.

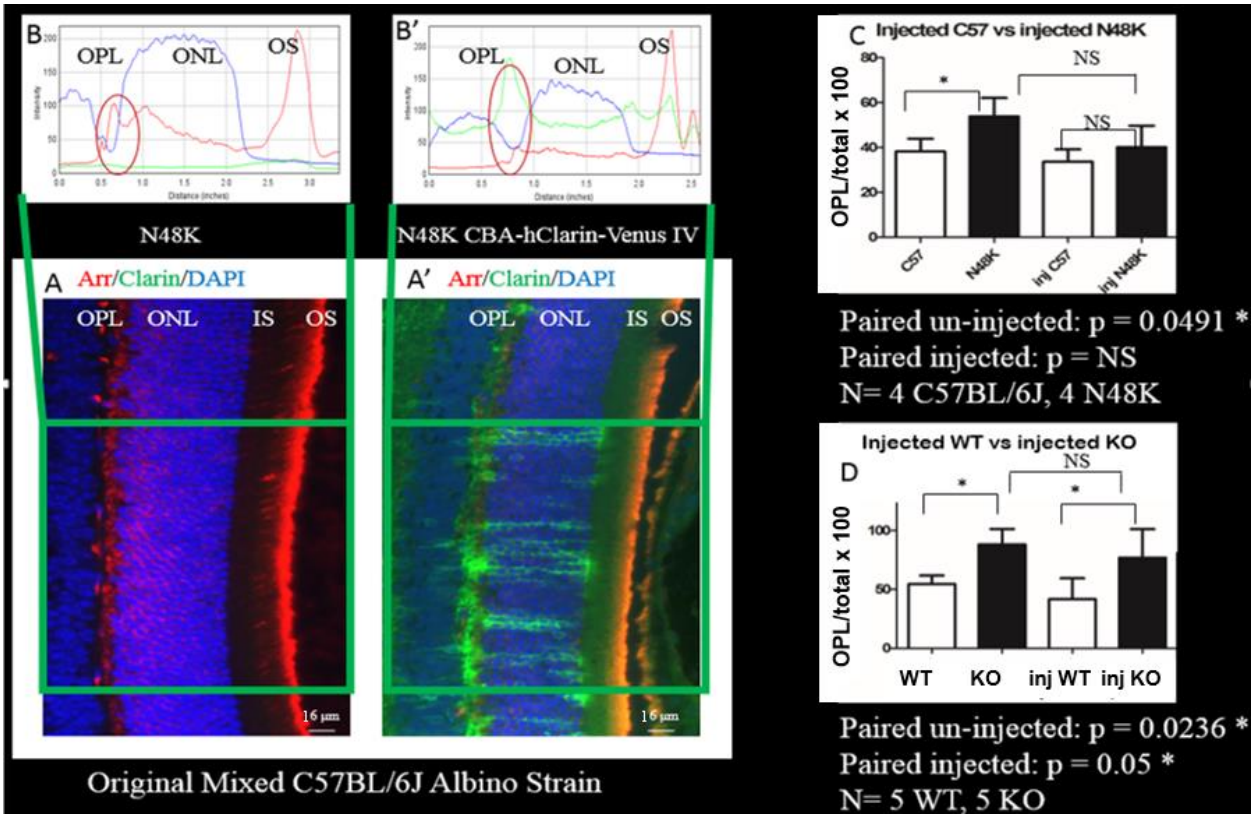

Figure 5-9. Arrestin-1 translocation quantification after intravitreal injection. A) Immunohistochemistry staining of the untreated left eye of an N48K KI mouse after 1 hour of light exposure. There is still a significant amount of arrestin-1 remaining at the OPL synapses. Arrestin-1 (red) and DAPI (blue). A') Immunohistochemistry staining of the treated right eye of an N48K KI mouse after 1 hour of light exposure. There is no longer a significant amount of arrestin-1 remaining at the OPL synapses in mice treated intravitreally with AAV2-Quad-YF-sc-smCBA-h*CLRN1*-HA. Arrestin-1 (red), CLRN1-HA (green), and DAPI (blue). B) Fluorescence intensity plot of the untreated left eye. B') Fluorescence intensity plot of the treated right eye. C) Average fluorescence intensity ratio of the OPL/OS in C57BL/6J WT vs N48K KI mice. There appears to be a decrease in the amount of arrestin-1 at the OPL synapses vs the OS, but the amount in the treated vs untreated N48K KI eyes is not significant even though there is no longer a difference between the KI and C57BL/6J WT mice. D) Average fluorescence intensity ratio of the OPL/OS in C57BL/6J Albino WT vs Albino *Clrn1* $^{-/-}$ KO mice. There appears to be no decrease in the amount of arrestin-1 at the OPL synapses vs the OS in the treated vs untreated *Clrn1* $^{-/-}$ KO eyes, and the ratio of arrestin-1 in the OPL/OS in the WT vs *Clrn1* $^{-/-}$ KO remained the same after treatment.

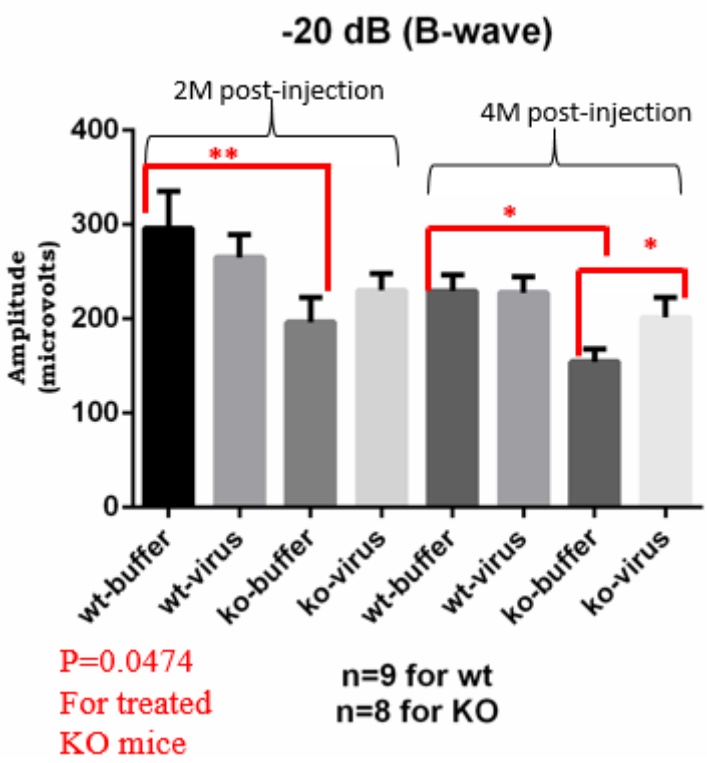

Figure 5-10. Evaluation of retinal function in WT vs *Clarin-1* $^{-/-}$ KO untreated and treated retinas following intravitreal delivery. Bar graph shows the average maximum ERG b-wave amplitudes in scotopic, dark-adapted conditions of untreated WT and *Clrn1* $^{-/-}$ KO control eyes, compared to AAV-treated eyes that received the full titer of AAV2-Quad-sc-smCBA-h*CLRN1*-HA vector (2 months and 4 months post-injection). Maximum b-wave amplitudes were not significantly lower than untreated controls at 2 or 4 months in the WT mice. *Clrn1* $^{-/-}$ KO mice at 2 months were slightly higher in the treated vs untreated eyes and the untreated *Clrn1* $^{-/-}$ KO mice had a significantly reduced ERG compared to WT, as shown above. At 4 months the *Clrn1* $^{-/-}$ KO treated eyes were significantly higher than the untreated eyes and the ERG from the untreated eyes remained significantly lower than the WT.

CHAPER 6
CONCLUSIONS

A primary complication with the USH mouse models is the majority have normal retinal function and morphology. Many studies for USH proteins localize them to the PR CC and calyceal processes in the retina and the stereocilia bundle on cochlear hair cells in the ear (5, 198). The USH3 protein, CLRN1, is the only USH protein not proven to be a component of these USH networks (3, 147, 194, 211). CLRN1 is believed to be a tetraspanin transmembrane protein that has a C-terminal PDZ binding domain with a suggested role in sensory synapses (4, 132). One issue with the previous *Clrn1*/Clrn1 data, is the retinal localization data is conflicting and may due to the different techniques utilized. The immunohistochemistry data localized Clrn1 at the CC in PR cells, and the *in situ* data showed *Clrn1* expression in the INL, most likely in Müller cells, with expression loss at 1 month old (53, 87, 241). Another group using retinal transcription profiling showed *Clrn1* expression only in starburst amacrine cells (207). Given this conflicting data, it was unclear which cell types in the retina express *Clrn1*/Clrn1. More recently, in zebrafish, Clrn1 was shown to localize to inner retinal cells and PR cells including cell-cell contacts between PR and Müller glial cells at the OLM with some faint expression in the GCL (93, 182). Clrn1 localization in the cochlea showed staining in the cochlear hair cells in the inner ear (93, 146, 182, 241). Recently, it has also been shown that Pch15, the USH1F protein, binds to the C-terminal tail of Clrn1 and that Clrn1 is essential for proper subcellular localization of PCH15 in the cochlear hair cells (169).

The zebrafish CC staining supports the subcellular localization of Clrn1 that I saw at the CC in PR cells with the NB-CLRN1 antibody in mice (Figure 3-2). Additionally, this antibody colocalizes with AAV-injected CLRN1, both via the subretinal or intravitreal

route (Figure 3-6) confirming the NB-CLRN1antibody recognizes Clrn1. The N48K KI mice, have Clrn1 localizing at the OS distal tips and/or RPE microvilli (Figure 3-4). The *Clrn1* $^{-/-}$ KO mice appear to have normal synapses, but N48K KI mice were not studied (4, 72, 87, 89, 169, 241, 242). Since other USH proteins were shown to play a role in sensory synapses, it would be useful to pursue in these mice (3, 135, 191-194).

Here I show that the *Clrn1* $^{-/-}$; rd1 $^{-/-}$ double KO mouse has no expression of the 250 aa isoform in WT or *Clrn1* $^{-/-}$ KO mice lacking PR cells, but the WT *Clrn1* $^{+/+}$; rd1 $^{-/-}$ mice lacking PR cells still express the 232 aa isoform (Figure 3-1C, D). The C57BL/6J mice containing PR cells express the 250 aa isoform, suggesting the 250 aa isoform is most likely expressed by PR cells and the 232 aa isoform is expressed by the inner retina (Figure 3-1). Additionally, quantitative RT-PCR could be optimized for isoform specific primers. This would inform us whether the original RT-PCR for the double *Clrn1*/rd1 WT and KO data is correct because I could compare whole retina to only inner retina and measure if it is really isoform 1 in the INL, isoform 2 in PR cells, and where isoform 3 may be expressed, if at all.

In addition to identifying where endogenous *Clrn1*/Clrn1 is expressed in the retina, I further attempted to identify a retinal phenotype in multiple mouse strains for *Clrn1* $^{-/-}$ KO and N48K KI mice. I identified a delay in arrestin-1 translocation from the OPL to the OS upon exposure to light (Figure 4-2). This is significant because other USH mouse models have reported a light induced delay in transducin movement but not arrestin-1 (176, 219). I further showed that N48K KI mice have a maintained ERG response after 1 hour of light exposure, indicating that under a 0 dB mesopic single flash light intensity N48K KI mice are still responsive to light (Figure 4-8). Given the

delay in arrestin-1 movement and maintained ERG response, I tested the ERG recovery response rate to see if with age there was a significant difference. This was previously shown in an arrestin-1 double KO mouse (235) where the study identified a novel prolonged photoresponse with altered rhodopsin recovery in these mice, but these mice have a completely normal ONL similar to my mice (235). Unfortunately, I was unable to see any difference in ERG recovery in the WT vs N48K KI A/J mice (Figure 4-9).

To further test whether or not the arrestin-1 delay and maintained ERG response indicate a potential mechanism for disease progression, I also looked at the ability to induce degeneration and PR cell death after a 4 hour bright light exposure. In WT A/J mice there was some significant PR cell loss in the ONL after 4 hours of light exposure at 2000 lux, however there was no decrease in ERG response, and this was therefore used as the control light intensity (Figure 4-10). When I assessed for both retinal degeneration and ERG loss after 2000 lux of light damage, the *Clrn1* -/- KO mice showed minimal degeneration in the superior retina whereas the N48K KI mice showed degeneration in both the superior and inferior retina, but neither was significantly different from the WT mice after light damage. When I looked at a loss of function by ERG analysis after light damage, the *Clrn1* -/- KO mice showed no significant decrease in ERG response; however, the N48K KI mice showed a significant decrease in ERG amplitude for the -10 and 0 Db a-wave intensities, and at every scotopic b-wave light intensity. This now further provides a quantifiable outcome parameter that I can assess for an AAV-mediated gene therapy phenotype rescue in the N48K KI mice in the future.

I also validated the A/J mouse strain has a reduced ERG compared to C57BL/6J mice, and *Clrn1* $^{-/-}$ KO A/J mice have a significant decrease in ERG amplitude compared

to WT A/J mice as they age as previously published (Figure 4-6, 4-7) (160, 217). Given these phenotypes between the *Clrn1* $^{-/-}$ KO and N48K KI mice, although they both possess a delay in arrestin-1 translocation, it seems that the *Clrn1* $^{-/-}$ KO phenotype is more related to a decreased b-wave ERG at dim light intensities, which may be due to an inner-retinal and not a PR cell phenotype. In contrast, the N48K KI phenotype is due to a maintained ERG response after light exposure, and loss of retinal function after light damage with a significantly reduced a- and b-wave ERG at all light intensities (Figure 4-11D, D'). This suggests the N48K KI phenotype is due to malfunctions in PR cells. This is significant because it means that even though both mutations are in the same protein, there may be different biological mechanisms inducing loss of retinal function and degeneration depending on the mutation. This is particularly relevant in the case of the N48K KI mutation, since it's the most prevalent mutation in USH3A patients.

I next assessed the gene therapy potential for *Clrn1/CLRN1*. First I looked at AAV-CLRN1 expression in the retina after subretinal or intravitreal injections with an AAV2-Quad-smCBA-h*CLRN1*-Venus tagged vector. Subretinal delivery showed AAV-CLRN1 in PR and RPE cells with the majority in the IS and ONL of PR cells and distinct punctate staining at the CC (Figure 5-1) (72). Intravitreally delivered AAV-CLRN1 was expressed in every retinal cell type, particularly in the INL and GCL. There is also significant staining in Müller cells based on the staining in their apical processes at the OLM (Figure 5-1). I originally tested the Venus-tagged construct because at the time there was not a Clrn1/CLRN1 antibody available however, a Venus-tagged construct would not be able to move forward for gene therapy treatment in the clinic.

I generated a C-terminal HA-Tagged AAV-CLRN1 vector in order to follow viral expression levels without altering Clrn1/CLRN1 protein structure. Unfortunately, when I tested the subretinal AAV2-Quad-Y-F-smCBA-h*ClLRN1*-HA construct, the virus was extremely toxic and killed the majority of PR cells at the injection site (Figre5-2). This was significantly reduced at a vector dilution of 1:1000 from the original titer and protein expression was still observed using an anti-HA antibody (Figure 5-3, 5-4). Furthermore, when I compared the full titer subretinal and intravitreal injections there appeared to be no toxicity in the intravitreally treated eyes, both functionally via ERG amplitudes, and structurally with no loss of PR cells (Figure 5-5). Given the CBA-HA vector toxicity, and the ability for the AAV-CLRN1 constructs to transfect multiple cell types, I needed to optimize for PR cell expression, a delivery method that is not toxic, and a capsid serotype and design that will target PR cells through both injection methods if possible.

To specifically target PR cells by subretinal and intravitreal delivery, I generated a construct driven by a PR specific GRK1 promoter with an HA-tag. First I performed OCT analysis 3 months post-treatment to assay for subretinal injection damage. The full titer GRK1 vector was extremely toxic, with complete loss of PR at the injection site. At a 1:10 dilution, there was still some cell death, and only at the 1:100 and 1:1000 dilutions was there no significant degeneration (Figure 5-6). When I assess the ERG response for each injection, the 1:10 dilution was extremely toxic to the retina and only the 1:100 and 1:1000 intravitreal injections did not show any significant loss in retinal function (Figure 5-7). With age, the 1:1000 dilution at 10 months old (8 months post-treatment) still showed no significant retinal degeneration, however, there was a significant loss of ERG amplitude for all scotopic light intensities in both the a- and b-

waves (Figure 5-8). This suggests that even though the initial treatment appeared safe and non-toxic, over time there is still some functional toxicity that results from the AAV2-Quad-Y-F-pTR-GRK1-h*CLRN1*-HA vector treatment. Given the possibility that there are different isoforms of Clrn1/CLRN1 present in different cell types, it seems that the currently preferred method for my gene therapy approach is either a subretinal delivery of CBA-hCLRN1-HA vector at a 1:1000 dilution dose of 8.43×10^9 vg/ml or an intravitreal delivery of CBA-hCLRN1-HA vector at a full titer dose of 8.43×10^{12} vg/ml.

To test for a potential treatment, I intravitreally injected the AAV2-Quad-smCBA-hCLRN1-HA construct into WT, *Clrn1* $^{-/-}$ KO, and N48K KI mice (Table 5-1, construct 11). I performed the arrestin-1 translocation experiment 1 month post-injection and the N48K mice showed some significant rescue of the arrestin-1 delay after light exposure compared to WT mice, but the untreated versus treated *Clrn1* $^{-/-}$ KO eyes did not show a significant difference (Figure 5-9). Because the arrestin-1 localization is not significantly different in WT vs N48K KI treated eyes, this is still a useful phenotype to screen for the success of a gene therapy treatment because they are behaving more like the WT mice.

I further wanted to attempt to rescue the reduced ERG b-wave phenotype in the *Clrn1* $^{-/-}$ KO mice using an intravitreal injection of the AAV2-Quad-smCBA-h*CLRN1*-HA construct. At 2 months post-injection there was no significant ERG rescue in treated vs untreated retinas, but at 4 months post-injection there was a significantly higher ERG amplitude in the treated vs untreated retinas (Figure 5-10). This is promising because it means that the AAV treatment was able to maintain a stable ERG response compared to the untreated control. A similar vector was used by a collaborator to test for AAV-mediated CLRN1 expression in cochlear hair cells in a new mouse model. Using *in situ*

hybridization they observed *CLRN1* expression in inner and outer cochlear hair cells as well as ganglion cells until 1 week post-natally (90). To test for a therapeutic rescue of the hearing loss phenotype in *Clrn1* $^{-/-}$ KO mice, they observed ABR (auditory brainstem response) thresholds in WT, *Clrn1* $^{-/-}$ KO untreated, and Clrn1 $^{-/-}$ KO treated mice. Mice were injected at P3 and analyzed 22 weeks post-injection. At all three ABR intensities tested (8, 16, and 32 kHz) they saw a significant rescue in ABR thresholds post-treatment in the *Clrn1* $^{-/-}$ KO mice (90). This AAV treatment can further be validated after retinal injections. Additionally, because the N48K KI mice also showed degeneration and a significant loss of ERG function post light damage, this can also be a potential assay to measure the success of a gene therapy treatment. If these phenotypic rescue experiments prove to be reliable and reproducible they can further be used to validate my viral vectors in order to translate my gene therapy into the clinic to treat patients.

In conclusion, I have shown that my novel NB-CLRN1 antibody stains the CC in PR cells and that it recognizes my injected viral construct through both a subretinal and intravitreal delivery. I have also identified a novel retinal phenotype of a delay of arrestin-1 movement upon exposure to light in both the KO and KI mice. I confirmed that the *Clrn1* $^{-/-}$ KO display a reduced ERG b-wave amplitude phenotype, in agreement with a recent study (217). I further showed that N48K KI mice are more susceptible to light damage compared to the WT and *Clrn1* $^{-/-}$ KO mice due to a loss of a- and b-wave ERG amplitude after light exposure. All of these previously unidentified phenotypes can now be employed to further screen my optimized AAV-vector designs to gain a statistically valid and reproducible approach to develop a gene therapy treatment for USH3A.

LIST OF REFERENCES

1. **Adams NA, Awadein A, and Toma HS.** The retinal ciliopathies. *Ophthalmic Genet* 28: 113-125, 2007.

2. **Adamus G, Zam ZS, Arendt A, Palczewski K, McDowell JH, and Hargrave PA.** Anti-rhodopsin monoclonal antibodies of defined specificity: characterization and application. *Vision Res* 31: 17-31, 1991.

3. **Adato A, Michel V, Kikkawa Y, Reiners J, Alagramam KN, Weil D, Yonekawa H, Wolfrum U, El-Amraoui A, and Petit C.** Interactions in the network of Usher syndrome type 1 proteins. *Hum Mol Genet* 14: 347-356, 2005.

4. **Adato A, Vreugde S, Joensuu T, Avidan N, Hamalainen R, Belenkiy O, Olender T, Bonne-Tamir B, Ben-Asher E, Espinos C, Millán JM, Lehesjoki AE, Flannery JG, Avraham KB, Pietrokovski S, Sankila EM, Beckmann JS, and Lancet D.** USH3A transcripts encode clarin-1, a four-transmembrane-domain protein with a possible role in sensory synapses. *Eur J Hum Genet* 10: 339-350, 2002.

5. **Ahmed ZM, Frolenkov GI, and Riazuddin S.** Usher proteins in inner ear structure and function. *Physiol Genomics* 45: 987-989, 2013.

6. **Ahmed ZM, Goodyear R, Riazuddin S, Lagziel A, Legan PK, Behra M, Burgess SM, Lilley KS, Wilcox ER, Griffith AJ, Frolenkov GI, Belyantseva IA, Richardson GP, and Friedman TB.** The tip-link antigen, a protein associated with the transduction complex of sensory hair cells, is protocadherin-15. *J Neurosci* 26: 7022-7034, 2006.

7. **Ahmed ZM, Kjellstrom S, Haywood-Watson RJ, Bush RA, Hampton LL, Battey JF, Riazuddin S, Frolenkov G, Sieving PA, and Friedman TB.** Double homozygous waltzer and Ames waltzer mice provide no evidence of retinal degeneration. *Mol Vis* 14: 2227-2236, 2008.

8. **Ahmed ZM, Riazuddin S, Ahmad J, Bernstein SL, Guo Y, Sabar MF, Sieving P, Griffith AJ, Friedman TB, Belyantseva IA, and Wilcox ER.** PCDH15 is expressed in the neurosensory epithelium of the eye and ear and mutant alleles are responsible for both USH1F and DFNB23. *Hum Mol Genet* 12: 3215-3223, 2003.

9. **Ahmed ZM, Riazuddin S, Bernstein SL, Ahmed Z, Khan S, Griffith AJ, Morell RJ, Friedman TB, and Wilcox ER.** Mutations of the protocadherin gene PCDH15 cause Usher syndrome type 1F. *Am J Hum Genet* 69: 25-34, 2001.

10. **Ahmed ZM, Riazuddin S, and Wilcox ER.** The molecular genetics of Usher syndrome. *Clin Genet* 63: 431-444, 2003.

11. **Akoury E, El Zir E, Mansour A, Mégarbané A, Majewski J, and Slim R.** A novel 5-bp deletion in Clarin 1 in a family with Usher syndrome. *Ophthalmic Genet* 32: 245-249, 2011.

12. **Armengot M, Salom D, Diaz-Llopis M, Millan JM, Milara J, Mata M, and Cortijo J.** Nasal ciliary beat frequency and beat pattern in retinal ciliopathies. *Invest Ophthalmol Vis Sci* 53: 2076-2079, 2012.

13. **Athanasiou D, Aguila M, Bevilacqua D, Novoselov SS, Parfitt DA, and Cheetham ME.** The cell stress machinery and retinal degeneration. *FEBS Lett* 587: 2008-2017, 2013.

14. **Bahloul A, Michel V, Hardelin JP, Nouaille S, Hoos S, Houdusse A, England P, and Petit C.** Cadherin-23, myosin VIIa and harmonin, encoded by Usher syndrome type I genes, form a ternary complex and interact with membrane phospholipids. *Hum Mol Genet* 19: 3557-3565, 2010.

15. **Barrong SD, Chaitin MH, Fliesler SJ, Possin DE, Jacobson SG, and Milam AH.** Ultrastructure of connecting cilia in different forms of retinitis pigmentosa. *Arch Ophthalmol* 110: 706-710, 1992.

16. **Beltran WA, Cideciyan AV, Guziewicz KE, Iwabe S, Swider M, Scott EM, Savina SV, Ruthel G, Stefano F, Zhang L, Zorger R, Sumaroka A, Jacobson SG, and Aguirre GD.** Canine retina has a primate fovea-like bouquet of cone photoreceptors which is affected by inherited macular degenerations. *PLoS One* 9: e90390, 2014.

17. **Belyantseva IA, Boger ET, Naz S, Frolenkov GI, Sellers JR, Ahmed ZM, Griffith AJ, and Friedman TB.** Myosin-XVa is required for tip localization of whirlin and differential elongation of hair-cell stereocilia. *Nat Cell Biol* 7: 148-156, 2005.

18. **Berbari NF, O'Connor AK, Haycraft CJ, and Yoder BK.** The primary cilium as a complex signaling center. *Curr Biol* 19: R526-535, 2009.

19. **Berger A, Cavallero S, Dominguez E, Barbe P, Simonutti M, Sahel JA, Sennlaub F, Raoul W, Paques M, and Bemelmans AP.** Spectral-domain optical coherence tomography of the rodent eye: highlighting layers of the outer retina using signal averaging and comparison with histology. *PLoS One* 9: e96494, 2014.

20. **Bermingham-McDonogh O, Corwin JT, Hauswirth WW, Heller S, Reed R, and Reh TA.** Regenerative medicine for the special senses: restoring the inputs. *J Neurosci* 32: 14053-14057, 2012.

21. **Bermingham-McDonogh O and Reh TA.** Regulated reprogramming in the regeneration of sensory receptor cells. *Neuron* 71: 389-405, 2011.

22. **Bilotta J and Saszik S.** The zebrafish as a model visual system. *Int J Dev Neurosci* 19: 621-629, 2001.

23. **Bonnet C and El-Amraoui A.** Usher syndrome (sensorineural deafness and retinitis pigmentosa): pathogenesis, molecular diagnosis and therapeutic approaches. *Curr Opin Neurol* 25: 42-49, 2012.

24. **Bonnet C, Grati M, Marlin S, Levilliers J, Hardelin JP, Parodi M, Niasme-Grare M, Zelenika D, Délépine M, Feldmann D, Jonard L, El-Amraoui A, Weil D, Delobel B, Vincent C, Dollfus H, Eliot MM, David A, Calais C, Vigneron J, Montaut-Verient B, Bonneau D, Dubin J, Thauvin C, Duvillard A, Francannet C, Mom T, Lacombe D, Duriez F, Drouin-Garraud V, Thuillier-Obstoy MF, Sigaudy S, Frances AM, Collignon P, Challe G, Couderc R, Lathrop M, Sahel JA, Weissenbach J, Petit C, and Denoyelle F.** Complete exon sequencing of all known Usher syndrome genes greatly improves molecular diagnosis. *Orphanet J Rare Dis* 6: 21, 2011.

25. **Bonnet C, Riahi Z, Chantot-Bastaraud S, Smagghe L, Letexier M, Marcaillou C, Lefèvre GM, Hardelin JP, El-Amraoui A, Singh-Estivalet A, Mohand-Saïd S, Kohl S, Kurtenbach A, Sliesoraityte I, Zobor D, Gherbi S, Testa F, Simonelli F, Banfi S, Fakin A, Glavač D, Jarc-Vidmar M, Zupan A, Battelino S, Martorell Sampol L, Claveria MA, Catala Mora J, Dad S, Møller LB, Rodriguez Jorge J, Hawlina M, Auricchio A, Sahel JA, Marlin S, Zrenner E, Audo I, and Petit C.** An innovative strategy for the molecular diagnosis of Usher syndrome identifies causal biallelic mutations in 93% of European patients. *Eur J Hum Genet* 24: 1730-1738, 2016.

26. **Bork JM, Peters LM, Riazuddin S, Bernstein SL, Ahmed ZM, Ness SL, Polomeno R, Ramesh A, Schloss M, Srisailpathy CR, Wayne S, Bellman S, Desmukh D, Ahmed Z, Khan SN, Kaloustian VM, Li XC, Lalwani A, Bitner-Glindzicz M, Nance WE, Liu XZ, Wistow G, Smith RJ, Griffith AJ, Wilcox ER, Friedman TB, and Morell RJ.** Usher syndrome 1D and nonsyndromic autosomal recessive deafness DFNB12 are caused by allelic mutations of the novel cadherin-like gene CDH23. *Am J Hum Genet* 68: 26-37, 2001.

27. **Boyd RF, Sledge DG, Boye SL, Boye SE, Hauswirth WW, Komáromy AM, Petersen-Jones SM, and Bartoe JT.** Photoreceptor-targeted gene delivery using intravitreally administered AAV vectors in dogs. *Gene Ther* 23: 223-230, 2016.

28. **Boye SE, Alexander JJ, Witherspoon CD, Boye SL, Peterson JJ, Clark ME, Sandefer KJ, Girkin CA, Hauswirth WW, and Gamlin PD.** Highly Efficient Delivery of Adeno-Associated Viral Vectors to the Primate Retina. *Hum Gene Ther* 27: 580-597, 2016.

29. **Boye SE, Boye SL, Lewin AS, and Hauswirth WW.** A comprehensive review of retinal gene therapy. *Mol Ther* 21: 509-519, 2013.

30. **Boye SE, Boye SL, Pang J, Ryals R, Everhart D, Umino Y, Neeley AW, Besharse J, Barlow R, and Hauswirth WW.** Functional and behavioral restoration of vision by gene therapy in the guanylate cyclase-1 (GC1) knockout mouse. *PLoS One* 5: e11306, 2010.

31. **Boye SL, Peshenko IV, Huang WC, Min SH, McDoom I, Kay CN, Liu X, Dyka FM, Foster TC, Umino Y, Karan S, Jacobson SG, Baehr W, Dizhoor A, Hauswirth WW, and Boye SE.** AAV-mediated gene therapy in the guanylate cyclase (RetGC1/RetGC2) double knockout mouse model of Leber congenital amaurosis. *Hum Gene Ther* 24: 189-202, 2013.

32. **Boye SL, Peterson JJ, Choudhury S, Min SH, Ruan Q, McCullough KT, Zhang Z, Olshevskaya EV, Peshenko IV, Hauswirth WW, Ding XQ, Dizhoor AM, and Boye SE.** Gene Therapy Fully Restores Vision to the All-Cone Nrl(-/-) Gucy2e(-/-) Mouse Model of Leber Congenital Amaurosis-1. *Hum Gene Ther* 26: 575-592, 2015.

33. **Bruewer AR, Mowat FM, Bartoe JT, Boye SL, Hauswirth WW, and Petersen-Jones SM.** Evaluation of lateral spread of transgene expression following subretinal AAV-mediated gene delivery in dogs. *PLoS One* 8: e60218, 2013.

34. **Byrne LC, Lin YJ, Lee T, Schaffer DV, and Flannery JG.** The expression pattern of systemically injected AAV9 in the developing mouse retina is determined by age. *Mol Ther* 23: 290-296, 2015.

35. **Caberlotto E, Michel V, Foucher I, Bahloul A, Goodyear RJ, Pepermans E, Michalski N, Perfettini I, Alegria-Prévot O, Chardenoux S, Do Cruzeiro M, Hardelin JP, Richardson GP, Avan P, Weil D, and Petit C.** Usher type 1G protein sans is a critical component of the tip-link complex, a structure controlling actin polymerization in stereocilia. *Proc Natl Acad Sci U S A* 108: 5825-5830, 2011.

36. **Calvert PD, Govardovskii VI, Arshavsky VY, and Makino CL.** Two temporal phases of light adaptation in retinal rods. *J Gen Physiol* 119: 129-145, 2002.

37. **Calvert PD and Makino CL.** The time course of light adaptation in vertebrate retinal rods. *Adv Exp Med Biol* 514: 37-60, 2002.

38. **Calvert PD, Schiesser WE, and Pugh EN.** Diffusion of a soluble protein, photoactivatable GFP, through a sensory cilium. *J Gen Physiol* 135: 173-196, 2010.

39. **Calvert PD, Strissel KJ, Schiesser WE, Pugh EN, and Arshavsky VY.** Light-driven translocation of signaling proteins in vertebrate photoreceptors. *Trends Cell Biol* 16: 560-568, 2006.

40. **Cao D, Pokorny J, and Grassi MA.** Isolated mesopic rod and cone electroretinograms realized with a four-primary method. *Doc Ophthalmol* 123: 29-41, 2011.

41. **Cardenas-Rodriguez M and Badano JL.** Ciliary biology: understanding the cellular and genetic basis of human ciliopathies. *Am J Med Genet C Semin Med Genet* 151C: 263-280, 2009.

42. **Chamling X, Seo S, Bugge K, Searby C, Guo DF, Drack AV, Rahmouni K, and Sheffield VC.** Ectopic expression of human BBS4 can rescue Bardet-Biedl syndrome phenotypes in Bbs4 null mice. *PLoS One* 8: e59101, 2013.

43. **Chang B, Hawes NL, Hurd RE, Davisson MT, Nusinowitz S, and Heckenlively JR.** Retinal degeneration mutants in the mouse. *Vision Res* 42: 517-525, 2002.

44. **Chang B, Hawes NL, Hurd RE, Wang J, Howell D, Davisson MT, Roderick TH, Nusinowitz S, and Heckenlively JR.** Mouse models of ocular diseases. *Vis Neurosci* 22: 587-593, 2005.

45. **Chih B, Liu P, Chinn Y, Chalouni C, Komuves LG, Hass PE, Sandoval W, and Peterson AS.** A ciliopathy complex at the transition zone protects the cilia as a privileged membrane domain. *Nat Cell Biol* 14: 61-72, 2011.

46. **Cideciyan AV, Aguirre GK, Jacobson SG, Butt OH, Schwartz SB, Swider M, Roman AJ, Sadigh S, and Hauswirth WW.** Pseudo-fovea formation after gene therapy for RPE65-LCA. *Invest Ophthalmol Vis Sci* 56: 526-537, 2014.

47. **Cideciyan AV, Hauswirth WW, Aleman TS, Kaushal S, Schwartz SB, Boye SL, Windsor EA, Conlon TJ, Sumaroka A, Pang JJ, Roman AJ, Byrne BJ, and Jacobson SG.** Human RPE65 gene therapy for Leber congenital amaurosis: persistence of early visual improvements and safety at 1 year. *Hum Gene Ther* 20: 999-1004, 2009.

48. **Cideciyan AV, Hauswirth WW, Aleman TS, Kaushal S, Schwartz SB, Boye SL, Windsor EA, Conlon TJ, Sumaroka A, Roman AJ, Byrne BJ, and Jacobson SG.** Vision 1 year after gene therapy for Leber's congenital amaurosis. *N Engl J Med* 361: 725-727, 2009.

49. **Cideciyan AV, Jacobson SG, Beltran WA, Sumaroka A, Swider M, Iwabe S, Roman AJ, Olivares MB, Schwartz SB, Komáromy AM, Hauswirth WW, and Aguirre GD.** Human retinal gene therapy for Leber congenital amaurosis shows advancing retinal degeneration despite enduring visual improvement. *Proc Natl Acad Sci U S A* 110: E517-525, 2013.

50. **Cideciyan AV, Roman AJ, Jacobson SG, Yan B, Pascolini M, Charng J, Pajaro S, and Nirenberg S.** Developing an Outcome Measure With High Luminance for Optogenetics Treatment of Severe Retinal Degenerations and for Gene Therapy of Cone Diseases. *Invest Ophthalmol Vis Sci* 57: 3211-3221, 2016.

51. **Colella P, Sommella A, Marrocco E, Di Vicino U, Polishchuk E, Garcia Garrido M, Seeliger MW, Polishchuk R, and Auricchio A.** Myosin7a deficiency results in reduced retinal activity which is improved by gene therapy. *PLoS One* 8: e72027, 2013.

52. **Colombo L, Sala B, Montesano G, Pierrottet C, De Cillà S, Maltese P, Bertelli M, and Rossetti L.** Choroidal Thickness Analysis in Patients with Usher Syndrome Type 2 Using EDI OCT. *J Ophthalmol* 2015: 189140, 2015.

53. **Cosgrove D and Zallocchi M.** Clarin-1 protein expression in photoreceptors. *Hear Res* 259: 117, 2010.

54. **Cosgrove D and Zallocchi M.** Usher protein functions in hair cells and photoreceptors. *Int J Biochem Cell Biol* 46: 80-89, 2014.

55. **Cremers FP, Kimberling WJ, Külm M, de Brouwer AP, van Wijk E, te Brinke H, Cremers CW, Hoefsloot LH, Banfi S, Simonelli F, Fleischhauer JC, Berger W, Kelley PM, Haralambous E, Bitner-Glindzicz M, Webster AR, Saihan Z, De Baere E, Leroy BP, Silvestri G, McKay GJ, Koenekoop RK, Millan JM, Rosenberg T, Joensuu T, Sankila EM, Weil D, Weston MD, Wissinger B, and Kremer H.** Development of a genotyping microarray for Usher syndrome. *J Med Genet* 44: 153-160, 2007.

56. **Czarnecki PG and Shah JV.** The ciliary transition zone: from morphology and molecules to medicine. *Trends Cell Biol* 22: 201-210, 2012.

57. **D'Amico F, Skarmoutsou E, and Stivala F.** State of the art in antigen retrieval for immunohistochemistry. *J Immunol Methods* 341: 1-18, 2009.

58. **da Cruz L, Dorn JD, Humayun MS, Dagnelie G, Handa J, Barale PO, Sahel JA, Stanga PE, Hafezi F, Safran AB, Salzmann J, Santos A, Birch D, Spencer R, Cideciyan AV, de Juan E, Duncan JL, Eliott D, Fawzi A, Olmos de Koo LC, Ho AC, Brown G, Haller J, Regillo C, Del Priore LV, Arditi A, Greenberg RJ, and Group AIS.** Five-Year Safety and Performance Results from the Argus II Retinal Prosthesis System Clinical Trial. *Ophthalmology* 123: 2248-2254, 2016.

59. **Dagnelie G, Christopher P, Arditi A, da Cruz L, Duncan JL, Ho AC, Olmos de Koo LC, Sahel JA, Stanga PE, Thumann G, Wang Y, Arsiero M, Dorn JD, Greenberg RJ, and Group AIS.** Performance of real-world functional vision tasks by blind subjects improves after implantation with the Argus® II retinal prosthesis system. *Clin Exp Ophthalmol* 45: 152-159, 2017.

60. **Dalkara D, Byrne LC, Klimczak RR, Visel M, Yin L, Merigan WH, Flannery JG, and Schaffer DV.** In vivo-directed evolution of a new adeno-associated virus for therapeutic outer retinal gene delivery from the vitreous. *Sci Transl Med* 5: 189ra176, 2013.

61. **Dalkara D, Byrne LC, Lee T, Hoffmann NV, Schaffer DV, and Flannery JG.** Enhanced gene delivery to the neonatal retina through systemic administration of tyrosine-mutated AAV9. *Gene Ther* 19: 176-181, 2012.

62. **Dalkara D, Kolstad KD, Caporale N, Visel M, Klimczak RR, Schaffer DV, and Flannery JG.** Inner limiting membrane barriers to AAV-mediated retinal transduction from the vitreous. *Mol Ther* 17: 2096-2102, 2009.

63. **Dalke C, Löster J, Fuchs H, Gailus-Durner V, Soewarto D, Favor J, Neuhäuser-Klaus A, Pretsch W, Gekeler F, Shinoda K, Zrenner E, Meitinger T, Hrabé de Angelis M, and Graw J.** Electroretinography as a screening method for mutations causing retinal dysfunction in mice. *Invest Ophthalmol Vis Sci* 45: 601-609, 2004.

64. **Davenport JR and Yoder BK.** An incredible decade for the primary cilium: a look at a once-forgotten organelle. *Am J Physiol Renal Physiol* 289: F1159-1169, 2005.

65. **Day TP, Byrne LC, Schaffer DV, and Flannery JG.** Advances in AAV vector development for gene therapy in the retina. *Adv Exp Med Biol* 801: 687-693, 2014.

66. **Daya S and Berns KI.** Gene therapy using adeno-associated virus vectors. *Clin Microbiol Rev* 21: 583-593, 2008.

67. **DE ROBERTIS E.** Electron microscope observations on the submicroscopic organization of the retinal rods. *J Biophys Biochem Cytol* 2: 319-330, 1956.

68. **Delprat B, Michel V, Goodyear R, Yamasaki Y, Michalski N, El-Amraoui A, Perfettini I, Legrain P, Richardson G, Hardelin JP, and Petit C.** Myosin XVa and whirlin, two deafness gene products required for hair bundle growth, are located at the stereocilia tips and interact directly. *Hum Mol Genet* 14: 401-410, 2005.

69. **Di Palma F, Holme RH, Bryda EC, Belyantseva IA, Pellegrino R, Kachar B, Steel KP, and Noben-Trauth K.** Mutations in Cdh23, encoding a new type of cadherin, cause stereocilia disorganization in waltzer, the mouse model for Usher syndrome type 1D. *Nat Genet* 27: 103-107, 2001.

70. **Di Palma F, Pellegrino R, and Noben-Trauth K.** Genomic structure, alternative splice forms and normal and mutant alleles of cadherin 23 (Cdh23). *Gene* 281: 31-41, 2001.

71. **Dinculescu A, Glushakova L, Min SH, and Hauswirth WW.** Adeno-associated virus-vectored gene therapy for retinal disease. *Hum Gene Ther* 16: 649-663, 2005.

72. **Dinculescu A, Stupay RM, Deng WT, Dyka FM, Min SH, Boye SL, Chiodo VA, Abrahan CE, Zhu P, Li Q, Strettoi E, Novelli E, Nagel-Wolfrum K, Wolfrum U, Smith WC, and Hauswirth WW.** AAV-Mediated Clarin-1 Expression in the Mouse Retina: Implications for USH3A Gene Therapy. *PLoS One* 11: e0148874, 2016.

73. **Donoso LA, Gregerson DS, Smith L, Robertson S, Knospe V, Vrabec T, and Kalsow CM.** S-antigen: preparation and characterization of site-specific monoclonal antibodies. *Curr Eye Res* 9: 343-355, 1990.

74. **Duncan JL, Richards TP, Arditi A, da Cruz L, Dagnelie G, Dorn JD, Ho AC, Olmos de Koo LC, Barale PO, Stanga PE, Thumann G, Wang Y, and Greenberg RJ.** Improvements in vision-related quality of life in blind patients implanted with the Argus II Epiretinal Prosthesis. *Clin Exp Optom* 100: 144-150, 2017.

75. **Eckmiller MS.** Defective cone photoreceptor cytoskeleton, alignment, feedback, and energetics can lead to energy depletion in macular degeneration. *Prog Retin Eye Res* 23: 495-522, 2004.

76. **Eckmiller MS.** Microtubules in a rod-specific cytoskeleton associated with outer segment incisures. *Vis Neurosci* 17: 711-722, 2000.

77. **Ekström P, Sanyal S, Narfström K, Chader GJ, and van Veen T.** Accumulation of glial fibrillary acidic protein in Müller radial glia during retinal degeneration. *Invest Ophthalmol Vis Sci* 29: 1363-1371, 1988.

78. **Eley L, Yates LM, and Goodship JA.** Cilia and disease. *Curr Opin Genet Dev* 15: 308-314, 2005.

79. **Elias RV, Sezate SS, Cao W, and McGinnis JF.** Temporal kinetics of the light/dark translocation and compartmentation of arrestin and alpha-transducin in mouse photoreceptor cells. *Mol Vis* 10: 672-681, 2004.

80. **Falk N, Lösl M, Schröder N, and Gießl A.** Specialized Cilia in Mammalian Sensory Systems. *Cells* 4: 500-519, 2015.

81. **Ferguson LR, Balaiya S, Grover S, and Chalam KV.** Modified protocol for in vivo imaging of wild-type mouse retina with customized miniature spectral domain optical coherence tomography (SD-OCT) device. *Biol Proced Online* 14: 9, 2012.

82. **Flannery JG and Visel M.** Adeno-associated viral vectors for gene therapy of inherited retinal degenerations. *Methods Mol Biol* 935: 351-369, 2013.

83. **Flannery JG, Zolotukhin S, Vaquero MI, LaVail MM, Muzyczka N, and Hauswirth WW.** Efficient photoreceptor-targeted gene expression in vivo by recombinant adeno-associated virus. *Proc Natl Acad Sci U S A* 94: 6916-6921, 1997.

84. **Frolenkov GI, Belyantseva IA, Friedman TB, and Griffith AJ.** Genetic insights into the morphogenesis of inner ear hair cells. *Nat Rev Genet* 5: 489-498, 2004.

85. **Garcia-Gonzalo FR and Reiter JF.** Scoring a backstage pass: mechanisms of ciliogenesis and ciliary access. *J Cell Biol* 197: 697-709, 2012.

86. **Garg A, Yang J, Lee W, and Tsang SH.** Stem Cell Therapies in Retinal Disorders. *Cells* 6, 2017.

87. **Geller SF, Guerin KI, Visel M, Pham A, Lee ES, Dror AA, Avraham KB, Hayashi T, Ray CA, Reh TA, Bermingham-McDonogh O, Triffo WJ, Bao S, Isosomppi J, Västinsalo H, Sankila EM, and Flannery JG.** CLRN1 is nonessential in the mouse retina but is required for cochlear hair cell development. *PLoS Genet* 5: e1000607, 2009.

88. **Geng R, Geller SF, Hayashi T, Ray CA, Reh TA, Bermingham-McDonogh O, Jones SM, Wright CG, Melki S, Imanishi Y, Palczewski K, Alagramam KN, and Flannery JG.** Usher syndrome IIIA gene clarin-1 is essential for hair cell function and associated neural activation. *Hum Mol Genet* 18: 2748-2760, 2009.

89. **Geng R, Melki S, Chen DH, Tian G, Furness DN, Oshima-Takago T, Neef J, Moser T, Askew C, Horwitz G, Holt JR, Imanishi Y, and Alagramam KN.** The mechanosensory structure of the hair cell requires clarin-1, a protein encoded by Usher syndrome III causative gene. *J Neurosci* 32: 9485-9498, 2012.

90. **Geng R, Omar A, Gopal SR, Chen DH, Stepanyan R, Basch ML, Dinculescu A, Furness DN, Saperstein D, Hauswirth W, Lustig LR, and Alagramam KN.** Modeling and Preventing Progressive Hearing Loss in Usher Syndrome III. *Sci Rep* 7: 13480, 2017.

91. **Geruschat DR, Richards TP, Arditi A, da Cruz L, Dagnelie G, Dorn JD, Duncan JL, Ho AC, Olmos de Koo LC, Sahel JA, Stanga PE, Thumann G, Wang V, and Greenberg RJ.** An analysis of observer-rated functional vision in patients implanted with the Argus II Retinal Prosthesis System at three years. *Clin Exp Optom* 99: 227-232, 2016.

92. **Glöckle N, Kohl S, Mohr J, Scheurenbrand T, Sprecher A, Weisschuh N, Bernd A, Rudolph G, Schubach M, Poloschek C, Zrenner E, Biskup S, Berger W, Wissinger B, and Neidhardt J.** Panel-based next generation sequencing as a reliable and efficient technique to detect mutations in unselected patients with retinal dystrophies. *Eur J Hum Genet* 22: 99-104, 2014.

93. **Gopal SR, Chen DH, Chou SW, Zang J, Neuhauss SC, Stepanyan R, McDermott BM, and Alagramam KN.** Zebrafish Models for the Mechanosensory Hair Cell Dysfunction in Usher Syndrome 3 Reveal That Clarin-1 Is an Essential Hair Bundle Protein. *J Neurosci* 35: 10188-10201, 2015.

94. **Gorlin RJ, Tilsner TJ, Feinstein S, and Duvall AJ.** Usher's syndrome type III. *Arch Otolaryngol* 105: 353-354, 1979.

95. **Govardovskii VI, Calvert PD, and Arshavsky VY.** Photoreceptor light adaptation. Untangling desensitization and sensitization. *J Gen Physiol* 116: 791-794, 2000.

96. **Greenberg KP, Lee ES, Schaffer DV, and Flannery JG.** Gene delivery to the retina using lentiviral vectors. *Adv Exp Med Biol* 572: 255-266, 2006.

97. **Gurevich VV, Hanson SM, Song X, Vishnivetskiy SA, and Gurevich EV.** The functional cycle of visual arrestins in photoreceptor cells. *Prog Retin Eye Res* 30: 405-430, 2011.

98. **Hanson SM, Cleghorn WM, Francis DJ, Vishnivetskiy SA, Raman D, Song X, Nair KS, Slepak VZ, Klug CS, and Gurevich VV.** Arrestin mobilizes signaling proteins to the cytoskeleton and redirects their activity. *J Mol Biol* 368: 375-387, 2007.

99. **Hao W, Wenzel A, Obin MS, Chen CK, Brill E, Krasnoperova NV, Eversole-Cire P, Kleyner Y, Taylor A, Simon MI, Grimm C, Remé CE, and Lem J.** Evidence for two apoptotic pathways in light-induced retinal degeneration. *Nat Genet* 32: 254-260, 2002.

100. **Harris BZ and Lim WA.** Mechanism and role of PDZ domains in signaling complex assembly. *J Cell Sci* 114: 3219-3231, 2001.

101. **Hata Y, Nakanishi H, and Takai Y.** Synaptic PDZ domain-containing proteins. *Neurosci Res* 32: 1-7, 1998.

102. **Hauswirth WW, Aleman TS, Kaushal S, Cideciyan AV, Schwartz SB, Wang L, Conlon TJ, Boye SL, Flotte TR, Byrne BJ, and Jacobson SG.** Treatment of leber congenital amaurosis due to RPE65 mutations by ocular subretinal injection of adeno-associated virus gene vector: short-term results of a phase I trial. *Hum Gene Ther* 19: 979-990, 2008.

103. **Hauswirth WW, Lewin AS, Zolotukhin S, and Muzyczka N.** Production and purification of recombinant adeno-associated virus. *Methods Enzymol* 316: 743-761, 2000.

104. **Hauswirth WW, Li Q, Raisler B, Timmers AM, Berns KI, Flannery JG, LaVail MM, and Lewin AS.** Range of retinal diseases potentially treatable by AAV-vectored gene therapy. *Novartis Found Symp* 255: 179-188; discussion 188-194, 2004.

105. **Haywood-Watson RJ, Ahmed ZM, Kjellstrom S, Bush RA, Takada Y, Hampton LL, Battey JF, Sieving PA, and Friedman TB.** Ames Waltzer deaf mice have reduced electroretinogram amplitudes and complex alternative splicing of Pcdh15 transcripts. *Invest Ophthalmol Vis Sci* 47: 3074-3084, 2006.

106. **Helga Kolb EF and Ralph N.** *Webvision : the organization of the retina and visual system*: [Bethesda, Md.] : National Library of Medicine : [National Center for Biotechnology Information], 2007., 2007.

107. **Herrera W, Aleman TS, Cideciyan AV, Roman AJ, Banin E, Ben-Yosef T, Gardner LM, Sumaroka A, Windsor EA, Schwartz SB, Stone EM, Liu XZ, Kimberling WJ, and Jacobson SG.** Retinal disease in Usher syndrome III caused by mutations in the clarin-1 gene. *Invest Ophthalmol Vis Sci* 49: 2651-2660, 2008.

108. **Herzog RW and Zolotukhin S.** Guide to Human Gene Therapy: World Scientific, 2010.

109. **Hildebrandt F, Benzing T, and Katsanis N.** Ciliopathies. *N Engl J Med* 364: 1533-1543, 2011.

110. **Huang D, Swanson EA, Lin CP, Schuman JS, Stinson WG, Chang W, Hee MR, Flotte T, Gregory K, and Puliafito CA.** Optical coherence tomography. *Science* 254: 1178-1181, 1991.

111. **Hudspeth AJ.** Integrating the active process of hair cells with cochlear function. *Nat Rev Neurosci* 15: 600-614, 2014.

112. **Insinna C and Besharse JC.** Intraflagellar transport and the sensory outer segment of vertebrate photoreceptors. *Dev Dyn* 237: 1982-1992, 2008.

113. **Ishikawa H and Marshall WF.** Ciliogenesis: building the cell's antenna. *Nat Rev Mol Cell Biol* 12: 222-234, 2011.

114. **Isosomppi J, Västinsalo H, Geller SF, Heon E, Flannery JG, and Sankila EM.** Disease-causing mutations in the CLRN1 gene alter normal CLRN1 protein trafficking to the plasma membrane. *Mol Vis* 15: 1806-1818, 2009.

115. **Jacobson SG, Acland GM, Aguirre GD, Aleman TS, Schwartz SB, Cideciyan AV, Zeiss CJ, Komaromy AM, Kaushal S, Roman AJ, Windsor EA, Sumaroka A, Pearce-Kelling SE, Conlon TJ, Chiodo VA, Boye SL, Flotte TR, Maguire AM, Bennett J, and Hauswirth WW.** Safety of recombinant adeno-

associated virus type 2-RPE65 vector delivered by ocular subretinal injection. *Mol Ther* 13: 1074-1084, 2006.

116. **Jacobson SG, Cideciyan AV, Aguirre GD, Roman AJ, Sumaroka A, Hauswirth WW, and Palczewski K.** Improvement in vision: a new goal for treatment of hereditary retinal degenerations. *Expert Opin Orphan Drugs* 3: 563-575, 2015.

117. **Jacobson SG, Cideciyan AV, Ratnakaram R, Heon E, Schwartz SB, Roman AJ, Peden MC, Aleman TS, Boye SL, Sumaroka A, Conlon TJ, Calcedo R, Pang JJ, Erger KE, Olivares MB, Mullins CL, Swider M, Kaushal S, Feuer WJ, Iannaccone A, Fishman GA, Stone EM, Byrne BJ, and Hauswirth WW.** Gene therapy for leber congenital amaurosis caused by RPE65 mutations: safety and efficacy in 15 children and adults followed up to 3 years. *Arch Ophthalmol* 130: 9-24, 2012.

118. **Jacobson SG, Matsui R, Sumaroka A, and Cideciyan AV.** Retinal Structure Measurements as Inclusion Criteria for Stem Cell-Based Therapies of Retinal Degenerations. *Invest Ophthalmol Vis Sci* 57: ORSFn1-9, 2016.

119. **Jacobson SG, Sumaroka A, Luo X, and Cideciyan AV.** Retinal optogenetic therapies: clinical criteria for candidacy. *Clin Genet* 84: 175-182, 2013.

120. **Jansen F, Kalbe B, Scholz P, Mikosz M, Wunderlich KA, Kurtenbach S, Nagel-Wolfrum K, Wolfrum U, Hatt H, and Osterloh S.** Impact of the Usher syndrome on olfaction. *Hum Mol Genet* 25: 524-533, 2016.

121. **Jenkins PM, McEwen DP, and Martens JR.** Olfactory cilia: linking sensory cilia function and human disease. *Chem Senses* 34: 451-464, 2009.

122. **Jin H, White SR, Shida T, Schulz S, Aguiar M, Gygi SP, Bazan JF, and Nachury MV.** The conserved Bardet-Biedl syndrome proteins assemble a coat that traffics membrane proteins to cilia. *Cell* 141: 1208-1219, 2010.

123. **Joensuu T, Blanco G, Pakarinen L, Sistonen P, Kääriäinen H, Brown S, Chapelle A, and Sankila EM.** Refined mapping of the Usher syndrome type III locus on chromosome 3, exclusion of candidate genes, and identification of the putative mouse homologous region. *Genomics* 38: 255-263, 1996.

124. **Joensuu T, Hämäläinen R, Lehesjoki AE, de la Chapelle A, and Sankila EM.** A sequence-ready map of the Usher syndrome type III critical region on chromosome 3q. *Genomics* 63: 409-416, 2000.

125. **Joiner AM, Green WW, McIntyre JC, Allen BL, Schwob JE, and Martens JR.** Primary Cilia on Horizontal Basal Cells Regulate Regeneration of the Olfactory Epithelium. *J Neurosci* 35: 13761-13772, 2015.

126. **Kalloniatis M, Nivison-Smith L, Chua J, Acosta ML, and Fletcher EL.** Using the rd1 mouse to understand functional and anatomical retinal remodelling and treatment implications in retinitis pigmentosa: A review. *Exp Eye Res* 150: 106-121, 2016.

127. **Katsanis N.** The continuum of causality in human genetic disorders. *Genome Biol* 17: 233, 2016.

128. **Kay CN, Ryals RC, Aslanidi GV, Min SH, Ruan Q, Sun J, Dyka FM, Kasuga D, Ayala AE, Van Vliet K, Agbandje-McKenna M, Hauswirth WW, Boye SL, and Boye SE.** Targeting photoreceptors via intravitreal delivery using novel, capsid-mutated AAV vectors. *PLoS One* 8: e62097, 2013.

129. **Kazmierczak P, Sakaguchi H, Tokita J, Wilson-Kubalek EM, Milligan RA, Müller U, and Kachar B.** Cadherin 23 and protocadherin 15 interact to form tip-link filaments in sensory hair cells. *Nature* 449: 87-91, 2007.

130. **Kee HL, Dishinger JF, Blasius TL, Liu CJ, Margolis B, and Verhey KJ.** A size-exclusion permeability barrier and nucleoporins characterize a ciliary pore complex that regulates transport into cilia. *Nat Cell Biol* 14: 431-437, 2012.

131. **Khan MI, Kersten FF, Azam M, Collin RW, Hussain A, Shah ST, Keunen JE, Kremer H, Cremers FP, Qamar R, and den Hollander AI.** CLRN1 mutations cause nonsyndromic retinitis pigmentosa. *Ophthalmology* 118: 1444-1448, 2011.

132. **Khan SH, Javed MR, Qasim M, Shahzadi S, Jalil A, and Rehman SU.** Domain analyses of Usher syndrome causing Clarin-1 and GPR98 protein models. *Bioinformation* 10: 491-495, 2014.

133. **Kim YK, Kim JH, Yu YS, and Ko HW.** Localization of primary cilia in mouse retina. *Acta Histochem* 115: 789-794, 2013.

134. **Kolstad KD, Dalkara D, Guerin K, Visel M, Hoffmann N, Schaffer DV, and Flannery JG.** Changes in adeno-associated virus-mediated gene delivery in retinal degeneration. *Hum Gene Ther* 21: 571-578, 2010.

135. **Kremer H, van Wijk E, Märker T, Wolfrum U, and Roepman R.** Usher syndrome: molecular links of pathogenesis, proteins and pathways. *Hum Mol Genet* 15 Spec No 2: R262-270, 2006.

136. **Krishnamoorthy V, Cherukuri P, Poria D, Goel M, Dagar S, and Dhingra NK.** Retinal Remodeling: Concerns, Emerging Remedies and Future Prospects. *Front Cell Neurosci* 10: 38, 2016.

137. **Ku CA, Chiodo VA, Boye SL, Goldberg AF, Li T, Hauswirth WW, and Ramamurthy V.** Gene therapy using self-complementary Y733F capsid mutant AAV2/8 restores vision in a model of early onset Leber congenital amaurosis. *Hum Mol Genet* 20: 4569-4581, 2011.

138. **Lagziel A, Ahmed ZM, Schultz JM, Morell RJ, Belyantseva IA, and Friedman TB.** Spatiotemporal pattern and isoforms of cadherin 23 in wild type and waltzer mice during inner ear hair cell development. *Dev Biol* 280: 295-306, 2005.

139. **Lagziel A, Overlack N, Bernstein SL, Morell RJ, Wolfrum U, and Friedman TB.** Expression of cadherin 23 isoforms is not conserved: implications for a mouse model of Usher syndrome type 1D. *Mol Vis* 15: 1843-1857, 2009.

140. **Lam S, Cao H, Wu J, Duan R, and Hu J.** Highly efficient retinal gene delivery with helper-dependent adenoviral vectors. *Genes Dis* 1: 227-237, 2014.

141. **Langham ME and Kramer T.** Decreased choroidal blood flow associated with retinitis pigmentosa. *Eye (Lond)* 4 (Pt 2): 374-381, 1990.

142. **Libby RT, Kitamoto J, Holme RH, Williams DS, and Steel KP.** Cdh23 mutations in the mouse are associated with retinal dysfunction but not retinal degeneration. *Exp Eye Res* 77: 731-739, 2003.

143. **Lindemann CB and Lesich KA.** Flagellar and ciliary beating: the proven and the possible. *J Cell Sci* 123: 519-528, 2010.

144. **Lopes VS, Boye SE, Louie CM, Boye S, Dyka F, Chiodo V, Fofo H, Hauswirth WW, and Williams DS.** Retinal gene therapy with a large MYO7A cDNA using adeno-associated virus. *Gene Ther* 20: 824-833, 2013.

145. **Luby-Phelps K, Fogerty J, Baker SA, Pazour GJ, and Besharse JC.** Spatial distribution of intraflagellar transport proteins in vertebrate photoreceptors. *Vision Res* 48: 413-423, 2008.

146. **Lukacs GL.** Proteostasis: Chaperoning for hearing loss. *Nat Chem Biol* 12: 388-389, 2016.

147. **Maerker T, van Wijk E, Overlack N, Kersten FF, McGee J, Goldmann T, Sehn E, Roepman R, Walsh EJ, Kremer H, and Wolfrum U.** A novel Usher protein network at the periciliary reloading point between molecular transport machineries in vertebrate photoreceptor cells. *Hum Mol Genet* 17: 71-86, 2008.

148. **Mathur P and Yang J.** Usher syndrome: Hearing loss, retinal degeneration and associated abnormalities. *Biochim Biophys Acta* 1852: 406-420, 2015.

149. **Mburu P, Mustapha M, Varela A, Weil D, El-Amraoui A, Holme RH, Rump A, Hardisty RE, Blanchard S, Coimbra RS, Perfettini I, Parkinson N, Mallon AM, Glenister P, Rogers MJ, Paige AJ, Moir L, Clay J, Rosenthal A, Liu XZ, Blanco G, Steel KP, Petit C, and Brown SD.** Defects in whirlin, a PDZ domain molecule involved in stereocilia elongation, cause deafness in the whirler mouse and families with DFNB31. *Nat Genet* 34: 421-428, 2003.

150. **McCall MA and Gregg RG.** Comparisons of structural and functional abnormalities in mouse b-wave mutants. *J Physiol* 586: 4385-4392, 2008.

151. **McEwen DP, Jenkins PM, and Martens JR.** Olfactory cilia: our direct neuronal connection to the external world. *Curr Top Dev Biol* 85: 333-370, 2008.

152. **McGee J, Goodyear RJ, McMillan DR, Stauffer EA, Holt JR, Locke KG, Birch DG, Legan PK, White PC, Walsh EJ, and Richardson GP.** The very large G-protein-coupled receptor VLGR1: a component of the ankle link complex required for the normal development of auditory hair bundles. *J Neurosci* 26: 6543-6553, 2006.

153. **McIntyre JC, Davis EE, Joiner A, Williams CL, Tsai IC, Jenkins PM, McEwen DP, Zhang L, Escobado J, Thomas S, Szymanska K, Johnson CA, Beales PL, Green ED, Mullikin JC, Sabo A, Muzny DM, Gibbs RA, Attié-Bitach T, Yoder BK, Reed RR, Katsanis N, Martens JR, and Program NCS.** Gene therapy rescues cilia defects and restores olfactory function in a mammalian ciliopathy model. *Nat Med* 18: 1423-1428, 2012.

154. **McIntyre JC, Williams CL, and Martens JR.** Smelling the roses and seeing the light: gene therapy for ciliopathies. *Trends Biotechnol* 31: 355-363, 2013.

155. **McLean WJ, Yin X, Lu L, Lenz DR, McLean D, Langer R, Karp JM, and Edge AS.** Clonal Expansion of Lgr5-Positive Cells from Mammalian Cochlea and High-Purity Generation of Sensory Hair Cells. *Cell Rep* 18: 1917-1929, 2017.

156. **Menini A, Lagostena L, and Boccaccio A.** Olfaction: from odorant molecules to the olfactory cortex. *News Physiol Sci* 19: 101-104, 2004.

157. **Michalski N, Michel V, Bahloul A, Lefèvre G, Barral J, Yagi H, Chardenoux S, Weil D, Martin P, Hardelin JP, Sato M, and Petit C.** Molecular characterization of the ankle-link complex in cochlear hair cells and its role in the hair bundle functioning. *J Neurosci* 27: 6478-6488, 2007.

158. **Millán JM, Aller E, Jaijo T, Blanco-Kelly F, Gimenez-Pardo A, and Ayuso C.** An update on the genetics of usher syndrome. *J Ophthalmol* 2011: 417217, 2011.

159. **Mourão A, Christensen ST, and Lorentzen E.** The intraflagellar transport machinery in ciliary signaling. *Curr Opin Struct Biol* 41: 98-108, 2016.

160. **Mustafi D, Maeda T, Kohno H, Nadeau JH, and Palczewski K.** Inflammatory priming predisposes mice to age-related retinal degeneration. *J Clin Invest* 122: 2989-3001, 2012.

161. **Nachury MV, Seeley ES, and Jin H.** Trafficking to the ciliary membrane: how to get across the periciliary diffusion barrier? *Annu Rev Cell Dev Biol* 26: 59-87, 2010.

162. **Nair KS, Hanson SM, Kennedy MJ, Hurley JB, Gurevich VV, and Slepak VZ.** Direct binding of visual arrestin to microtubules determines the differential subcellular localization of its splice variants in rod photoreceptors. *J Biol Chem* 279: 41240-41248, 2004.

163. **Nair KS, Hanson SM, Mendez A, Gurevich EV, Kennedy MJ, Shestopalov VI, Vishnivetskiy SA, Chen J, Hurley JB, Gurevich VV, and Slepak VZ.** Light-dependent redistribution of arrestin in vertebrate rods is an energy-independent process governed by protein-protein interactions. *Neuron* 46: 555-567, 2005.

164. **Najafi M, Maza NA, and Calvert PD.** Steric volume exclusion sets soluble protein concentrations in photoreceptor sensory cilia. *Proc Natl Acad Sci U S A* 109: 203-208, 2012.

165. **Naso MF, Tomkowicz B, Perry WL, and Strohl WR.** Adeno-Associated Virus (AAV) as a Vector for Gene Therapy. *BioDrugs*, 2017.

166. **Nishio SY, Takumi Y, and Usami SI.** Laser-capture micro dissection combined with next-generation sequencing analysis of cell type-specific deafness gene expression in the mouse cochlea. *Hear Res* 348: 87-97, 2017.

167. **Noben-Trauth K, Zheng QY, and Johnson KR.** Association of cadherin 23 with polygenic inheritance and genetic modification of sensorineural hearing loss. *Nat Genet* 35: 21-23, 2003.

168. **O'Connor AK, Malarkey EB, Berbari NF, Croyle MJ, Haycraft CJ, Bell PD, Hohenstein P, Kesterson RA, and Yoder BK.** An inducible CiliaGFP mouse model for in vivo visualization and analysis of cilia in live tissue. *Cilia* 2: 8, 2013.

169. **Ogun O and Zallocchi M.** Clarin-1 acts as a modulator of mechanotransduction activity and presynaptic ribbon assembly. *J Cell Biol* 207: 375-391, 2014.

170. **Overlack N, Maerker T, Latz M, Nagel-Wolfrum K, and Wolfrum U.** SANS (USH1G) expression in developing and mature mammalian retina. *Vision Res* 48: 400-412, 2008.

171. **Pakarinen L, Karjalainen S, Simola KO, Laippala P, and Kaitalo H.** Usher's syndrome type 3 in Finland. *Laryngoscope* 105: 613-617, 1995.

172. **Pakarinen L, Tuppurainen K, Laippala P, Mäntyjärvi M, and Puhakka H.** The ophthalmological course of Usher syndrome type III. *Int Ophthalmol* 19: 307-311, 1995.

173. **Pan B, Askew C, Galvin A, Heman-Ackah S, Asai Y, Indzhykulian AA, Jodelka FM, Hastings ML, Lentz JJ, Vandenberghe LH, Holt JR, and Géléoc GS.** Gene therapy restores auditory and vestibular function in a mouse model of Usher syndrome type 1c. *Nat Biotechnol* 35: 264-272, 2017.

174. **Parmeggiani F, De Nadai K, Piovan A, Binotto A, Zamengo S, and Chizzolini M.** Optical coherence tomography imaging in the management of the Argus II retinal prosthesis system. *Eur J Ophthalmol* 27: e16-e21, 2017.

175. **Peachey NS and Ball SL.** Electrophysiological analysis of visual function in mutant mice. *Doc Ophthalmol* 107: 13-36, 2003.

176. **Peng YW, Zallocchi M, Wang WM, Delimont D, and Cosgrove D.** Moderate light-induced degeneration of rod photoreceptors with delayed transducin translocation in shaker1 mice. *Invest Ophthalmol Vis Sci* 52: 6421-6427, 2011.

177. **Pennesi ME, Michaels KV, Magee SS, Maricle A, Davin SP, Garg AK, Gale MJ, Tu DC, Wen Y, Erker LR, and Francis PJ.** Long-term characterization of retinal degeneration in rd1 and rd10 mice using spectral domain optical coherence tomography. *Invest Ophthalmol Vis Sci* 53: 4644-4656, 2012.

178. **Petit C.** Usher syndrome: from genetics to pathogenesis. *Annu Rev Genomics Hum Genet* 2: 271-297, 2001.

179. **Petrs-Silva H, Dinculescu A, Li Q, Deng WT, Pang JJ, Min SH, Chiodo V, Neeley AW, Govindasamy L, Bennett A, Agbandje-McKenna M, Zhong L, Li B, Jayandharan GR, Srivastava A, Lewin AS, and Hauswirth WW.** Novel properties of tyrosine-mutant AAV2 vectors in the mouse retina. *Mol Ther* 19: 293-301, 2011.

180. **Petrs-Silva H, Dinculescu A, Li Q, Min SH, Chiodo V, Pang JJ, Zhong L, Zolotukhin S, Srivastava A, Lewin AS, and Hauswirth WW.** High-efficiency transduction of the mouse retina by tyrosine-mutant AAV serotype vectors. *Mol Ther* 17: 463-471, 2009.

181. **Petrs-Silva H and Linden R.** Advances in gene therapy technologies to treat retinitis pigmentosa. *Clin Ophthalmol* 8: 127-136, 2014.

182. **Phillips JB, Västinsalo H, Wegner J, Clément A, Sankila EM, and Westerfield M.** The cone-dominant retina and the inner ear of zebrafish express the ortholog of CLRN1, the causative gene of human Usher syndrome type 3A. *Gene Expr Patterns* 13: 473-481, 2013.

183. **Pietola L, Aarnisalo AA, Abdel-Rahman A, Västinsalo H, Isosomppi J, Löppönen H, Kentala E, Johansson R, Valtonen H, Vasama JP, Sankila EM, and Jero J.** Speech recognition and communication outcomes with cochlear implantation in Usher syndrome type 3. *Otol Neurotol* 33: 38-41, 2012.

184. **Pinto LH, Invergo B, Shimomura K, Takahashi JS, and Troy JB.** Interpretation of the mouse electroretinogram. *Doc Ophthalmol* 115: 127-136, 2007.

185. **Plantinga RF, Kleemola L, Huygen PL, Joensuu T, Sankila EM, Pennings RJ, and Cremers CW.** Serial audiometry and speech recognition findings in Finnish Usher syndrome type III patients. *Audiol Neurootol* 10: 79-89, 2005.

186. **Plantinga RF, Pennings RJ, Huygen PL, Sankila EM, Tuppurainen K, Kleemola L, Cremers CW, and Deutman AF.** Visual impairment in Finnish Usher syndrome type III. *Acta Ophthalmol Scand* 84: 36-41, 2006.

187. **Rachel RA, Li T, and Swaroop A.** Photoreceptor sensory cilia and ciliopathies: focus on CEP290, RPGR and their interacting proteins. *Cilia* 1: 22, 2012.

188. **Ramamurthy V and Cayouette M.** Development and disease of the photoreceptor cilium. *Clin Genet* 76: 137-145, 2009.

189. **Ratnam K, Västinsalo H, Roorda A, Sankila EM, and Duncan JL.** Cone structure in patients with usher syndrome type III and mutations in the Clarin 1 gene. *JAMA Ophthalmol* 131: 67-74, 2013.

190. **Reidel B, Goldmann T, Giessl A, and Wolfrum U.** The translocation of signaling molecules in dark adapting mammalian rod photoreceptor cells is dependent on the cytoskeleton. *Cell Motil Cytoskeleton* 65: 785-800, 2008.

191. **Reiners J, Märker T, Jürgens K, Reidel B, and Wolfrum U.** Photoreceptor expression of the Usher syndrome type 1 protein protocadherin 15 (USH1F) and its interaction with the scaffold protein harmonin (USH1C). *Mol Vis* 11: 347-355, 2005.

192. **Reiners J, Nagel-Wolfrum K, Jürgens K, Märker T, and Wolfrum U.** Molecular basis of human Usher syndrome: deciphering the meshes of the Usher protein network provides insights into the pathomechanisms of the Usher disease. *Exp Eye Res* 83: 97-119, 2006.

193. **Reiners J, Reidel B, El-Amraoui A, Boëda B, Huber I, Petit C, and Wolfrum U.** Differential distribution of harmonin isoforms and their possible role in Usher-1 protein complexes in mammalian photoreceptor cells. *Invest Ophthalmol Vis Sci* 44: 5006-5015, 2003.

194. **Reiners J, van Wijk E, Märker T, Zimmermann U, Jürgens K, te Brinke H, Overlack N, Roepman R, Knipper M, Kremer H, and Wolfrum U.** Scaffold protein harmonin (USH1C) provides molecular links between Usher syndrome type 1 and type 2. *Hum Mol Genet* 14: 3933-3943, 2005.

195. **Reiter JF, Blacque OE, and Leroux MR.** The base of the cilium: roles for transition fibres and the transition zone in ciliary formation, maintenance and compartmentalization. *EMBO Rep* 13: 608-618, 2012.

196. **Ribeiro JC, Oliveiros B, Pereira P, António N, Hummel T, Paiva A, and Silva ED.** Accelerated age-related olfactory decline among type 1 Usher patients. *Sci Rep* 6: 28309, 2016.

197. **Ryals RC, Boye SL, Dinculescu A, Hauswirth WW, and Boye SE.** Quantifying transduction efficiencies of unmodified and tyrosine capsid mutant AAV vectors in vitro using two ocular cell lines. *Mol Vis* 17: 1090-1102, 2011.

198. **Sahly I, Dufour E, Schietroma C, Michel V, Bahloul A, Perfettini I, Pepermans E, Estivalet A, Carette D, Aghaie A, Ebermann I, Lelli A, Iribarne M, Hardelin JP, Weil D, Sahel JA, El-Amraoui A, and Petit C.** Localization of Usher 1 proteins to the photoreceptor calyceal processes, which are absent from mice. *J Cell Biol* 199: 381-399, 2012.

199. **Saihan Z, Webster AR, Luxon L, and Bitner-Glindzicz M.** Update on Usher syndrome. *Curr Opin Neurol* 22: 19-27, 2009.

200. **Sankila EM, Pakarinen L, Kääriäinen H, Aittomäki K, Karjalainen S, Sistonen P, and de la Chapelle A.** Assignment of an Usher syndrome type III (USH3) gene to chromosome 3q. *Hum Mol Genet* 4: 93-98, 1995.

201. **Schultz JM, Bhatti R, Madeo AC, Turriff A, Muskett JA, Zalewski CK, King KA, Ahmed ZM, Riazuddin S, Ahmad N, Hussain Z, Qasim M, Kahn SN, Meltzer MR, Liu XZ, Munisamy M, Ghosh M, Rehm HL, Tsilou ET, Griffith AJ, Zein WM, Brewer CC, and Friedman TB.** Allelic hierarchy of CDH23 mutations causing non-syndromic deafness DFNB12 or Usher syndrome USH1D in compound heterozygotes. *J Med Genet* 48: 767-775, 2011.

202. **Sedmak T and Wolfrum U.** Intraflagellar transport molecules in ciliary and nonciliary cells of the retina. *J Cell Biol* 189: 171-186, 2010.

203. **Sedmak T and Wolfrum U.** Intraflagellar transport proteins in ciliogenesis of photoreceptor cells. *Biol Cell* 103: 449-466, 2011.

204. **Senften M, Schwander M, Kazmierczak P, Lillo C, Shin JB, Hasson T, Géléoc GS, Gillespie PG, Williams D, Holt JR, and Müller U.** Physical and functional interaction between protocadherin 15 and myosin VIIa in mechanosensory hair cells. *J Neurosci* 26: 2060-2071, 2006.

205. **Seo S, Mullins RF, Dumitrescu AV, Bhattarai S, Gratie D, Wang K, Stone EM, Sheffield V, and Drack AV.** Subretinal gene therapy of mice with Bardet-Biedl syndrome type 1. *Invest Ophthalmol Vis Sci* 54: 6118-6132, 2013.

206. **Shichida Y and Morizumi T.** Mechanism of G-protein activation by rhodopsin. *Photochem Photobiol* 83: 70-75, 2007.

207. **Siegert S, Cabuy E, Scherf BG, Kohler H, Panda S, Le YZ, Fehling HJ, Gaidatzis D, Stadler MB, and Roska B.** Transcriptional code and disease map for adult retinal cell types. *Nat Neurosci* 15: 487-495, S481-482, 2012.

208. **Siemens J, Kazmierczak P, Reynolds A, Sticker M, Littlewood-Evans A, and Müller U.** The Usher syndrome proteins cadherin 23 and harmonin form a complex by means of PDZ-domain interactions. *Proc Natl Acad Sci U S A* 99: 14946-14951, 2002.

209. **Simons DL, Boye SL, Hauswirth WW, and Wu SM.** Gene therapy prevents photoreceptor death and preserves retinal function in a Bardet-Biedl syndrome mouse model. *Proc Natl Acad Sci U S A* 108: 6276-6281, 2011.

210. **Slepak VZ and Hurley JB.** Mechanism of light-induced translocation of arrestin and transducin in photoreceptors: interaction-restricted diffusion. *IUBMB Life* 60: 2-9, 2008.

211. **Sorusch N, Wunderlich K, Bauss K, Nagel-Wolfrum K, and Wolfrum U.** Usher syndrome protein network functions in the retina and their relation to other retinal ciliopathies. *Adv Exp Med Biol* 801: 527-533, 2014.

212. **Sumaroka A, Matsui R, Cideciyan AV, McGuigan DB, Sheplock R, Schwartz SB, and Jacobson SG.** Outer Retinal Changes Including the Ellipsoid Zone Band in Usher Syndrome 1B due to MYO7A Mutations. *Invest Ophthalmol Vis Sci* 57: OCT253-261, 2016.

213. **Sun LW, Johnson RD, Langlo CS, Cooper RF, Razeen MM, Russillo MC, Dubra A, Connor TB, Han DP, Pennesi ME, Kay CN, Weinberg DV, Stepien KE, and Carroll J.** Assessing Photoreceptor Structure in Retinitis Pigmentosa and Usher Syndrome. *Invest Ophthalmol Vis Sci* 57: 2428-2442, 2016.

214. **Sung CH and Chuang JZ.** The cell biology of vision. *J Cell Biol* 190: 953-963, 2010.

215. **Sung CH and Tai AW.** Rhodopsin trafficking and its role in retinal dystrophies. *Int Rev Cytol* 195: 215-267, 2000.

216. **Szymanska K and Johnson CA.** The transition zone: an essential functional compartment of cilia. *Cilia* 1: 10, 2012.

217. **Tian G, Lee R, Ropelewski P, and Imanishi Y.** Impairment of Vision in a Mouse Model of Usher Syndrome Type III. *Invest Ophthalmol Vis Sci* 57: 866-875, 2016.

218. **Tian G, Zhou Y, Hajkova D, Miyagi M, Dinculescu A, Hauswirth WW, Palczewski K, Geng R, Alagramam KN, Isosomppi J, Sankila EM, Flannery JG, and Imanishi Y.** Clarin-1, encoded by the Usher Syndrome III causative gene, forms a membranous microdomain: possible role of clarin-1 in organizing the actin cytoskeleton. *J Biol Chem* 284: 18980-18993, 2009.

219. **Tian M, Wang W, Delimont D, Cheung L, Zallocchi M, Cosgrove D, and Peng YW.** Photoreceptors in whirler mice show defective transducin translocation and are susceptible to short-term light/dark changes-induced degeneration. *Exp Eye Res* 118: 145-153, 2014.

220. **Tian M, Zallocchi M, Wang W, Chen CK, Palczewski K, Delimont D, Cosgrove D, and Peng YW.** Light-induced translocation of RGS9-1 and Gβ5L in mouse rod photoreceptors. *PLoS One* 8: e58832, 2013.

221. **Toth CA, Narayan DG, Boppart SA, Hee MR, Fujimoto JG, Birngruber R, Cain CP, DiCarlo CD, and Roach WP.** A comparison of retinal morphology viewed by optical coherence tomography and by light microscopy. *Arch Ophthalmol* 115: 1425-1428, 1997.

222. **Trapani I, Puppo A, and Auricchio A.** Vector platforms for gene therapy of inherited retinopathies. *Prog Retin Eye Res* 43: 108-128, 2014.

223. **Ueki Y, Chollangi S, Le YZ, and Ash JD.** gp130 activation in Müller cells is not essential for photoreceptor protection from light damage. *Adv Exp Med Biol* 664: 655-661, 2010.

224. **Ueki Y, Wang J, Chollangi S, and Ash JD.** STAT3 activation in photoreceptors by leukemia inhibitory factor is associated with protection from light damage. *J Neurochem* 105: 784-796, 2008.

225. **Västinsalo H, Jalkanen R, Bergmann C, Neuhaus C, Kleemola L, Jauhola L, Bolz HJ, and Sankila EM.** Extended mutation spectrum of Usher syndrome in Finland. *Acta Ophthalmol* 91: 325-334, 2013.

226. **Västinsalo H, Jalkanen R, Dinculescu A, Isosomppi J, Geller S, Flannery JG, Hauswirth WW, and Sankila EM.** Alternative splice variants of the USH3A gene Clarin 1 (CLRN1). *Eur J Hum Genet* 19: 30-35, 2011.

227. **Wachtmeister L.** Oscillatory potentials in the retina: what do they reveal. *Prog Retin Eye Res* 17: 485-521, 1998.

228. **Wei Q, Ling K, and Hu J.** The essential roles of transition fibers in the context of cilia. *Curr Opin Cell Biol* 35: 98-105, 2015.

229. **Weil D, El-Amraoui A, Masmoudi S, Mustapha M, Kikkawa Y, Lainé S, Delmaghani S, Adato A, Nadifi S, Zina ZB, Hamel C, Gal A, Ayadi H, Yonekawa H, and Petit C.** Usher syndrome type I G (USH1G) is caused by mutations in the gene encoding SANS, a protein that associates with the USH1C protein, harmonin. *Hum Mol Genet* 12: 463-471, 2003.

230. **Wheway G, Parry DA, and Johnson CA.** The role of primary cilia in the development and disease of the retina. *Organogenesis* 10: 69-85, 2014.

231. **Williams CL, Li C, Kida K, Inglis PN, Mohan S, Semenec L, Bialas NJ, Stupay RM, Chen N, Blacque OE, Yoder BK, and Leroux MR.** MKS and NPHP modules cooperate to establish basal body/transition zone membrane associations and ciliary gate function during ciliogenesis. *J Cell Biol* 192: 1023-1041, 2011.

232. **Williams CL, Uytingco CR, Green WW, McIntyre JC, Ukhanov K, Zimmerman AD, Shively DT, Zhang L, Nishimura DY, Sheffield VC, and Martens JR.** Gene Therapeutic Reversal of Peripheral Olfactory Impairment in Bardet-Biedl Syndrome. *Mol Ther*, 2017.

233. **Williams DS.** Usher syndrome: animal models, retinal function of Usher proteins, and prospects for gene therapy. *Vision Res* 48: 433-441, 2008.

234. **Wolfrum U and Schmitt A.** Rhodopsin transport in the membrane of the connecting cilium of mammalian photoreceptor cells. *Cell Motil Cytoskeleton* 46: 95-107, 2000.

235. **Xu J, Dodd RL, Makino CL, Simon MI, Baylor DA, and Chen J.** Prolonged photoresponses in transgenic mouse rods lacking arrestin. *Nature* 389: 505-509, 1997.

236. **Yan D and Liu XZ.** Genetics and pathological mechanisms of Usher syndrome. *J Hum Genet* 55: 327-335, 2010.

237. **Yang J, Liu X, Zhao Y, Adamian M, Pawlyk B, Sun X, McMillan DR, Liberman MC, and Li T.** Ablation of whirlin long isoform disrupts the USH2 protein complex and causes vision and hearing loss. *PLoS Genet* 6: e1000955, 2010.

238. **Yaqoob Z, Wu J, and Yang C.** Spectral domain optical coherence tomography: a better OCT imaging strategy. *Biotechniques* 39: S6-13, 2005.

239. **Yoshimura H, Oshikawa C, Nakayama J, Moteki H, and Usami S.** Identification of a novel CLRN1 gene mutation in Usher syndrome type 3: two case reports. *Ann Otol Rhinol Laryngol* 124 Suppl 1: 94S-99S, 2015.

240. **Zallocchi M, Binley K, Lad Y, Ellis S, Widdowson P, Iqball S, Scripps V, Kelleher M, Loader J, Miskin J, Peng YW, Wang WM, Cheung L, Delimont D, Mitrophanous KA, and Cosgrove D.** EIAV-based retinal gene therapy in the shaker1 mouse model for usher syndrome type 1B: development of UshStat. *PLoS One* 9: e94272, 2014.

241. **Zallocchi M, Meehan DT, Delimont D, Askew C, Garige S, Gratton MA, Rothermund-Franklin CA, and Cosgrove D.** Localization and expression of clarin-1, the Clrn1 gene product, in auditory hair cells and photoreceptors. *Hear Res* 255: 109-120, 2009.

242. **Zallocchi M, Meehan DT, Delimont D, Rutledge J, Gratton MA, Flannery J, and Cosgrove D.** Role for a novel Usher protein complex in hair cell synaptic maturation. *PLoS One* 7: e30573, 2012.

243. **Zheng QY, Ding D, Yu H, Salvi RJ, and Johnson KR.** A locus on distal chromosome 10 (ahl4) affecting age-related hearing loss in A/J mice. *Neurobiol Aging* 30: 1693-1705, 2009.

244. **Zhong H, Eblimit A, Moayedi Y, Boye SL, Chiodo VA, Chen Y, Li Y, Nichols RM, Hauswirth WW, Chen R, and Mardon G.** AAV8(Y733F)-mediated gene therapy in a Spata7 knockout mouse model of Leber congenital amaurosis and retinitis pigmentosa. *Gene Ther* 22: 619-627, 2015.

245. **Zolotukhin S, Potter M, Zolotukhin I, Sakai Y, Loiler S, Fraites TJ, Chiodo VA, Phillipsberg T, Muzyczka N, Hauswirth WW, Flotte TR, Byrne BJ, and Snyder RO.** Production and purification of serotype 1, 2, and 5 recombinant adeno-associated viral vectors. *Methods* 28: 158-167, 2002.

246. **Zou J, Mathur PD, Zheng T, Wang Y, Almishaal A, Park AH, and Yang J.** Individual USH2 proteins make distinct contributions to the ankle link complex during development of the mouse cochlear stereociliary bundle. *Hum Mol Genet* 24: 6944-6957, 2015.

BIOGRAPHICAL SKETCH

Rachel Michelle Stupay was born and raised in Frankfort, Illinois and graduated from Lincoln Way East High School in the spring of 2004. Growing up Rachel trained as a professional ballet dancer with The School of Ballet Chicago for over a decade. She performed with the Joffrey Ballet of Chicago for four consecutive years and was a Dancewear Catalog Model for Leo's Dancewear during that time. From 2004-2005 Rachel was a Post-Graduate with Ballet Met in Columbus, OH. She was then offered a company contract with the Alabama ballet from 2006-2008. During this time Rachel was also a Sales Lead/ Key-holder and Credit Card Coach for Ann Taylor Inc.

In 2007, Rachel returned to undergraduate school at the University of Alabama at Birmingham. In 2009 she was awarded a Genetics Summer Research Internship and a Summer Internship in Biomedical Sciences in 2010 where she worked in Dr. Bradley K. Yoder's laboratory. Rachel first became interested in studying Ciliopathies through her work in Dr. Yoder's lab where her research consisted of executing a *Caenorhabiditis elegans* mutagenesis screen to identify novel ciliopathy disease-causing alleles (Stupay RM et al, 2009 https://www.uab.edu/inquiro/images/Archives/Volume_3.pdf, pages 37-45; Stupay RM et al, 2010 https://www.uab.edu/inquiro/images/Archives/Volume_4.pdf, pages 55-61) (231). Rachel graduated with a bachelor's degree from UAB in the spring of 2011 with a major in Molecular Biology and a minor in Biochemistry.

Rachel was accepted into the University of Florida's Interdisciplinary Program in Biomedical Sciences and began graduate school in the fall of 2011. In 2012 Rachel joined the lab of Dr. William W. Hauswirth and was appointed a Graduate Fellow on an NIH Ophthalmology Training Grant. Her thesis project involved studying an Usher Syndrome Type 3A (USH3A) mouse model in order to define a retinal phenotype and

establish a therapeutic approach for treatment (72). Rachel has extensive experience with working with mice on several ophthalmologic assays including: ERG (LKC and Espion systems), optical coherence tomography (OCT) (Heidelburg Spectralis and Bioptigen systems), fundoscopy, and optokinetics as well as extensive breeding, and genotyping. Rachel is also experienced in Cryostat and paraffin microtome fixation and sectioning for histology, qPCR, PCR, western blotting, and AAV vector cloning.

Rachel graduated with her doctoral degree in the fall of 2017 and subsequently moved to Cleveland, Ohio to work as a post-doctoral fellow with Dr. Brian D. Perkins in the Cole Eye Institute at the Cleveland Clinic. Her postdoctoral studies are focused on using zebrafish as a model organism to study photoreceptor degeneration in ciliopathy models that mimic patient phenotypes and how the cilia protein mutations disrupt normal cellular pathways.